Development of a Design Process for Solar-Powered HALE Aircraft Configurations

Benedict Bartels

Technische Universiteit Delft

TU Delft Delft University of Technology

Challenge the future

Development of a Design Process for Solar-Powered HALE Aircraft Configurations

by

Benedict Bartels

in partial fulfillment of the requirements for the degree of

Master of Science
in Aerospace Engineering

at the Delft University of Technology,
to be defended publicly on Tuesday January 18, 2022 at 02:00 PM.

Supervisor:	Dr. ir. G. la Rocca,	
	Ir. C. Liersch	
Thesis committee:	Dr. ir. G. la Rocca,	TU Delft
	Dr. ir. AH. van Zuijlen,	TU Delft
	Dr. ir. MFM Hoogreef,	TU Delft
	Dipl.-Ing. C. Liersch,	German Aerospace Center

Wordcount: $22,999 + 35x200 = 29,999$

Alte Straße 8, Veltheim (Ohe), Niedersachsen, Germany, 38173
Student 4247353, TUDelft, AE, b.j.bartels@student.tudelft.nl

TU Delft Delft University of Technology

Abstract

High-flying autonomous aircraft are meant to be deployed in the stratosphere for days or even months. These aircraft share different applications from and several advantages over satellites. Therefore, such aircraft are an interesting subject for research and commercial applications. They are expected to be powered by solar energy and thus heavily depend on their mission profile.
An integrated, multidisciplinary design process is proposed to provide a fast way to evaluate an extensive parameter space while requiring minimum input parameters. This process is realised by developing a process which incorporates several critical disciplines required for a high-flying autonomous aircraft, implemented into a software-tool. The underlying disciplines include the basic aerodynamics and structural analysis of an aircraft, which must be connected with a mission analysis approach, considering the constantly changing irradiation conditions and the resulting aircraft power management and constant re-evaluation of aircraft parameters.
The aircraft's dependence on solar energy led to the implementation of a time-based, iterative sizing approach which relied on handbook formulas and empirical estimation methods. The tool ultimately consists of different levels, permitting the use of a core process to evaluate aircraft configurations and missions and provide aircraft performance estimates for researchers and designers. This core process can further be used by outer levels for parametric studies, enabling users to change the basic parameters of the aircraft or the mission definition. These studies can be used to compare aircraft parameter configurations or to conduct use case analysis of a given aircraft. The tool is shown to be capable of evaluating the parameter space for the intended aircraft and mission configurations. Exemplary studies using the mission analysis algorithm revealed that the results where highly sensitive to irradiation compared to what was expected from earlier studies from the literature, ultimately influencing all aircraft parameters due to highly dynamic parameter relations. For example, the effect of adjustable solar panels can be rated using simple comparison experiments, which attest an efficiency increase for low irradiation angles with adjustable panels despite an included drag and weight penalty. This thesis and the included methods helps to close a gap between analytic aircraft analysis approaches and CPU-intensive 3D-simulations for high-flying autonomous aircraft. Future projects will have a detailed overview of battery management required for high-flying autonomous aircraft, and a process supporting aircraft assessment and design for faster research and development.

List of Figures

List of Tables

Nomenclature

α	=	angle of attack [°]
α_0	=	zero-lift angle of attack [°]
α_eff	=	resulting angle of attack with lift induced effects [°]
α_i	=	angle of attack due to lift induced effects [°]
Δ_t	=	time step length $[s]$
Δ_{Re}	=	difference in Reynolds numbers$[s]$
η	=	efficiency factor [−]
γ	=	flight path angle [°]
Γ	=	circulation [−]
Γ_0	=	circulation at $y = 0$ [−]
ω	=	battery energy density $\left[\frac{Wh}{kg}\right]$
σ	=	direct stress $[Pa]$
ρ	=	mass density $[kg/m^3]$
τ_G	=	Glauert factor [−]
Φ	=	aircraft bank angle [°]
a	=	lift coefficient curve slope [−]
A	=	area $[m^2]$
AR	=	aspect ratio [−]
b	=	wing span $[m]$
B_i	=	inner material (wall) strength (horizontal) $[m]$
B_o	=	outer material (wall) strength (horizontal) $[m]$
c_d	=	2D airfoil drag coefficient [−]
c_f	=	Friction coefficient [−]
c_l	=	2D airfoil lift coefficient [−]
C_D	=	3D wing drag coefficient [−]
$C_{D,0}$	=	3D wing drag coefficient at zero lift [−]
$C_{D,i}$	=	3D wing induced drag coefficient [−]
C_L	=	3D wing lift coefficient [−]
d	=	distance $[m]$
d_{nl}	=	distance from neutral line $[m]$
D	=	drag force $[N]$
D'	=	distributed drag force $[N]$
D_f	=	skin friction drag $[N]$
D_i	=	inner diameter $[m]$
D_p	=	lift induced drag ——waht? $[N]$
D_o	=	outer diameter $[m]$
e	=	Oswald efficiency factor [−]
e_v	=	span efficiency factor [−]
E_{bat}	=	total battery capacity $[Wh]$
F	=	force $[N]$
F'	=	distributed force $[N]$
g	=	load factor [−]

$ground$	=	referred to ground usage $[-]$
h	=	altitude $[m]$
H_i	=	inner material (wall) strength (vertical) $[m]$
H_o	=	inner material (wall) strength (vertical) $[m]$
K	=	drag-due-to-lift factor $[-]$
l	=	length $[m]$
L	=	lift force $[N]$
L'	=	distributed (span-wise) lift force $[N]$
L_{VT}, L_{HT}	=	vertical / horizontal tail distance to wing quarter-chord $[m]$
m	=	mass $[kg]$
M	=	moment $[Nm]$
M'	=	distributed moment $[Nm]$
n	=	number of instances $[-]$
P	=	power $[W]$
S	=	projected (planform) wing area $[m^2]$
R	=	radius $[m]$
R_i	=	inner radius $[m]$
R_o	=	outer radius $[m]$
Re	=	Reynolds number $[-]$
Re_{min}	=	minimum Reynolds number to be considered $[-]$
RC	=	Rate of climb $\left[\frac{m}{s}\right]$
t	=	time $[s]$
T	=	thrust force $[N]$
v	=	velocity $\left[\frac{m}{s}\right]$
v_∞	=	freestream velocity $\left[\frac{m}{s}\right]$
V	=	volume $[m^3]$
w_s	=	sink rate $[m/s]$
W	=	weight force $[N]$
W'	=	distributed weight force $[N]$
$x_{rel.W}$	=	aircraft flight direction relative to the wind direction $[^\circ]$

Subscript

0	:	origin
∞	:	infinity/freestream
ac	:	aircraft
af	:	airfoil
av	:	available
bat	:	battery
$cycle$	:	mission cycle period used for analysis
d	:	2D drag
day	:	day

def	:	deficit
D	:	3D drag
eff	:	effective
f	:	(skin) friction
$fuse$	:	fuselage
HT/VT	:	horizontal tail / vertical tail
i	:	induced
$interp$	:	interpolated
irr	:	irradiation
kin	:	kinetic
l	:	2D lift
lam	:	laminar (flow)
$load$	:	loading
$lower$	:	lower surface
lvl	:	level flight
L	:	3D lift
LE	:	leading edge
m	:	mean
max	:	maximum
min	:	minimum
mat	:	material
$night$	:	night
nl	:	neutral line
p	:	pressure
$panel$	:	solar panel
pl	:	payload
pot	:	potential
$prop$	:	propulsion
rel	:	relative
req	:	required
rib	:	structural element located in wing
$ribs$	:	structural elements located in wing
sf	:	surface
$skin$	:	outer skin of volumetric structure
$solar$	:	solar energy
$spar$	:	wing spar
$sparcirc$	:	wing spar circumference
$storage$	:	storage space, located mainly or only in aircraft wing
sys	:	aircraft systems
t	:	time
$tail$	:	aircraft tail
$turb$	:	turbulent
T	:	thrust
$upper$	:	upper surface
$wind$	:	values, parameters and components referred to the wind

$wing$	:	values, parameters and components referred to the aircraft wing
x	:	x-axis
y	:	y-axis
z	:	z-axis

Abbreviations and Acronyms

$CPACS$	:	Common Parametric Aircraft Configuration Schema
CSV	:	comma-separated values
DOF	:	degree of freedom
DLR	:	German Aerospace Center
$HALE$	:	high-altitude long-endurance
$HTML$	:	hypertext markup language
$ICAO$	:	International Civil Aviation Organization
LLT	:	lifting line theory
$MTOW$	:	maximum take off weight
UAV	:	unmanned aerial vehicle
UML	:	unified modelling language
VLM	:	vortex lattice method
XML	:	extensible markup language

Contents

Chapter 1

Introduction

Today, satellites or expensive aircraft operations are used in many applications. Telecommunication, earth observation, environmental research, surveillance and other tasks are often performed by a complex infrastructure based on satellites. These satellites require substantial investments for production, placement into orbit and constant operation. For tasks of a limited duration, such as environmental research tasks in polar regions, the use of manned aircraft can be an interesting but also expensive alternative to satellites.
High-altitude long-endurance (HALE) platforms are a specialised type of aircraft designed to fly in the stratosphere at altitudes above 15,000m for hours, days or months. The flight altitude of these platforms reduces their distance from the ground, especially when compared to satellites. HALE platforms' distance from the ground is considerably lower than for satellites, permitting the use of lighter, simpler and even cheaper technology (see [1, 2, 3]). While flying closer to the ground than a satellite, they are still placed above commercial traffic, as well as above most weather-related influences. Other than these advantages HALE platforms hold over satellites, they can also be used for tasks where they are not just a substitute.
For example, they can be deployed temporarily and on short notice to perform ground support tasks in conflict areas or environmental research tasks. In contrast to satellites in lower orbits passing rapidly over a specific area, HALE aircraft platforms can fly constantly over a specific area. Based on these factors, it can be stated that HALE aircraft platforms hold great potential for specific applications.

HALE aircraft are expected to have limited power available for propulsion. Therefore, the aircraft's mass is a critical factor and must be minimised. Eliminating the need for a human pilot and the corresponding aircraft systems reduces the mass of non-load-bearing parts of the aircraft. This reduction in mass is also favourable, as HALE flights can be exhausting or even dangerous for human pilots. Such unmanned aerial vehicles (UAVs) can lead to lower costs and smaller aircraft structures, as well as fewer limitations due to human factors, ultimately resulting in new potential mission scenarios (see [2]).

At high altitudes, propulsion systems and the aerodynamic generation of lift are not very efficient due to atmospheric conditions. A combustion engine is even more problematic compared to an electric engine due to the air mass required for a working combustion process. Even though chemical energy storage systems (such as the fuel required for combustion engines) have a much higher specific energy density $\omega \left[\frac{Wh}{kg}\right]$, rechargeable electrochemical systems, such as batteries, are favourable in this context. Solar energy is available at flight altitude and does not require expensive refuelling by other aircraft, which is, again, more cost-effective and favourable for the implementation of a constant mission. The combination of critical aerodynamic performance at high altitudes and the low energy density of batteries leads to an aircraft design which must be extremely lightweight and energy efficient to fulfil its intended mission. Furthermore, the energy harvested during daylight must sufficiently power the propulsion system and enable the aircraft to store sufficient energy for night-time. With today's technology, the first concepts of HALE aircraft remain under development. These aircraft are at the cutting edge of what is technically possible, and feasible design parameters for such aircraft configurations are still limited.

Industry and research facilities have been working on high-altitude platforms using different approaches. Airbus has been researching the Zephyr concept (depicted in Figure 1.1a), which holds different records, including endurance flight with a duration of more than 25 days (see [4]). This aircraft uses a lightweight airframe combined with solar panels integrated into the structure of its outer surface, resulting in a low-weight platform. Proposed by Keidel in [2], the SOLITAIR concept from Figure 1.1b is a different configuration for a similar use case. This concept makes use of adjustable solar panels mounted on top of the fuselage. These solar panels are pivot-mounted and enable the turning of the panels towards incoming sunlight, resulting in a higher irradiation harvest efficiency. Keidel's research shows that adjustable solar panels might serve the intended purpose despite their weight and drag penalty.

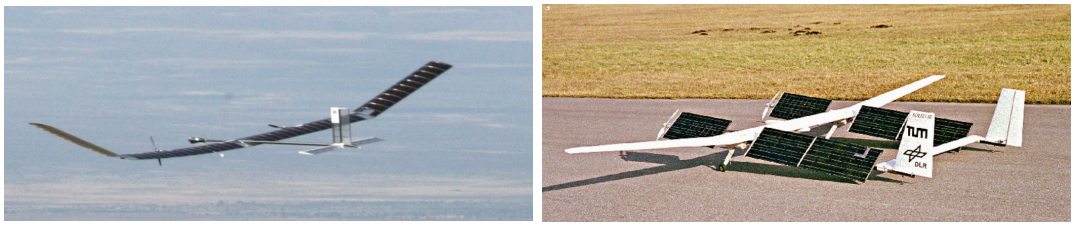

(a) Airbus Zephyr prototype from [5] (b) SOLITAIR demonstrator by Keidel [2]

Figure 1.1: Industrial HALE concept by Airbus and an alternative concept for solar cell integration by Keidel.

Research by [1, 2, 6, 7, 8] has focused on solar HALE aircraft and reviewed

different aspects of these platforms. A high-AR glider configuration which uses electrical power to harness solar energy has been suggested as the best approach by [1, 2, 6, 7]. An electrical solar aircraft is required to be equipped with a specific type of batteries and solar cells, in order to deliver feasible results. Further information about other approaches, solar cells and batteries are summarised in the literature study [9], based on [1, 2, 10, 11]. All reviewers picked up exemplary configurations and situations, while research by Liersch and Schopferer [8] focused on a more general approach. In their study, aerodynamic and structural performance was analysed for differing trajectories and mission scenarios around the world, instead of selecting a specific mission. This was realised using an analytic approach and an automated 3D trajectory optimisation process. The results revealed that the number of batteries required is a key parameter for solar HALE aircraft. The battery capacity required is highly dependent on mission profile, as well as the solar and atmospheric conditions at the latitudinal position. A strong contingency of the feasibility of the HALE aircraft platform on its main design parameters – low-energy flight capabilities and power management in combination with the appropriate battery size – emphasises the need for a specialised analysis procedure. Until now, most research has either analysed an exemplary aircraft configuration and mission scenario or combined an analytical approach with the use of a CPU-intensive tool for trajectory analysis. Therefore, earlier approaches missed a dynamic connection between the different required disciplines by focusing only on specific configurations or sub-problems.

As HALE platforms become more important in future research projects and commercial applications, an efficient method for evaluating such platforms will be required. Having an estimate of aircraft performance and required battery capacity can help to assess the feasibility of a configuration or to find boundary parameters for a specific aircraft design. A tool which includes solar HALE aircraft analysis capabilities can therefore be utilised in research or development projects on this topic. While such a tool delivers performance estimates for aircraft design development, the knowledge acquired through this thesis can be used for future analysis and optimisation processes for solar HALE aircraft designs.

Based on the potential use of such a tool, the results of [8] emphasise that a simple analysis within an iterative design and an analysis process could be used in a software-based design and assessment system for solar HALE aircraft. This system should evaluate the solar and atmospheric conditions and include separate disciplinary analysis procedures for aircraft performance, based on the specific properties of solar HALE platforms.
The intention of this thesis is therefore to develop a design and analysis tool for solar-powered HALE aircraft to estimate aircraft performance during the predesign stage. How can a broad range of aircraft configurations and requirements be incorporated into a tool, while requiring a minimal set of known parameters?

To answer respective questions, this thesis identifies an approach to incorporating basic theory into a software assessment tool, specific to solar HALE aircraft. The preliminary knowledge required is based on statistics for solar and glider aircraft, while most aspects are based on physical estimates for aerodynamics as well as aircraft structure. The implementation of these understandings into a tool, while keeping it modular as well as integrable into other integration environments, is the primary focus of this work. The tool is based on a multi-level architecture. The core level utilises knowledge about aircraft systems and aerodynamics to analyse a single aircraft and size its battery according to the defined mission. This knowledge about aircraft systems and aerodynamics is then distributed into different sub-systems working independently from each other. In contrast, outer level modules utilise the core level modules to complete comparison and optimisation tasks. The most important analysis procedure is based on the mission profile of a solar HALE aircraft. While other researchers have analysed a three-dimensional trajectory and neglected the dynamic relations between aircraft parameters and the battery required, this tool is intended to focus on a simplified mission and battery sizing. This requires minimal user input through a generalisation of aircraft parameters and the use of estimation techniques. The establishment of the tool enables the realisation of performance estimates for a specific mission, without having any knowledge about the required design. The purpose of the intended tool, which is called LEVEL0, is to conduct performance analysis. A simplified, level-based tool working on the a low-level design approach.

This thesis is structured based on the requirements needed to successfully complete the aforementioned task, guiding the reader from an initial concept to the final implementation and results. First, some characteristics of solar HALE aircraft, upon which the later implementation is based, are discussed. To define functional goals for this thesis, requirements and boundary conditions are introduced, followed by a basic concept, which shows a first sketch of the intended implementation. To understand the required theories for implementation, the relevant theoretical disciplines are then introduced and described. Disciplinary implementation is discussed in the next chapter, revealing the methodology for the study, including the tool structure and workflow. For verification reasons, the subsequent chapter compares extracts of LEVEL0 to well-known results. This verification is then connected with examples from LEVEL0, showing use cases and calculated results for different tool components, followed by a conclusion to the thesis.

Chapter 2

Requirements and Concept for the Design Tool

Based on the idea of an “integrated multidisciplinary design process” by Liersch [8], different questions must be answered to establish a concept for a tool and then formulate appropriate requirements. The process should include a design approach to quickly analyse different aircraft configurations based on the solar-powered HALE aircraft concept. With regard to the specific design process, the following questions arise:

- What are the parameters and requirements for the HALE aircraft platform, and how can these requirements be incorporated into a design and assessment tool?
- To build a tool for this task, what is the minimum set of parameters needed to investigate such an aircraft configuration?
- A solar aircraft evaluation is based on its mission profile. How can such a profile be implemented while using a minimum set of parameters and minimal CPU time?
- After combining the requirements, disciplines and input data, what would the final concept look like?

These questions guide the process described in this report. The software tool developed in this process illustrates basic principles resulting from these questions. The tool to be developed is referred to as ”LEVEL0” from this point on.

2.1 Requirements and Parameters

To formulate a concept for a tool and guide the design process, requirements must be established. First, the general tool criteria are formulated using requirements and parameters for the disciplines required to conceptually model a

HALE aircraft.

General requirements

The intended tool is meant to provide help in the design process for easy and fast sizing and assessment of solar-powered HALE aircraft configurations, using a mission simulation and aircraft comparison. The assumption is that there is no known data about aircraft size and performance; therefore, the tool must deliver results based on a minimum input basis. Earlier projects, as in [8], used a CPU-intensive trajectory analysis and fully detailed aircraft models. As LEVEL0 must rapidly deliver an estimation, a comparison with these tools emphasises the need for simplified mission analysis, an analysis which includes the most relevant factors for solar HALE aircraft while compensating for CPU-intensive factors with low impact on overall aircraft performance.

Aircraft evaluation
The tool must be able to analyse single aircraft configurations and compare multiple aircraft to each other.

Batch processing
The tool should be able to include modern computers' ability to utilise different threads and processing methods. This might incorporate batch processing with distributed threads, based on available CPU cores.

Modularity
For future development and maintenance, the tool should be developed in a modular fashion. Therefore, the different disciplinary modules must be independent of each other.

Input and output
The user should provide the required input parameters. The final results must be displayed in some common format which can be read by the user. Text files, plots and automated report files would be offered as outputs from the final tool.

Analysis results
The process should provide the user with a range of analysis capabilities, assisting in conducting an interpretation of the results. This includes optional outputs of all values occurring during analysis. A simple output of, for example, a resulting aircraft size and mass would not be sufficient.

Minimal input variables
For a first estimate, most analysis parameters should be computed by the tool, requiring a minimal number of input values from the user. This can be arranged by using pre-programmed formulas or estimates for specific situations. For example, a user could provide a mission location, a mission date and an aircraft

configuration boundary based on simplified size boundaries and then leave the rest to the tool.

Input format
User input defines the mission and the basic geometric parameters. Database input, such as airfoil data, consists of different parts needed for further evaluation or aerodynamic analysis of the aircraft. The input files must be readable and editable by the user through a specified XML-based data format. which is further described in Section 4.1.1.

Error handling
Errors must be handled and reported using a function to log events.

Reporting
Final results should be organised in an automated report. This report can be given in text form or using plots and HTML files for easy readability.

LEVEL0 must cover different disciplines such as aerodynamics, flight mechanics and structural analysis. The requirements for the specified tool and its associated disciplines are now briefly explained, offering the first conceptual ideas of what they shall fulfil and what the tool requires.

Aircraft Geometry
With as little input data from the user, the tool must gather further geometric data, using statistical and mathematical methods to complete the aircraft data required for analysis.

- Requirements:
  - Fuselage length and diameter must be estimated based on wing parameters.
  - The position and size of the wings and the tail must be estimated.
  - Moment equilibrium, affecting the force and mass relation between different different components, may be neglected.
  - Based on estimation, the position of the centre of gravity (COG) may be neglected.
- Parameters for LEVEL0:
  - Wing span and area as a basis for aircraft sizing
  - Solar cell integration type
  - Statistical data for fuselage and tail sizing

Mission and performance

- Requirements:
  - Aerodynamic coefficients for atmospheric conditions must be computed.
  - Solar irradiation must be computed relative to time, altitude and the global position of the aircraft.
  - The tool must include an altitude mission profile to model different power criteria for day and night flights.
  - Performance is based on force equilibrium during mission flight.
  - The propulsion system (including solar cells and batteries) may be modelled by assuming efficiency factors.
  - Precise simulation of irradiation income based on location, time and altitude
  - The analysis shall be based on time steps to factor in variable solar irradiation.
- Parameters for LEVEL0:
  - Mission start and end time
  - Global position (longitudinal and latitudinal)
  - Mission altitude range
  - Wind speed profile
  - Efficiencies of the solar panels, batteries and propulsion system
  - Payload power consumption profile
  - Option to choose for powered descent
  - Option to choose for limited climbing flight capability
  - Temperature deviation from the standard atmosphere

Aerodynamics

- Requirements:
  - It should be possible to import arbitrary aeorfoils without interaction.
  - Small Reynolds numbers ($Re <= 50,0000$) should be analysable.
  - 2D-airfoil analysis and 3D-wing analysis must be possible.
  - Elliptical lift distribution should be considered.
  - Lift and drag forces of the tail may be estimated using empirical formulas.
  - Fuselage drag may be estimated using surface drag.

- Parameters for LEVEL0:
  - 2D-airfoil name required for use of the airfoil parameters saved in database.
  - Minimum and maximum aircraft velocity boundaries.
  - Efficiency factor to quantify lift-induced downwash effects.

Structures
To compute aerodynamic forces, an aircraft's mass is required. The required values for mass may either be calculated based on statistics or through physical analysis of the components.

- Requirements:
  - Wing mass and tail mass can be estimated based on the same theoretical basis and the same module.
  - Wing mass is scaled using occurring aerodynamic forces.
  - Fuselage mass estimation may be based on forces on tail and wing.
  - Aircraft system mass may be estimated as a fraction of the total aircraft mass.
- Parameters for LEVEL0:
  - Material constants for structural components

2.2 Concept

Based on the specified requirements, this thesis aims to develop a tool that can conduct a solar HALE aircraft assessment process. An initial sketch of this process is shown in Figure 2.1.

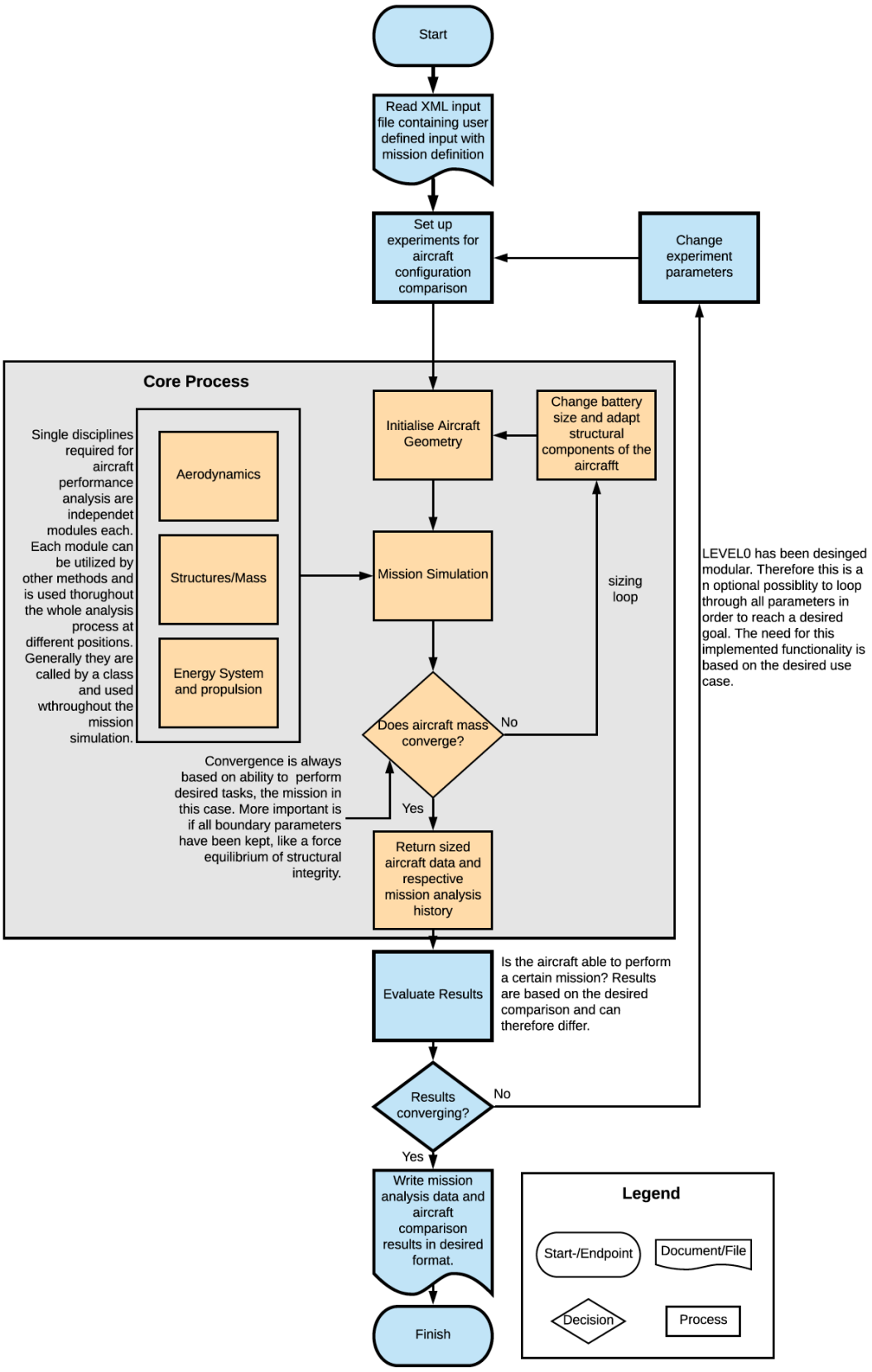

Figure 2.1: Initial concept of HALE design process.

The tool may consist of different process levels, inheriting different parts of the solar HALE aircraft assessment. The core process is intended to evaluate a single aircraft configuration. It initialises the aircraft geometry, performs a mission simulation and evaluates the mission analysis results. The results include the aircraft's performance, mass, battery data and mission history. The aerodynamic, performance and mass parameters required for these steps are provided by the implemented modules, each representing a single discipline. Before a mission has been analysed, it is not possible to determine how much energy can be harvested by the solar panels or how much energy is required for a flight. This introduces an iterative approach to determining battery and structural sizing for every single aircraft configuration to be analysed based on a mission analysis. While the iterative process is meant to size the battery for the aircraft, all structural components of the aircraft should also be re-evaluated. The core process should be a stand-alone process, but should also be usable as a sub-process.

To evaluate different aircraft configurations, the core process is embedded within an outer level process, which uses the input files given to set up different experiments and re-direct the required aircraft configurations to the core process for evaluation. It should be possible to evaluate the results of the core process and reuse them for further analysis steps. Due to the expected quantity of calculations, a parallelisation of analysis processes should be possible.

To realise and explain this concept, the different disciplines involved are explained in Chapter 3, followed by explanations of the resulting system in Chapter 4 and of exemplary results in Chapter 5. The different sections have been reduced to the most important facts necessary to understanding the realisation and operation of LEVEL0.

Chapter 3

Disciplines introduced in LEVEL0

The requirements formulated in Section 2.1 and general aircraft requirements must be represented in LEVEL0 by the included disciplines. For an autonomous aircraft, relying solely on solar energy and depending heavily on the individual mission, aerodynamic and mass considerations must be evaluated for all possible cases. To account for all these factors in a single tool, the required disciplines are briefly explained in this chapter. An explanation of general aircraft topology is followed by descriptions of mission analysis, aerodynamics and structural analysis.

3.1 Aircraft Layout

The layout for a solar HALE aircraft follows different requirements, which are determined by a particular application. These requirements can be based on different design parameters concerning speed, operation altitude, distance to cover within a limited timeframe, a defined payload mass, the UAV being stowed within a limited volume or the required launch method, as stated by [1]. Approaches to the design of an HALE aircraft, such as those of [1], Keidel[2] or Liersch[8], are based on a specific mission profile, payload and aircraft size. In particular, the mission parameters are fixed without closer analysis of mission progress or possible alternatives related to required battery capacity. A goal of LEVEL0 is to use a generalised approach, including aircraft performance estimates. By using aircraft design and mission analysis, which are applicable for mission and design parameters, a comparison of a broad range of aircraft and mission parameters is possible.

In accordance with Keidel [2] and Noth [1], a HALE aircraft fulfils different design characteristics in order to satisfy the considered mission scenarios.

- High aspect ratio wing: High aspect ratio reduces the induced drag, in-

creasing the lift-to-drag ratio, which is beneficial for aircraft performance

- Low wing loading: The lower the aircraft mass, the lower the required aerodynamic and propulsive forces. This also reduces the total structural load.
- Uniformly distributed mass: Distributing mass uniformly over the whole area reduces local structural load. This implies the distribution of payload over wing span.
- No gear or small landing gear: As the aircraft is supposed to fly quasi-permanently at a high altitude, the landing gear is of ancillary importance.
- Carbon-fibre construction: This reduces the total aircraft mass while making it possible to shape the wing, fuselage and tail in an optimised way. Simultaneously, this keeps aircraft structural integrity at least equivalent to other materials such as aluminium-built structures.
- Optional adjusting solar cells: Keidel suggested the use of irradiation-oriented, pivot-mounted solar cells to optimise irradiation harvest during flight.

Aircraft which have similar properties to the abovementioned include glider aircraft. These aircraft use aspect ratios between $30 \leq AR \leq 60$ while having a low structural mass. A glider-like configuration for a high-altitude aircraft has also been proposed by different authors, such as [1, 2, 6, 8], and can be used to represent a close to optimal HALE aircraft configuration.
The abovementioned aircraft configuration can be used as a starting point for LEVEL0 to adequately scale the residual components. Typical properties such as wingspan, fuselage or tail size can be deduced from existing aircraft of the mentioned type. General wing parameters, such as span and aspect ratio, can be used to scale remaining aircraft components. These values can then be compared with a specific database containing parameters of comparable aircraft to find parameters close to the base configuration for performance analysis. This method enables the tool to deduce an estimation of the most general geometric parameters from existing aircraft based on customisable data. The length and diameter of the fuselage can be estimated using the database containing comparable aircraft. Using tail volume coefficients, as described in [12], the actual sizes of the tail surfaces can be estimated based on the distances between wing and tail. The aircraft geometry assumption concept is displayed in Figure 3.1.

The aircraft is initially parametrised using a simplified geometry concept used as initiation point. This simplified geometry is based on wing size input parameters and is subsequently further estimated through statistical data and formulas. The inputs are part of the implementation of LEVEL0, as discussed in Section 4.1. The wing is assumed to be shaped such that a quasi-elliptical lift distribution is

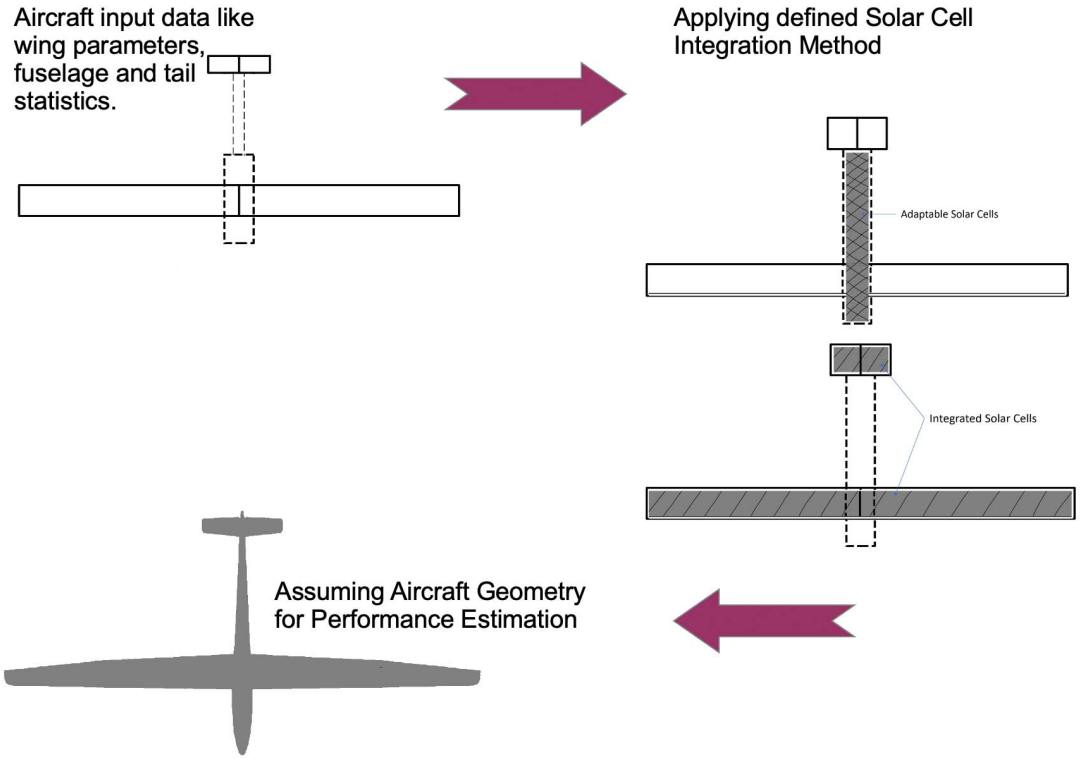

Figure 3.1: Aircraft geometry input, solar cell integration assumption and final geometric estimation in LEVEL0.

reached. This aligns with that of most glider aircraft and super elliptical wings, thereby allowing for its assumption in conducting mass estimation.
In line with [1, 2, 13], solar cells can be integrated in different ways, among which integration into the outer layers of the sandwich construction seems the most promising when attempting to reach a low airframe mass. An alternative concept by [2] suggests the integration of adjustable solar cell systems on the aircraft. Based on a pivot-mounted mechanical mechanism, this concept turns the solar cells towards irradiation for a maximised incidence angle, resulting in higher solar cell efficiency as used for the demonstrator in Figure 1.1b. Compared with the typical approach, the total cell surface area is smaller when the cells are integrated into the fuselage. This method increases drag and aircraft mass. Examples of solar cell implementation for both concepts can be found in Figure 1.1. However, the aircraft assumed in LEVEL0 does not have to match these examples.
Using these simplified geometric input data and solar cell system assumptions, the following performance analysis and mass estimate is conducted, assuming a glider- like aircraft design estimation.

3.2 Mission Analysis

In accordance with Schopferer in [8] the irradiation, altitude profile and wind speeds are crucial to the intended design of a solar aircraft, therefore they present the basics of mission performance analysis.

For a complete optimisation and analysis of wind speeds and solar irradiation in flight, the trajectories must be optimised and analysed step by step, as Schopferer did in [8]. The trajectories examined by Schopferer have been appended in Section A.2 and are based on maximum harvested energy while using a minimum energy approach. This kind of analysis includes aircraft flight path angles as well as trajectory optimisation, which requires a substantial amount of CPU time. Trajectory optimisation includes a three-dimensional model of the aircraft and trajectory path model. While aircraft movement in a three-dimensional space has six degrees of freedom (DOFs), this is reduced to three DOFs in a two-dimensional environment, and decreases further with less dimensions. Every DOF also influences other parameters, such as solar irradiation angles and panel shading, not to mention aircraft aerodynamics. In particular the irradiation analysis is CPU intensive. Reducing the number of DOF, or possible aircraft flight path angles, also reduces the number of flight conditions in which the required parameters must be computed, thereby reducing CPU time. A comparison between a straight flight assumption and trajectory flight, as appended in A.1, has shown a difference of $<= 4\%$ in resulting power. Therefore, straight flight assumption without lateral movement has been chosen for this analysis process. Due to the minimal difference assumed, an altitude and time-based estimation should return a similar aircraft performance estimation as three-dimensional trajectory analysis. The chosen analysis closes a gap between the 3D mission analysis and a simple analytic approach, while keeping the possibility to include the correlations between irradiation, aerodynamics, structural mechanics and flight performance.

At sunrise or sunset, the irradiation harvest can have an influence on aircraft performance. Either the batteries may already be loaded while the incoming irradiation power is not yet sufficient for climbing flight or the climbing or descending flight can be adapted to the incoming irradiation. This can either be done by adapting the rate of ascent or descent, as it is also possible to consider a powered descent to support gliding flight. Therefore, a time-dependent mission analysis with the following assumptions has been chosen:

- Steady flight for level, climbing and descending flight;
- Battery parameters and performance independent of temperature;
- Constant mass during whole flight;
- Propulsive force parallel with the aircraft's body axis;

- Propulsion capable of using complete harvested energy, considering propulsive efficiency parameters and boundary conditions;
- Shut down propulsion does not create additional drag due to mechanisms such as folding propellers and
- Solar energy distribution changing due to reduced DOFs approached by using an efficiency constant based on irradiation analysis.

Solar energy is computed using a customised model based on the solar model by Brizon [14]. The customised model includes parallel computation, database storage capabilities, interpolation techniques and an implementation of an extended application programming interface. The customisations have been made in favour of faster data access for the software tool and less required CPU time. The approach of irradiation analysis itself has been kept unchanged and is thus not part of this thesis. It is assumed that the aircraft uses all harvested solar energy, which is dependent on incoming irradiation and solar panel efficiency. The harvested energy is primarily used for propulsion, while excess energy is used to recharge the batteries. To store additional energy, the mission profile allows climbing through the defined day or night altitude required, up to a maximum set altitude. A sketch and example of this is included in the following subsection.

A detailed propulsion model has not been integrated, as there are too many electric propulsion systems available and the possibilities to integrate propulsion are manifold. However, propulsion has been considered by providing efficiency and mass factors. The range of the propulsive force required for the intended aircraft is subsequently defined by the range of required power for level and climbing flights. The maximum possible propulsive force can be limited by setting a maximum climb angle, which is discussed in Section 4.1.

To optimise energy efficiency, the core of LEVEL0 aims to find the minimum battery mass necessary, assuming a fixed energy density, to fulfil a user-defined mission within the given parameters. A mission profile includes level, climbing and descending flight, ordered in a specific pattern, and is discussed in this chapter. To compute the required power in the different flight modes, the analysis process makes use of the force equilibrium fixed to the aircraft body frame with the assumption of a steady flight.

General equations for motion are based on the forces exerted on the aircraft based on aircraft weight W force, drag D force, thrust T force and lift L force, which can also be found in Figure D.3. Based on these forces, basic equations of motion can be set up using $\sum F_{x,y,z} = 0$. Using small angle approximation, steady flight, thrust vector $\alpha_T = 0$ and $Dv = P_{req}$, $Tv = P_{av}$, $V \sin\gamma \hat{=}$rate of climb (RC), can be merged into Equation (3.1).

$$\begin{cases} \sum F_x : P_{av} - P_{req} - WRC = 0 \\ \sum F_y = 0 \\ \sum F_z : L - W\cos\gamma = 0 \text{ with } \cos\gamma = 1 \end{cases} \tag{3.1}$$

The conservation of energy and thus the use of maximum available solar irradiation energy for a fast climb and the use of solar irradiation during descent to keep potential energy as long as possible are essential. This results in a climb and descend performance computed based on incoming solar irradiation rather than on propulsion performance or optimised en route velocity.

The power available P_{av}, or harvested power, for the assumed solar aircraft is related to the power available by solar irradiation P_{irr}, which has been harvested by solar panels with an efficiency η_{panel}, as can be seen in Equation (3.2).

$$P_{av,solar} = \eta_{panel} P_{irr} \tag{3.2}$$

The power required by the aircraft (P_{req}) is equipped with an efficiency constant η_{ac} in Equation (3.3) in order to model propulsive and electric effects.

$$P_{req} = \frac{1}{\eta_{ac}} Dv \tag{3.3}$$

The aircraft requires power for flight and harvests power through the solar panels. The resulting power deficit P_{def} is defined through Equation (3.4).

$$P_{def} = P_{req} - P_{av} \tag{3.4}$$

The energy stored in the battery is based on Equation (3.5). The maximum capacity is based on the assumed battery mass and energy density, while the charging process is based on overshoot power harvested. All of this is assumed to be computed for the

$$E_{bat} = \sum_{t=0}^{t_{cycle}} P_{load}\Delta_t \text{ with } P_{load} = -P_{def} \text{ if } P_{def} \leq 0 \tag{3.5}$$

Evaluating the horizontal force equilibrium in Equation (3.1) returns the following formulas in Equation (3.6), in line with what was determined in [15]. The rate of climb RC is the vertical velocity of the aircraft based on the power equilibrium.

$$RC = \frac{P_{av} - P_{req}}{W} \tag{3.6}$$

If there is no irradiation available, the aircraft uses pure gliding flight or battery energy. Propulsive efficiency changes based on altitude. Therefore, the aircraft is assumed to hold the lowest possible altitude defined while on the mode for battery power only. If there is more energy available than required for the lowest

possible altitude flight, the aircraft uses as much incoming solar irradiation as possible and therefore less battery power.

As discussed in [16], the sink rate w_s of a glider aircraft (the estimated aircraft with propulsion switched off) can be computed using speed and horizontal flight path angle, as can be seen in Equation (3.7).

$$w_s = v \sin\left(\gamma\right) \text{ with } \tan\gamma = \frac{W}{L} \tag{3.7}$$

The mission duration for a solar HALE aircraft is meant to be defined as a long duration flight over weeks, months or even years. The most critical part for aircraft performance is its high-altitude flight. Holding at an altitude or even climbing at high altitudes requires more energy due to the low density of the surrounding gases, making this a critical mission phase. Assuming a climb with completely filled batteries and maximum incoming irradiation, as well as a solar HALE aircraft being able to fly in high altitudes, climbing always concludes at mission altitude. The time for a climb is based on the given inputs and maximum climb limits, but according to the assumptions made in this study, a climb is not critical. This is based on the fact, that in lower altitudes, the power required is lower, while irradiation is assumed to be similar. Furthermore, while it is possible to analyse the full mission cycle of months or years, the mission cycle in LEVEL0 inherits a cycle of exemplary days. Otherwise, the CPU time would increase to an extent that would render an expedient analysis impossible. Therefore, the climb and the descent are not part of the mission analysis cycle.

Altitudes for day and night flights, based on irradiation level, are the determining values for aircraft status as well as for a mission success or failure. The aircraft tries to reach the defined altitudes using solar energy during the day, while storing overshoot energy. If the target altitudes cannot be reached, the mission has failed. If the used battery capacity is insufficient for flying through the night, it is increased in the following iteration.
A typical mission extract is shown as a sketch in Figure 3.2a. The aircraft runs through different phases, divided into segments based on irradiation phases and battery status. An example of how these phases are given as a result is shown in Figure 3.2.

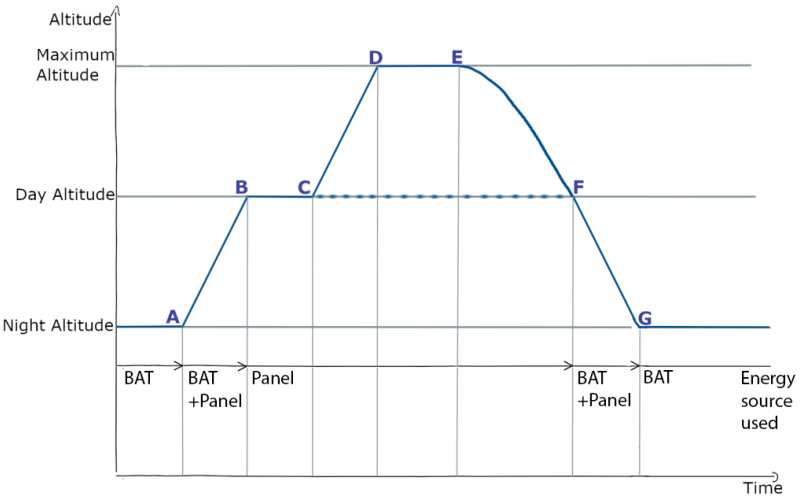

(a) Theoretical mission decision points.

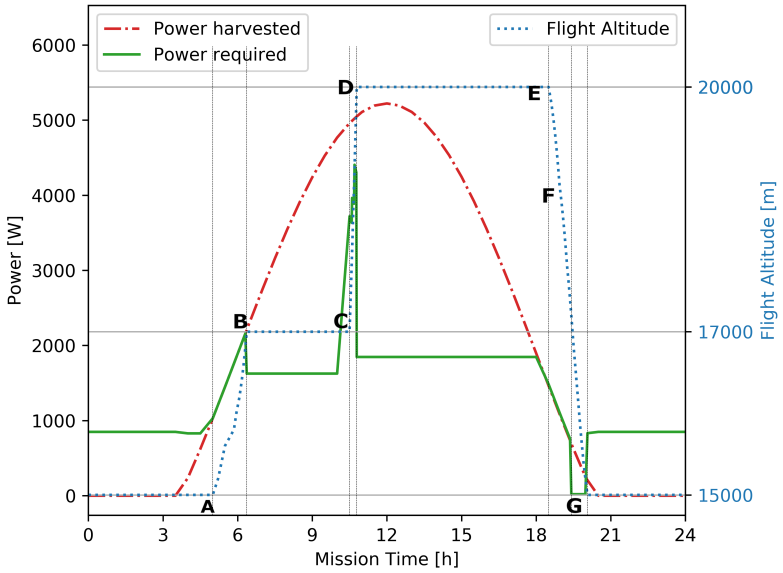

(b) LEVEL0 output - Power harvested related to power required.

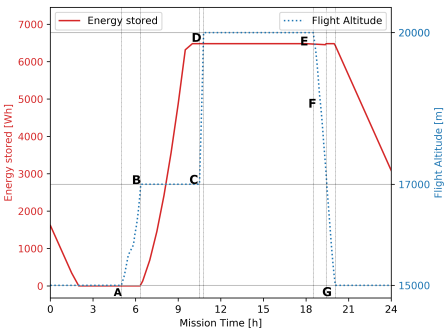

(c) LEVEL0 output - Energy stored in batteries.

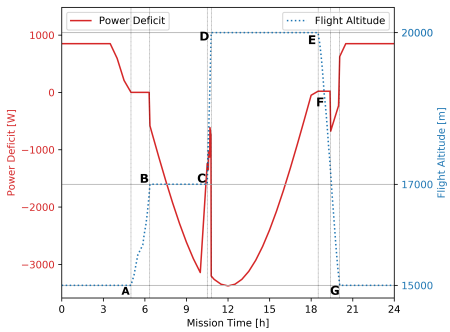

(d) LEVEL0 output - Power deficit.

Figure 3.2: LEVEL0 24 h example based on the theoretical mission decision points in Figure 3.2a.

The phases a solar powered HALE aircraft runs through are defined by changes in the power ratio of aircraft and irradiation and are explained below. A shortened overview of these phases is appended in Table C.1.

Phase A to B
Point **A** is marked at the first irradiation strong enough for the aircraft to climb. In terms of irradiation power harvested, the "daylight" phase of a mission starts with incoming irradiation. At this point the aircraft is supposed to climb up to "day altitude". Shortly before Point **A** , the power from irradiation P_{irr}, and the resulting harvested power P_{av} are insufficient to power the aircraft for level or even climbing flight, resulting in the positive, but decreasing power deficit seen in Figure 3.2d. As long as the power required is greater than the power available $P_{req} \geq P_{av}$, the aircraft is relying on battery power and holding its altitude.

At some Point **A**, the amount of power available becomes high enough to support the aircraft in level flight. At this point, the power drained from the battery is assumed to approach zero, as the aircraft should solely use harvested solar power P_{av}. The power required at this point is covered by the incoming irradiation; thus, $P_{av} \geq P_{req}$ in Figure 3.2b and $P_{def} \leq 0$ in Figure 3.2d. The aircraft's rate of climb is adapted according to the available power, as in Figure 3.2b. With increasing solar irradiation power, the rate of climb potentially reaches a defined maximum. Therefore, the power available exceeds the power required $P_{av} > P_{req}$. As such, the power deficit decreases, and the battery can be charged; $E_{bat} \geq 0$ in Figure 3.2c due to a negative deficit.

Phase B to C
The aircraft reaches the "day altitude" and stops climbing. Therefore, the aircraft holds its altitude and requires power for level flight at the current altitude. At this point, $P_{av} \geq P_{req}$ for level flight. Excess power is used to charge batteries; thus, $P_{def} \leq 0$ with decreasing P_{def}. This implies that the battery is charged with increasing $E_{bat} \geq 0$ in Figure 3.2c. It is important to notice that the power required at the "day altitude" is higher than the power required at "night altitude" in Figure 3.2b. This is based on air density, requiring the aircraft to fly faster to produce the required amount of lift.

Phase C to D
If the aircraft batteries are fully charged, it is possible to use incoming solar irradiation to store potential energy. For the assumed solar aircraft, this would mean that the aircraft uses only solar irradiation power available to climb, while leaving the battery at 100% charged status. Therefore, the required energy P_{req} increases in Figure 3.2b for climbing flights. As the aircraft only uses incoming solar irradiation for climbing flights, the power deficit again increases, as can be seen in Figure 3.2d. The energy stored E_{bat} stays constant in Figure 3.2c.
The required power must be less than or equal to the power available to only use incoming solar irradiation energy. As in Phase A, the climbing phase can be limited using either a power limitation or a climb angle limitation from within

the process. If the power available is not sufficient to climb using solar power only, indicating that $P_{av} < P_{req}$ in climbing, the aircraft maintains its altitude. Therefore, this phase or aircraft action is optional and is based on the optimal case of a strong irradiation energy overshoot.

Phase C to F
If power available is not sufficient to climb while only using solar irradiation ($P_{av} < P_{req}$ in climbing), the aircraft holds its altitude, and a climb to gain potential energy is not performed. Therefore, the cycle directly moves on to **F**. This case is not included in this example.

Phase D to E
The maximum flight altitude is reached. This means that even if solar irradiation energy is still available, the aircraft is not allowed to climb further to gain potential energy. Still, the power available is greater than or equal to the power required, as seen in Figure 3.2b, which also means that the power deficit $P_{def} < 0$. Level flight is assumed, and the aircraft holds its altitude as long as possible based on solar irradiation energy available.

Phase E to F
At the current flight altitude, the solar irradiation power harvested becomes insufficient for holding level flight. Therefore, the aircraft has to descend to a lower altitude to keep $P_{req} \leq P_{av}$. This can be done using gliding flight or a propelled descent, while always keeping $P_{req} \leq P_{av}$ and $E_{bat} = 100\%$. The choice of descent is based on the boundary condition to store as much potential energy as possible. In this phase, the power required adapts to the power available, such that $P_{req} = P_{av}$ as depicted in Figure 3.2b. As the battery power is not used at this point, the energy stored does not vary, as can be seen in Figure 3.2c.

Phase F to G
As soon as a propelled descent would result in a higher rate of descent than a pure gliding flight, the propulsion is assumed to be switched off, and the propeller is retracted. This status holds until "night altitude" is reached. The battery and available solar irradiation are then used to power aircraft control systems and payload. Therefore, $P_{req} \leq P_{av}$ at this point. In the assumed optimal case, shown in Figure 3.2, the power available in Figure 3.2b is greater than the power required, and the power deficit in Figure 3.2d is thus negative ($P_{def} \leq 0$).

Phase G to A
The lowest allowed altitude, the "night altitude" is reached. The aircraft is now using the battery to power all aircraft systems. This status is preserved until solar irradiation is detected again and the cycle restarts. In this case, $P_{req} > P_{av}$ as is seen in Figure 3.2b, $P_{def} > 0$, as is seen in Figure 3.2d, and E_{bat} decreases, as can be seen in Figure 3.2c.

3.3 Aerodynamics

HALE aircraft are designed for high altitudes at low speeds, in contrast to commercial or sports aircraft. For a near optimal solution, using an elliptical lift distribution, an approach initially based on a trapezoidal wing planform, can be assumed. In accordance with lifting line theory, as detailed in [17, 18], elliptical lift distribution and high AR are typically preferred for glider aircraft. This also corresponds with research by [1, 2, 8, 19] who proposed high-AR glider-like configurations for solar HALE aircraft. Some of the information used for this thesis, including further details on 2D airfoils, 3D wings and elliptical lift distributions, can be found in Anderson [17].

Assuming an elliptical lift distribution, the underlying analysis procedure can be based on a 2D airfoil analysis used in conjunction with handbook formulas. The 2D airfoil is assumed to be distributed over the whole span. The aerodynamics of an infinite wing can then be computed using XFoil [20]. This tool has several advantages, making it a good choice for a first aerodynamic estimation.

- As it is the goal of LEVEL0 to be able to analyse different aircraft configurations for a high range of Reynolds numbers, XFoil delivers these capabilities by being proven reliable for low Reynolds numbers of $RE \leq 500,000$.
- To obtain an adequate drag estimate, a viscous drag analysis is possible.
- XFoil can be controlled using external batch scripts or even through direct communication from third-party tools such as LEVEL0.
- XFoil is extremely lightweight and does not require much CPU time.
- XFoil has proven itself over many years and delivers reliable results for many cases.

3.3.1 From 2D to 3D

Wing aerodynamics is one of the main components in LEVEL0 due to the impact of the aerodynamic surfaces on aircraft performance. Therefore, a simple lift coefficient assumption did not seem sufficiently accurate. A "2.5D analysis" has been chosen to obtain a reasonable estimate of real wing performance and structural capabilities. Acquired 2D results can be used to estimate the 3D finite wing coefficients based on pressure imbalances on a finite wing compared to those on an infinite wing. Anderson [17] has written a more detailed explanation.

Due to downwash of a finite wing, an airfoil section senses a smaller angle of attack α_{eff} then the geometric angle of attack α. Thus, $\alpha_{eff} = \alpha - \alpha_i$, as explained by Anderson [17]. This results in smaller angle of attack in theory,

expressed in terms of a reduced lift coefficient for 3D wing. The resulting lift coefficient for a 3D wing is computed using the lift curve slope a, which is obtained using Equation (3.8) from [17]. With a as the lift curve slope for a finite elliptic wing, a_0 is the according slope for an infinite wing, as depicted in Figure D.1. Values of τ_G depending on aspect ratio and wing taper were first calculated by Glauert in [21], while it can be assumed that $\tau_G = 0$ for elliptical lift distributions.

$$a = \frac{a_0}{1 + \left(\frac{a_0}{\pi AR}\right)\left(1 + \tau_G\right)} \tag{3.8}$$

Using the slope a from Equation (3.8), the lift coefficient for a 3D wing can be obtained by using Equation (3.9). At zero lift, there are no induced effects; as a result, $\alpha = \alpha_{eff}$, which results in the same α_0 at $c_l = C_L$ for both finite and infinite wings in accordance with [17]. A graphical representation is appended in Figure D.1. Therefore, to compute the C_L polar for the finite wing, Equation (3.9) must be initiated at $\alpha_i = \alpha_0$.

$$C_L = a\left(\alpha - \alpha_i\right) \tag{3.9}$$

Drag for an infinite wing consists of parasitic drag and lift-induced drag $C_{D,i}$, while the parasitic drag consists of pressure drag D_p and drag due to skin friction D_f as in Equation (3.10). Therefore, the total drag coefficient C_D for a finite airfoil can be computed using Equation (3.11), as was done in [12]. The induced drag occurs due to lift-induced effects and is therefore dependent on the wing's lift coefficient C_L, as is calculated in Equation (3.12). According to classical wing theory, the induced drag coefficient of a 3D wing with an elliptical lift distribution equals the square of the lift coefficient divided by the product of the aspect ratio AR and π as stated by [12]. Most wings actually do not have a perfect elliptical lift distribution, and such a distribution also does not account for separation drag. Therefore, the K factor $K = \frac{1}{\pi Ae}$ includes the "Oswald span efficiency factor" e, which is a correction factor representing a 3D wing's change in drag with lift. In line with [12], values for e normally fall between the range of $0.7 \leq e \leq 0.85$, while for an elliptical wing, it tends to come closer to $e = 1.0$, as such a wing represents the optimal distribution. Following these steps, the total drag coefficient for a 3D wing can be computed using Equation (3.13).

$$C_{D,0} = \frac{D_f + D_p}{1/2\rho v^2 S} \tag{3.10}$$

$$C_D = C_{D,0} + C_{D,i} \tag{3.11}$$

$$\Leftrightarrow C_D = c_d + C_L^2 K \tag{3.12}$$

$$\Leftrightarrow C_D = c_d + \frac{C_L^2}{\pi ARe} \tag{3.13}$$

The lift force is elliptically distributed since it results from the elliptical circulation distribution Γ, as appended in Figure D.2. With Γ_0 representing the circulation at wing span $y = 0$. This elliptical distribution is defined as in Equation (3.14) and is used to compute the lift per span distribution based on the circulation, such as in Equation (3.15), which was provided by [17].

$$\Gamma(y) = \Gamma_0 \sqrt{1 - (\frac{2y}{b})^2} \tag{3.14}$$

$$L'(y) = \rho v_\infty \Gamma(y) \tag{3.15}$$

Total lift force can be computed using the integral over the whole span, as seen in Equation (3.16).

$$L = \int_{-\frac{b}{2}}^{\frac{b}{2}} L'(y)\,\mathrm{d}y \tag{3.16}$$

$$\Leftrightarrow L = \frac{\pi}{4} \rho v_\infty \Gamma_0 b$$

$$\Leftrightarrow \Gamma_0 = \frac{4L}{\pi \rho v_\infty b} \tag{3.17}$$

As the total surface beneath an ellipse is $\frac{\pi}{4}$ times the area of the enclosing rectangle, the already known lift force computed using the XFoil can be related to the distribution at $y = 0$, as is seen in Equation (3.17). Using Γ_0, the lift per span $L'(y)$ can be computed using Equation (3.14) and Equation (3.15), as shown in Equation (3.18).

$$L'(y) = \rho v_\infty \Gamma_0 \sqrt{1 - (\frac{2y}{b})^2}$$

$$\Leftrightarrow L'(y) = \frac{4L}{\pi b} \sqrt{1 - (\frac{2y}{b})^2} \tag{3.18}$$

3.3.2 Other Components

The wing is not the only component which influences the aircraft's aerodynamics. The fuselage, tail and excrescences also have an influence on the aircraft's aerodynamics. For simplicity, the following assumptions have been made:

- There are no excrescences on the aircraft that have an influence on aerodynamics (e.g., engine nacelles).
- The fuselage and tail do not contribute to total aircraft lift or downforce.

- A laminar boundary layer is assumed. This includes zero velocity of the fluid on the aircraft's surface and an increasing velocity with greater distance.
- The propeller only creates thrust force.

Therefore, the tail and the fuselage only contribute to the aircraft's drag and mass. The tail and wings share the same theoretical basis. The fuselage drag may be estimated using a skin friction coefficient for laminar and turbulent flow using Equation (3.19) from [22]:

$$c_f = c_{f,lam} \times d_{lam} + c_{f,turb} \times \left(1 - d_{lam}\right) = \frac{1.328}{Re} \times d_{lam} + \frac{0.074}{Re^{\frac{1}{5}}} \times \left(1 - d_{lam}\right) \quad (3.19)$$

In accordance with the drag equation from [22], the total drag force of the fuselage can be computed using Equation (3.20) based on the dynamic drag and the fuselage surface area A_{fus}.

$$D_{fuse} = c_f \frac{1}{2} \rho v^2 A_{fuse} \quad (3.20)$$

The interference drag for the fuselage and the tail must also be considered. As discussed in [23], a flow disturbance at the wing-to-fuselage junction may lead to separation and vortex shedding in which the viscous layer is weakened. According to [22, 23], interference can be estimated using an efficiency factor. The fuselage interference for a monoplane leads to a span efficiency factor $e_v = 0.948$, indicating a negative influence of about 5%. For the tail, a similar negative influence can be assumed.

3.4 Structural Model

Total aircraft structural mass is required to estimate the required forces, which include lift, drag and propulsion force in flight. According to [1, 12], there are different approaches to mass estimation.

Noth [1] utilised mass estimation approaches from Stender [24], Rizzo [25], Guglieri and others. Noth investigated a more precise prediction model for high-flying aircraft, which can be compared to the solar HALE aircraft model assumed in this thesis. These reference models are based on a broad range of relevant aircraft types, including which are different prototypes, UAVs, HALE aircraft, manned glider aircraft and others.
Such approaches utilise data referring to the aircraft as a whole, instead of distinguishing between its individual components. As mentioned in 2.1, a modular approach is one of the requirements for LEVEL0. Therefore, an approach based

on statistics and structural mechanics has been chosen, distinguishing between the most important components of the aircraft. A similar approach was used in [8, 13].

The different aircraft components are modelled and analysed individually, using the required components. Component sizing is completed based on wing size, payload and aerodynamic forces. The total wing mass is assumed to consist of several components, including the main components for general wing structures used on most general aviation aircraft. It consists of the following components:

- 1: Surface sandwich construction, foil or metal sheet
- 2: Span-wise distributed ribs along the wing chord
- 3: Main wing spar

In line with research reported in [1, 2, 8, 13], the wing construction should also include the following components.

- Solar cells
- Surface sandwich construction (potentially including solar cells)
- Surface foil
- Span-wise distributed ribs along the wing chord
- Main wing spar (rectangular, box shaped)

The upper surface of the wing consists of solar cells and a surface sandwich construction underneath. Due to the low aircraft velocities assumed, the lower side of the wing can be covered using foil clamped onto the wing ribs. As with a simplified wing, the wing of a high-altitude aircraft is assumed to be based on a box-shaped main wing spar and span-wise distributed ribs along the wing chord. The number of ribs has been determined based on experiences from previous research projects (see [13]). Different options for surface and wing layout have also been discussed in literature studies [9].

The included tail surfaces and wing surfaces are structured based on the same theoretical basis. The difference in structural mass is mainly dependent on the forces working on the surfaces. As the goal is to estimate the mass of the different structures, both tail surfaces and the wing have been assumed using the same approach. The tail surfaces are expected to be a wing-like structure with a spar, ribs, potential solar panels and a skin foil.

The mass estimation method is able to differentiate between the different aircraft components, based on physics and earlier research used in [8, 13]. This enables the implementation of a more detailed system in the future and fulfils

the requirement of a modular approach. Earlier research in [1, 2, 8, 13] has also showed that the range of possible estimated results for aircraft mass of a HALE aircraft is excessively large for the narrow range of combinations of aircraft performance and payloads which are actually feasible. Thus, the informational value of the mentioned estimation methods and the chosen analytical method are expected to limit the final results, while the analytical approach used has the capability to be refined. Nevertheless, Noth's [1] analytical approach has been integrated into LEVEL0 to provide an initial estimate for the aircraft mass iteration algorithm.

3.4.1 Wing-Like Structures

Solar cells and wing skin mass can be approximated using the outer surface of the airfoil, integrating it over the wing span. In line with the approach in [13], the possibility of choosing different materials for the upper and lower wing surfaces must be considered. The airfoil skin can be described using the x and y axes for the airfoil chord line and thickness, respectively, using the airfoil leading edge as the origin. The resulting skin mass $m_{wing,skin}$ can be derived using Equation (3.21).

$$m_{wing,skin} = 2(m_{skin,upper} + m_{skin,lower}) \int_0^{b/2} (\sum_{i=0} (x_i^2 + z_i^2)^{0.5}) \, \mathrm{d}y \tag{3.21}$$

The ribs are distributed over the span, following an estimate. The number of ribs n_{ribs} over span, as well as the rib thickness B_{ribs} are estimated based on practical experiences from earlier demonstrators, resulting in the rib volume in Equation (3.22) and mass Equation (3.23).

$$V_{ribs} = \sum_{i=0}^{n_{wing,ribs}} B_{rib,i} A_{rib,i} \tag{3.22}$$

$$m_{ribs} = \rho_{wing,ribs} V_{ribs} \tag{3.23}$$

The central component in a wing is the spar, which is assumed to carry the main aerodynamic forces and represents the load-bearing connective component between wings and fuselage. Using aerodynamic forces and weight force due to components, the loads on the wing structure can be used to size the spar. To size the spar, it is important to distinguish between different cases. During flight, the aerodynamic forces and a weight force exert a moment on the wing spar, while during start or landing at low speeds, the aerodynamic force may be negligible. At this point, forces on the wing due to pure component weight

during ground contact are the determining forces. Despite the theory behind the analysis being the same, these two cases must be computed separately during analysis.
The lift per span distribution $L'(y)$ and the weight per span distribution $W'(y)$ exert forces in the z direction on the spar. From the basic force equilibrium in Equation (3.24), the reaction force F_z can be derived using the force equilibrium in z direction from Equation (3.25). Additionally, as there is no axial force present in this contemplation, the reaction force F_y in y direction is $F_y = 0$. The force equilibrium in Equation (3.24) to Equation (3.25) for the forces shown in Figure 3.3 determines the forces to be considered for wing spar sizing.

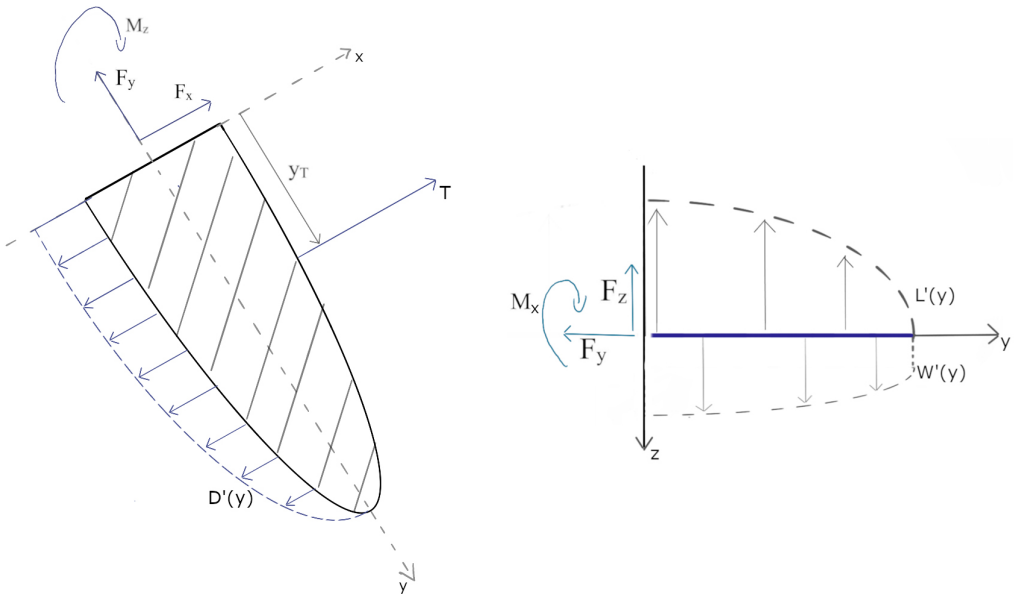

(a) X-y-plane. (b) Y-z-plane.

Figure 3.3: Schematic view of forces on half wing span

$$\sum \vec{F} = 0 \tag{3.24}$$

$$\Leftrightarrow \begin{aligned} F_x &= T - \int_0^{\frac{b}{2}} D'(y)\,\mathrm{d}y \\ F_y &= 0 \\ F_z &= -\int_0^{\frac{b}{2}} L'(y)\,\mathrm{d}y + \int_0^{\frac{b}{2}} W'(y)\,\mathrm{d}y \end{aligned} \tag{3.25}$$

From this point on, forces in the x direction are neglected, as they are assumed not to determine the spar size due to the wing shell's construction. The sketched forces in Figure 3.3a and Figure 3.3b work orthogonally to the span and thus exert a shear force on the spar. The wing spar shear force $F_z'(y)$ distributed over span can be computed using an integral of Equation (3.25). Using the definition

from [26], the bending moment can be found by integrating that shear force $F'_z(y)$ over the whole span. In accordance with [26], the bending moment can be used to compute the maximum direct stress at distance d_{nl} from the neutral line. The cross-section of the assumed spar referred to is shown in Figure 3.4b and has been chosen based on research by Juergenhake [13]. The referring forces and moments are shown in Figure 3.4a .

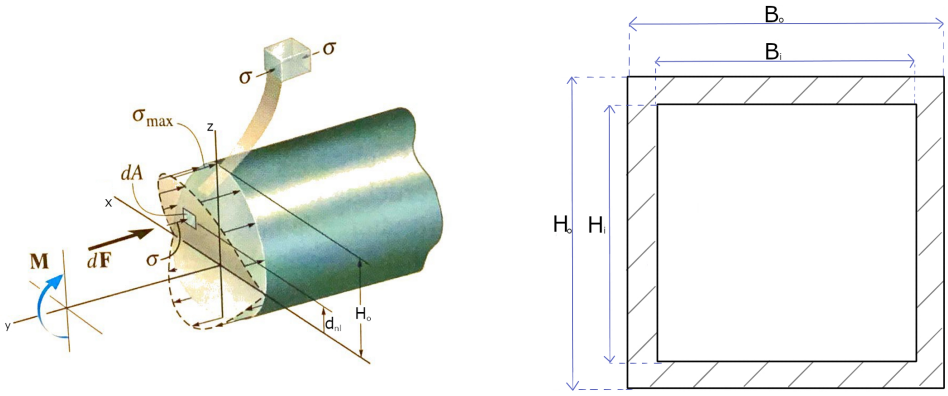

(a) Direct stress over a beam from [26]. (b) Schematic spar cross-section.

Figure 3.4: Schematic spar depiction

The neutral line for the cross-section in Figure 3.4b is assumed to be at $H_o/2$ of the symmetrical cross section. Therefore, the distance from the neutral line is $d_{nl} = H_o/2$. Using Equation (3.26), the maximum direct stress allowed must be compared to the maximum stress which can occur in the spar σ_{max}.

$$\sigma_{mat} - \frac{M'_x(y)H_o}{\frac{2}{12}(B_oH_o^3 - B_iH_i^3)} \geq 0 \tag{3.26}$$

Using the determined spar dimensions, the spar volume and mass can be computed using Equation (3.27) and Equation (3.28).

$$V_{spar} = 2\int_0^{b/2} (H_oB_o - H_iB_i)\,\mathrm{d}y \tag{3.27}$$

$$m_{spar} = \rho_{spar}V_{spar} \tag{3.28}$$

Since the mass of all components and the component volume are now known, the total storage volume $V_{storage}$ available within the wing can be determined using Equation (3.29).

$$V_{storage} = (2\int_0^{b/2} A_{af}\,\mathrm{d}y - V_{spar} - V_{ribs})const. \tag{3.29}$$

3.4.2 Fuselage

The assumed influence of the fuselage on the total aircraft weight of the aircraft is at about 10%, which is again addressed in 5.2. This assumption made for the fuselage has a marginal influence on the total aircraft weight for a HALE aircraft. For aerodynamic reasons, the fuselage is assumed to be similar to a glider aircraft fuselage. It is thicker at the front and becomes thinner towards the end. In reality, this fuselage form includes stringers as well as longerons. This construction can basically bear all loads and allows for a thinner outer frame for the fuselage. These structures cannot be described and analysed easily for aircraft of all sizes within a single algorithm; instead, they require a large number of boundaries and assessments for all aircraft. Therefore, such additional structures have not been incorporated into the wing mass analysis and are thus not part of the fuselage analysis. The fuselage is assumed to be modelled in the form as depicted in Figure 3.5, following the concept for circular beams in Figure 3.4a.

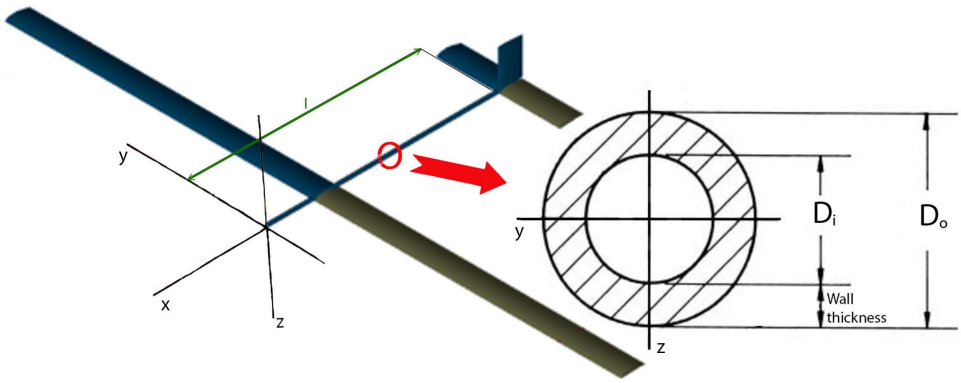

Figure 3.5: Fuselage diagram of aircraft concept, based on [8].

The bending moment calculated through Equation (3.30) is the determining parameter used for sizing. For the moment exerted on the fuselage, the system mass m_{sys} and the force exerted by the tail F_{tail} are involved. The system mass is distributed within the wing and the fuselage, while the total mass of the aircraft systems is is estimated to be exerted on the aircraft's centre of mass, located in the wing root. The tail force F_{tail} is exerted at distance l_{fuse}. Distance l_{fuse}, in this case, is estimated to be the distance between the wing and the tail, as this creates the critical moment.

$$M = gF_{tail}l_{fuse} \tag{3.30}$$

Using the given diameter and Equation (3.31), it is possible to compute the diameter of the inner fuselage based on possible stress σ.

$$
\begin{aligned}
\sigma &= \frac{M d_{nl}}{I} \\
\Leftrightarrow \sigma &= \frac{64 M d_{nl}}{\pi(D_o^4 - D_i^4)} \text{ With } D_o = 2R_o \text{ and } D_i = 2R_i \\
\Leftrightarrow \sigma &= \frac{32 M D_o}{\pi(D_o^4 - D_i^4)} \text{ With } D_o/2 = d_{nl} \\
\Leftrightarrow D_i &= \left(D_o^4 - \frac{32 M D_o}{\pi \sigma}\right)^{\frac{1}{4}}
\end{aligned} \tag{3.31}
$$

The fuselage mass can then be computed using Equation (3.32).

$$
m_{fuse} = l_{fuse} \frac{\pi}{4} (D_o^2 - D_i^2) \rho_{fuse} \tag{3.32}
$$

Chapter 4

Developed System "LEVEL0"

The development of this system involves the realisation of the concept (Section 2.2) and the integration of the various associated disciplines (Chapter 3). These disciplines require specific input parameters, which are briefly described below. The resulting tool using these inputs is described by an overview of its simplified structure.

4.1 Input and Output

The input and output files give an overview of what the tool includes within its analysis and also what the various parameters are used for. The inputs have been defined according to the requirements and parameters described in Section 2.1. There are different types of files required throughout the whole process. These files are used for input and output as well as for temporary or internal storage of the tool parameters.

4.1.1 User Input file

The inputs of LEVEL0 are based on different files in different formats. These input files include mandatory and optional user inputs as well as files required for aerodynamic or structural analysis during the computation process.

The user input file is based upon the CPACS data format developed by the DLR in 2005 [27]. CPACS is a universal, XML-based data format with individual sections for each tool. The use of the CPACS file format fulfils the requirement that the tool must be compatible with other CPACS-based tools used within the DLR. In Table 4.1, the main inputs for a standard mission are summarised. As this does not display all possible inputs, extended inputs have been appended

in Table C.3.

	(1) Parameter Name	(2) Parameter Variable	(3) Unit	(4) Description
(a)	span	b	m	Aircraft span
(b)	area	S	m^2	Projected wing area
(c)	datetime_start	-	–	Date and time of estimated or exemplary mission start
(d)	datetime_end	-	–	Date and time of estimated or exemplary mission end
(e)	latitude	-	°	Positional latitude of desired mission
(f)	longitude	-	°	Date and time of estimated or exemplary mission end
(g)	payloadmass	m_{pl}	kg	Payload mass to be carried
(h)	windspeed	v_{wind}	km/h	Altitude dependent wind speed profile
(i)	detaltemp	-	°	Altitude dependent deviant temperature profile
(j)	velocityrange	-	m/s	Aircraft velocity range to be considered
(k)	airfoilname	-	–	Name of the assumed wing airfoil profile file
(l)	airfoilname_tail	-	–	Name of the assumed tail airfoil profile file
(m)	timestep	Δ_t	s	Minimum timesteps for analysis to be assumed between analysis steps
(n)	altituderange	h	m	Aicraft altitude range for day (maximum) and night (minimum) flight
(o)	maxaltitude	h_{max}	m	Maximum altitude independent of "altituderange", for extra potential energy
(p)	deltaaltitude	Δh	m	Minimum altitude steps to be analysed
(q)	maximumforce	g_{max}	–	Maximum gravitational forces to be considered
(r)	maximumforce_ground	$g_{max,ground}$	°	Maximum gravitational forces considered without lift force available
(s)	propefficiency	η_{prop}	–	Efficiency constant used as propulsion surrogate
(t)	batenergydensity	ω	Wh/kg	Battery energy density
(u)	batvolume	-	kg/m^3	Battery volume estimation used in analysis
(v)	batstart	-	–	Procentual battery status at estimated mission analysis start
(w)	paneleff	η_{panel}	–	Efficiency constant assumed for the solar panels
(x)	panelcoverage	-	–	Coverage of the upper wing/tail surface with solar cells
(y)	payload_powerconsumptionday	-	W	Energy consumption of payload during daylight
(z)	payload_powerconsumptionnight	-	W	Energy consumption of payload without light

Table 4.1: Main input parameters for LEVEL0 with highlighted minimum input parameters for LEVEL0.

The minimum parameters for defining aircraft geometry and desired mission are based on Section 3.1 and Section 3.2. The initial values to start sizing the aircraft are based on the wing parameters *(a)* to *(b)*, while other size parameters are based on statistics and are calculated by LEVEL0. As a baseline, the mission requires data for time and position, defined in *(c)* to *(f)*. If the aircraft is required to carry a payload, this must be defined in *(g)*. These parameters are mandatory. For most applications, the other inputs can be left as defined in a standard input file already delivered with the tool; therefore, they are referred to as optional. Parameters are not fixed within the tool itself to maintain flexibility. The parameters in a standard input file are chosen based on preliminary research results. Some of them can vary over time or with aircraft configurations, such as the propulsive efficiency of the aircraft or the solar panel efficiency.

The surrounding atmospheric conditions can be set by using the temperature (option *(i)*) or the wind speed (option *(h)*). For example, a known drop in air temperature or the existence of strong winds in the operation area can influence aerodynamics or minimum aircraft speed. For a direct influence on the aircraft velocity, the velocity range in *(j)* can be set accordingly, or the aerodynamic properties can be heavily influenced using a different airfoil in *(k)*. Other important parameters include the aircraft altitude in *(n)* and maximum allowed altitude in *(o)*. These parameters define the altitude profile previously

mentioned in Figure 3.2a. This altitude profile determines the minimum altitude for day and night flight and the maximum possible altitude which may be reached to gain extra potential energy if the batteries are fully charged.

Therefore, this altitude profile is a key parameter for mission analysis. All other parameters do have a direct influence on mission progress. Thus, it is important to show that they are considered during a mission analysis; otherwise, they are mostly self-explanatory. It is also possible to run a search for specific values or to batch process different configurations for the sake of comparison. The respective values coincide with the absolute minimum parameters in Table 4.1.

4.1.2 ”Data Input” files

Various aspects of conceptual aircraft design in LEVEL0 are covered by separate database files which are editable, exchangeable or both. Therefore, they are also described as additional input files or data input files. To fit the tool appropriately for use, they are saved as text files, XML files or pickle files. Pickle files are based on a Python module to convert an object hierarchy into a byte-stream and the other way around; they are used to save Python-specific data into a file. As various disciplines require their own individual databases, the most important databases are listed below:

- Airfoil database: airfoil coordinate source files and their respective analysis results
- Solar energy database: irradiation data
- Geometry database: aircraft geometry data
- Materials database: material constants

4.1.3 Output files

LEVEL0 produces different kinds of output files, depending on the use cases defined in the ”Experiments”-level (see Section 4.6), or for a single aircraft analysis in the ”Core Process”-level (see Section 4.3). The different output cases are briefly described in this section. Exemplary results and outputs can then be found in Chapter 5.

Single aircraft analysis

For single aircraft analysis, there are different outputs included.

- A CPACS file, containing the inputs with best parameter values found during analysis.

- An HTML report file, containing diagrams and statistics for mission analysis.
- An ASCII text file, containing aircraft evaluation data used as a source for the report file.

In general, the input CPACS file is copied and updated with new data after each analysis. Every aircraft analysis creates an automatic report, which contains all data required for a user to evaluate the results. These results are reported in the form of plots within an HTML report as well as a file containing the listed data if the user wants to re-evaluate this data with a custom method. Within the report, the user can find

- main input parameters,
- mass breakdown,
- geometry parameters,
- height and power analysis,
- battery status over time and
- convergence history.

Examples of the report output can be found in Section 5.4.

Aircraft batch analysis

For the comparison of multiple aircraft, the abovementioned report and multiple output files would not be helpful because the sheer number of files to be analysed manually would be excessive. It is nevertheless possible to create reports for each defined analysis by reusing one of the automatically created batch files. The comparison results are then summarised within different plots.

Aircraft configuration comparison

A configuration comparison for changing aircraft span and area cam be conducted. The different configurations are compared for a specified mission with a range of values for battery energy density ω, or fixed value ω. This way, it is possible to evaluate the performance of different span and area combinations for a specified mission. The assessment criteria for this comparison are either the total aircraft mass or a weighting function $f(\omega, m)$ which uses a measure including aircraft mass and a value for battery-specific energy density. The weighting function has been chosen in order to return a compromise between aircraft mass (m) and required specific energy density (ω), as aircraft mass is not always a sufficient criteria as further explained in Section 4.4. Exemplary results can be found in Figure 5.10.

Worldmap aircraft comparison

This constitutes an exemplary comparison of different aircraft configurations using multiple positional latitudes and timestamps for the same mission. It shows at which locations and at what time of the year a chosen configuration can be used to fulfil a defined mission. An example is displayed in Figure 5.12.

4.2 General Implementation

Following the requirements, LEVEL0 must be able to evaluate single aircraft as well as multiple aircraft. Furthermore, it must be modular and enable the user to extend or exchange single components within LEVEL0. To fulfil this goal, the tool has been constructed in different levels, as displayed in Figure 4.1.

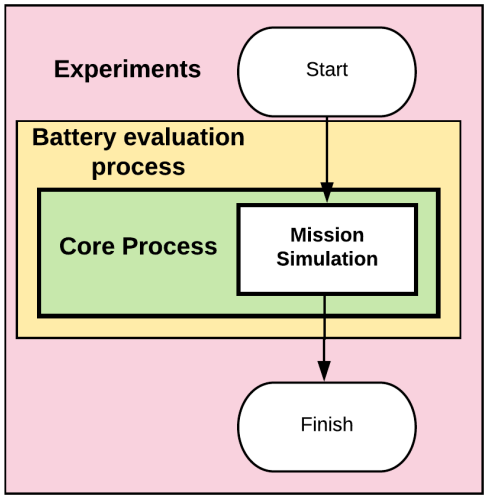

Figure 4.1: LEVEL0 Level architecture.

As shown in Figure 4.1, LEVEL0 is distributed into different levels for modularity. A core process executes the mission analysis process for a single aircraft and inherits all analysis functions, assembling the different theoretical modules from Chapter 3. This analysis process can be utilised by higher-level processes ("Battery Evaluation Process" and "Experiments") to determine specific values or perform experiments analysing multiple aircraft configurations.

The different tool components must be implemented according to different aspects. Aerodynamics and structural analysis tools are supposed to be implemented such that they can be exchanged for other modules, while mission analysis and geometric theory are part of the essential core process of LEVEL0.

Therefore, the following disciplines have been integrated in two ways. On the one hand, there are parts integrated inside other classes or modules to fulfil a single task. On the other hand, there are sub-modules implemented in a stand-alone class. The implementation of a theoretical module into a single class has several advantages. Due to the object-oriented approach, it is possible to instantiate several objects using the same class. This can become handy for the wing and tail surfaces of an aircraft. Additionally, classes can be created and tested as stand-alone objects and structured data access. A class, as well as the relations between classes and modules within a software tool, can be described through UML diagrams. These diagrams describe the inherited relations between different modules, which can, for example, include class attributes and methods as well as other associated aspects between different modules.

The modular setup of LEVEL0 has also been chosen to allow for the possibility of using all available CPUs on a computer. Multicore processing is one of the integrated features. Today, most computers have multiple cores and threads available, introducing the possibility of computing several things at the same time, independent of each other. Utilising all available threads has several advantages.

1. Efficiency: A process uses all available processor resources instead of leaving many available resources in idle mode.

2. Scalability: With a higher number of cores available, the process requires less total computation time and scales with CPU capability.

3. Responsiveness: If an unforeseen event occurs on one thread, this event can be compensated for using other threads.

This feature has been integrated for all modules which conduct independent calculations, such as in the following examples:

1. Customised solar irradiation analysis based on module by Brizon,

2. 2D airfoil analysis using XFoil and

3. A core process executing an iterative mission simulation.

Multicore analysis is automatically executed if a user enables the option within the input file described in Section 4.1.1. The multicore analysis creates temporary folders for each individual thread. Using the thread numbers, these different temporary folders are all assigned a unique identifier. All required data files are copied to individual folders, and each thread reads and writes only within the individual folder. At the end, each threads returns individual results to the coordinating process. Multicore implementation has been an important part of the realisation of LEVEL0 but does not have any influence on an individual theory or implementation of a single module. Therefore, it is an important part

of the software tool itself but is not discussed further within this thesis.

To describe how the specific disciplines are incorporated into a tool, different aspects must be considered. A brief description of the structure is therefore required. However, the modules also use the theory described to fulfil the intended purpose. This theory has been implemented using software code; additionally, some modules use an external tool to retrieve the data to be used. This process of theoretical implementation is thus an important part of the description process.

4.3 LEVEL0 Levels - Core Process

The analysis process for an aircraft is based on the analysis of the different theoretical fields in Chapter 3. The different theoretical modules have been implemented into classes and utilised within an aggregation class ("Aircraft Assembly"), as shown in Figure 4.2.

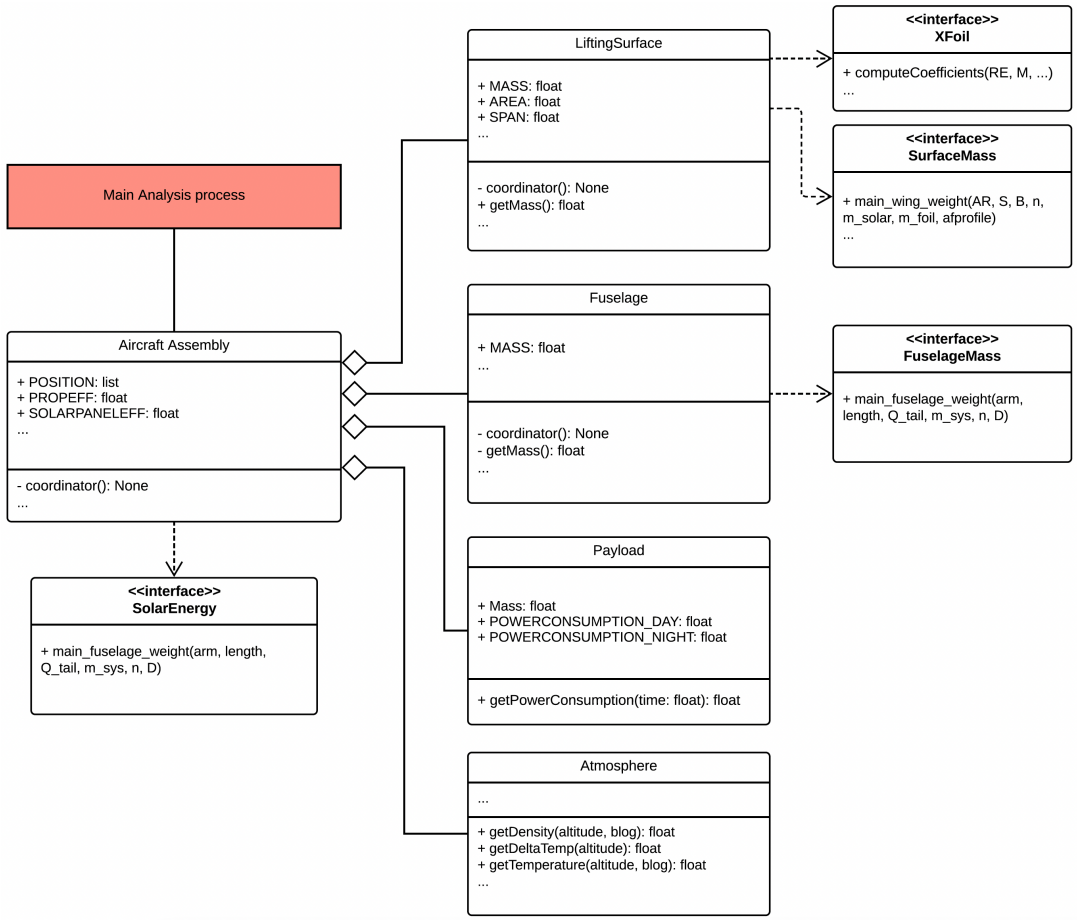

Figure 4.2: Simplified UML diagram displaying the core process software components.

Generally, the main analysis functions are separated into different functions. These analysis and comparison functions, which conduct mission analyses or aircraft comparisons, require aerodynamic and structural performance data from the aircraft. The aircraft data is computed using an ”Aircraft Assembly” class, which connects and uses aircraft component classes and gathers and interprets the data retrieved from the individual components.
The main class ”Aircraft assembly” delivers data for the main analysis and instantiates the aircraft components. The aircraft components with the wing and tail surfaces are represented by “LiftingSurface”, “Fuselage” and “Payload”. Coding-wise, another class utilised by the ”aircraft assembly” is the “Atmosphere”, as this allows all functions to have access to the atmospheric functions required. This method of implementation has proven to be faster than the use of an imported library even though the constantly required storage of atmospheric parameters ultimately requires more memory.
Upon initialisation the aircraft components make a first analysis of their individual sub-disciplines and store the results within the appropriate class. This way, “Aircraft Assembly” can retrieve the required parameters by using speci-

fied interfaces from the individual classes, without having any knowledge of the implemented theory or the eventually required sub-processes. The required parameters in every class can also be stored more efficiently, as it is not necessary to use temporary storage variables. Due to this approach, “Aircraft Assembly” cannot exist without the lower classes, as it utilises these classes to conduct the implemented analysis procedures. However, the lower classes are able to exist as stand-alone classes. The lower classes and their referring sub-disciplines analysis are independent of each other.

The individual classes include the specific disciplines for each individual component. A “LiftingSurface” class, which is used to instantiate the wing or a tail surface, inherits the aerodynamics of an aerodynamic surface as well as a mass estimation method based on a corresponding structure. A “Fuselage” class inherits the corresponding methods for the aerodynamics and mass estimation of a fuselage. This allows the main ”Aircraft Assembly” class to utilise these sub-classes without having deeper knowledge of their respective theories.

These different classes and modules work with each other to form a process which sums up all the individual analysis components. In this case, the “Core Process” builds the basic process for LEVEL0, as displayed in Figure 4.3. All theoretical models described in Chapter 3 are included and summarised in this process workflow. It is important to notice, that the different classes are a practical programming approach, while the processes are an approach for the require solar HALE aircraft analysis process.

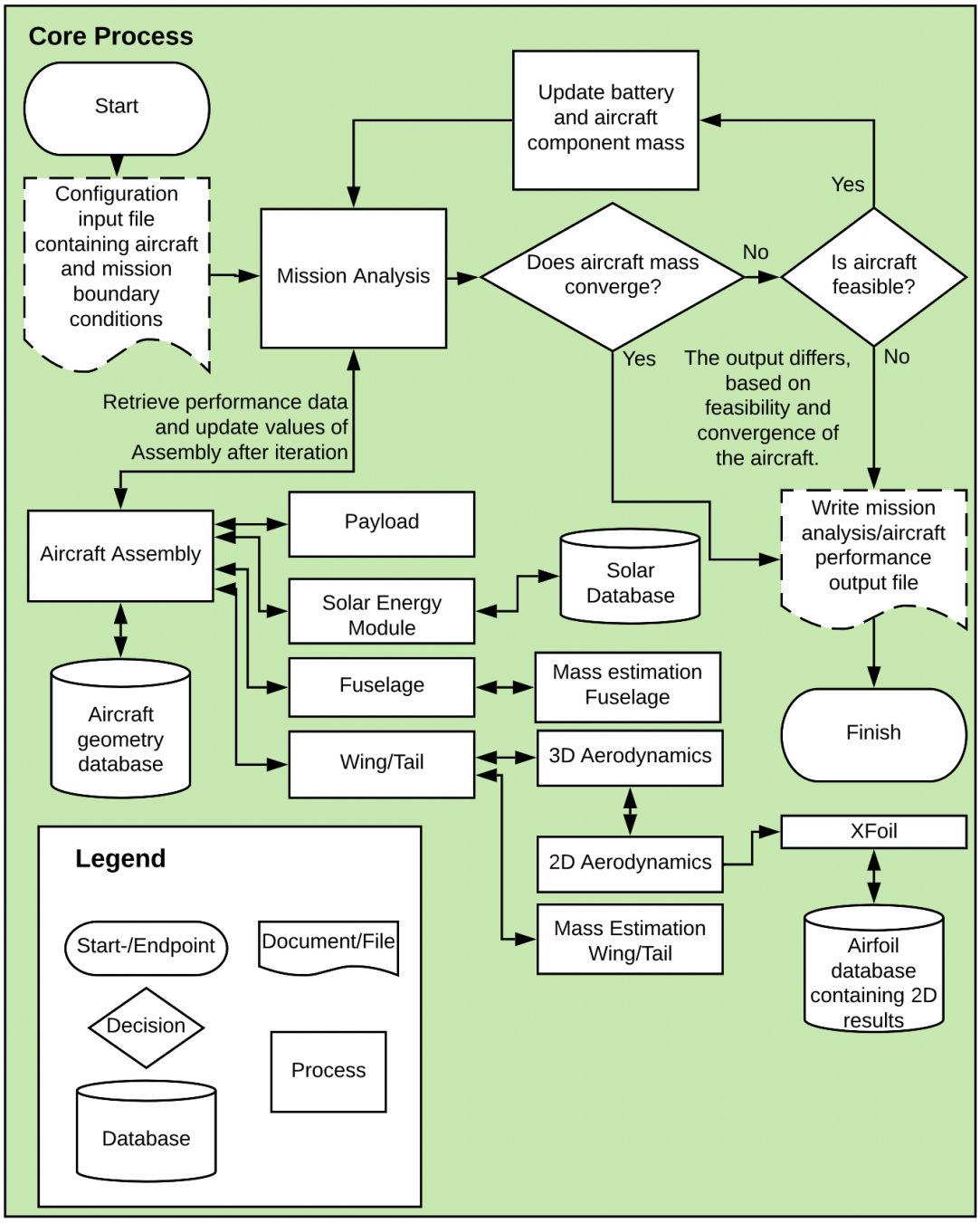

Figure 4.3: Workflow for the LEVEL0 core process.

An input file is given to the core analysis module, which first passes the data to aircraft aggregation to instantiate the required classes. The "Aircraft Assembly" utilises the given input data and database files to set up an aircraft geometry to work with based on statistical data from the geometry database file mentioned in Section 4.1.1. When the aircraft is initialised, the mission analysis simulation starts. During an analysis, performance data is requested from the aircraft aggregation. It requests the required data from the included classes, processes

the data and returns it to the mission analysis.
This also means that there is a continuous exchange of data between the mission analysis and "Aircraft Assembly", as well as the component classes. There is just one exception to this continuous data exchange. Wing and tail aerodynamics is derived from 2D airfoil data, computed by XFoil. The XFoil data is computed or loaded from the database at the very beginning with the instantiation of the corresponding class.
When the mission analysis has been completed, the results are tested for convergence. In case of divergence, the battery mass is updated, and the mission analysis cycle restarts. In case of a restart of the mission analysis cycle, the aircraft parameters in "Aircraft Assembly" are updated based on the new battery mass. This automatically includes a re-evaluation of the aircraft components and thus of the aircraft's performance parameters. The mission simulation ends with a convergence and feasibility check. Convergence is generally reached when the aircraft's total mass converges within a defined error parameter. A converging approach can still fail based on the following cases.

- Battery volume required exceeds available storage volume in aircraft;
- Structural fail occurs due to required forces;
- Aircraft does not reach defined altitude limits;
- Required energy exceeds available energy per day; and
- Required energy exceeds maximum available battery storage for currently defined aircraft.

Generally, the output differs based on the status of convergence and feasibility. It does not matter if the configuration is feasible and diverged, or if it is not, an output file is always produced, including respective results.

4.3.1 Mission Analysis

Mission analysis is part of a central coordinator function using "Aircraft Assembly", utilising all component sub-modules as shown in Figure 4.2. The analysis function is required to have access to all of the aircraft performance data. Therefore, mission analysis has full access to "Aircraft Assembly", which organises all sub-module data. This is also included in the workflow depicted in Figure 4.3.
The aircraft performance analysis is embedded using two loops. The first, internal loop contains the "mission time loop", described underneath. This analysis loops an analysis function through the mission time, evaluating the aircraft's performance based on fixed aircraft mass parameters. The second, outer loop contains the aircraft mass iteration loop, an iterative approach utilising the inner "mission time loop" to determine a converging battery and aircraft mass. This loop was previously described in Figure 4.3, and runs the "mission time loop" iteratively.

Mission time loop

An aircraft with a defined structural mass is given to the analysis and used to simulate a given mission based on timesteps. The loop restarts for every timestep, starting from the initial date to the final date. The respective start and end dates are given in Table 4.1. The analysis is embedded using a while loop with a counter. The process utilises the aircraft performance parameters to loop through the required mission. The complete loop is displayed in Figure 4.4.

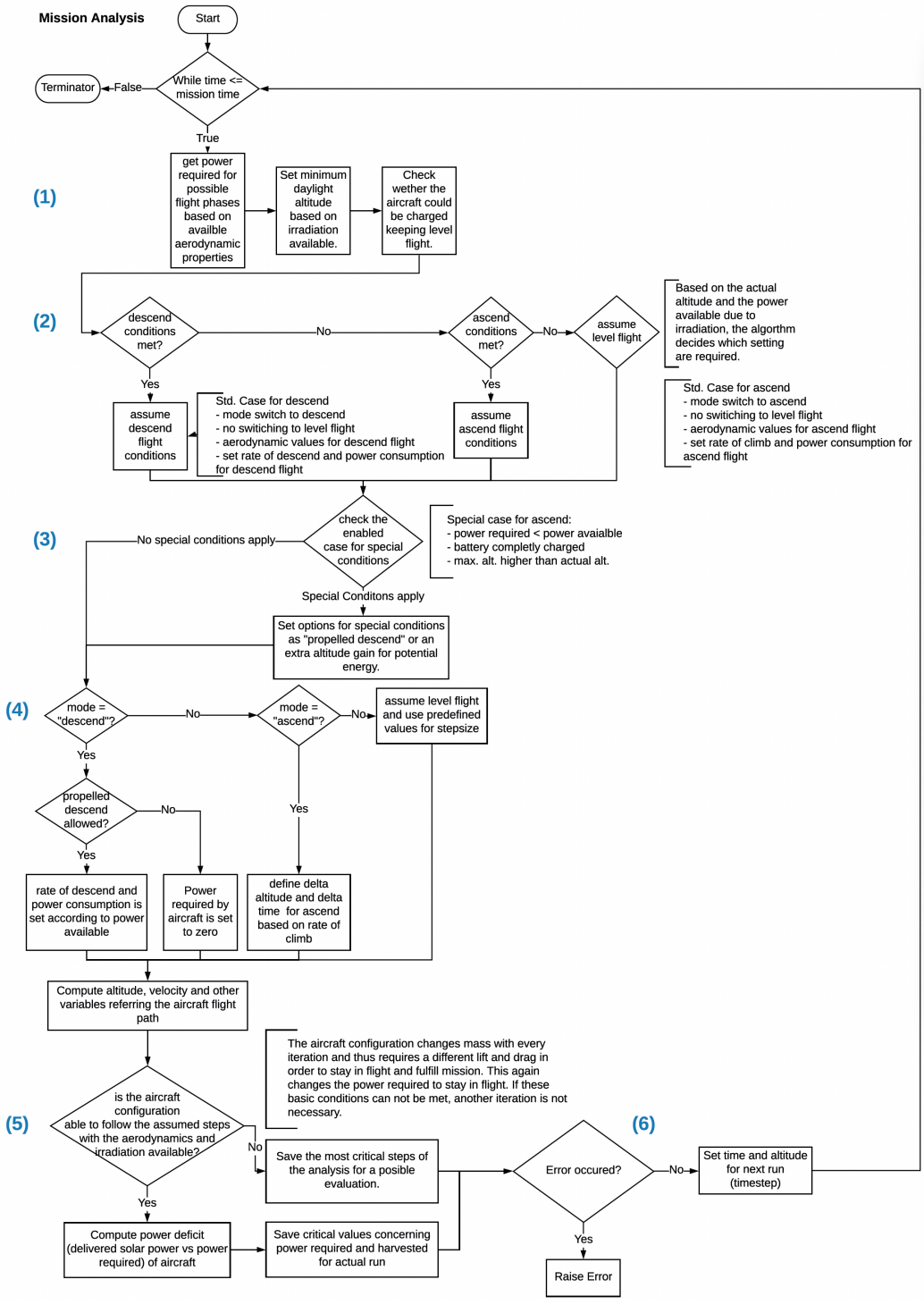

Figure 4.4: Scheme of mission implementation for mission performance evaluation loop.

At marking (1) in Figure 4.4, the aerodynamic values are prepared for later use. These values are always based on the assumption of minimum power requirement to maintain altitude, climb or descend. The required aerodynamic

values are computed first to compare and prepare for the flight mode required. The minimum altitude is set based on the available irradiation. By definition, the "day altitude" h_{day} described in Section 3.2 is assumed to be a minimum flight altitude to be reached at a positive solar irradiation, while "night altitude" h_{night} is assumed at all other times. With an assumption per timestep of the required power, available power and solar power, it is possible to make an assumption of the energy deficit per day, assuming a level flight at current altitude. If the assumed incoming energy is much lower than the minimum energy required during the day, the algorithm automatically stops.
To find the optimal flight conditions at **(2)** for the required step, the algorithm assumes level flight at current altitude as the standard condition. Depending on the current flight and environmental conditions, the algorithm chooses whether the flight mode has to be switched to either descending or ascending flight and sets the referring parameters. These parameters are mostly based on setting the required power, a target altitude, time and altitude step size and energy parameters. The subsequent enumeration displays some of the main markers for different flight conditions. As this are theoretical thoughts, the algorithm is prepared for these cases, but they do not have to occur during analysis or in reality.

- Level Flight
  - Set mode to "level" to maintain altitude.
  - Set used flight path angle such that the aircraft holds altitude with minimum power required.
  - If solar irradiation is available, try not to use battery power.
  - Use excess power available for battery charging.
- Ascending Flight
  - Set mode to "ascend" to gain altitude.
  - Set flight path angle according to a power available while considering maximum rate of climb.
  - If excess power is available, use it for battery charging.
- Descending Flight
  - Set mode to "descend" to decrease flight altitude.
  - Set flight path angle according to either the minimum rate of descent or the power available for propelled descent.
  - Use as much irradiation power as available.

After selecting a mode, it is possible to check for special conditions at **(3)**, if enabled. These options contain the possibility of making a propulsion-supported descent or of gaining additional potential altitude based on irradiation income.

- Powered descent
  - Set mode to ”descendprop” for propulsion-supported descent.
  - Use all incoming irradiation energy to use for propulsion instead of using gliding flight.
  - Switch to gliding flight (”descend”) when the rate of descent for propelled flight rises higher than for gliding flight.
- Gain extra potential altitude.
  - Set mode to ”ascend” flight in place of ”level” flight and ascend to maximum allowed altitude.
  - Keep battery fully charged during flight.

As the algorithm has now evaluated the flight modes, the regarding options are now executed by setting the correct values for the regarding time step at **(4)**. If the options for descent or ascent are not set, the algorithm assumes level flight conditions. Assuming the flight path mode, it is now possible to set the power parameters and compute the energy balance for the current timestep. This also includes computing the aircraft's altitude, rate of climb, velocity and other parameters necessary to define the next step during the mission.
These values are then checked for their feasibility at **(5)**. These checks include examining whether the aircraft can hold altitude, ascend or descend and generally follow a defined mission. When a check is passed, the results are used to compute a power deficit or, generally, the current energy balance of the aircraft. Depending on whether or not the values have passed the check, the algorithm store either the results of the current run or dummy values. As results are used to return an output, failed results or incomplete results would cause errors in results printing.
If no error occurs at **(6)**, the results are stored, and the following timestep is analysed utilising the results of the current steps. The timestep, as well as the altitude step size, can vary depending on the algorithm. For a mid-day level flight, a high step size saves CPU time and data due to fewer required analysis points. While in ascending flights, every reduction increases the possibility of decreasing the precision of the result.
If all conditions apply and no errors have appeared, the results are passed onto the next timestep, and the loop is restarted with values from the current run.

The step size of these time and altitude steps used for mission analysis have an influence on the total analysis behaviour. As for every step-based analysis method, the number of steps can add unnecessary CPU time or influence results. Even misleading results can occur, as the number of steps may be too few, and crucial events, such as beginning irradiation, can be missed.

4.3.2 Aerodynamics

The theory for the required aerodynamic analysis (see Section 3.3) is implemented within an independent module and handles all computation steps. It is initiated by creating a new instance of an aerodynamic surface class, as can be seen in Figure 4.2. Atmospheric data required is pulled from a module based on the international standard atmosphere [28], by Liersch.

At initiation, the module sets all parameters and automatically computes the coefficients for the given airfoil and wing geometry. Based on the defined velocity and altitude range of the aircraft, the algorithm defines the required values for XFoil based on Reynolds number and Mach number and then utilises them for coefficient computation. If possible, the results computed and stored earlier are loaded from the database (see Section 4.1.2).

The computation of the required values is depicted in 2D airfoil and 3D wing coefficients and forces. XFoil has been chosen for the 2D analysis of the given airfoil. The programmed XFoil interface used for this purpose, included in the overview in Figure 4.2, delivers a broad range of communication and analysis options and is also usable independently of LEVEL0. Despite the control which the XFoil interface offers, all 2D airfoil analysis methods are implemented within an independent module. All 3D analysis methods are implemented with the "LiftingSurface" class, utilising the aforementioned 2D module.
As it cannot be predicted at which point an airfoil might stall, it has been determined that each angle of attack must be analysed one by one within XFoil. This way, it is possible to stop the analysis at a minimum lift coefficient, maximum lift coefficient, airfoil stall or after a defined number of divergent analysis attempts. This method maintains a higher degree of stability. Consequently, after each analysis step from XFoil, the interface implemented in LEVEL0 analyses the returned results to decide whether to compute further or to stop the XFoil analysis loop.
The results read from XFoil are stored within an internal data structure and, if enabled, are also stored within a Python data file for reuse in later analysis processes. This prevents unnecessary recalculation of airfoil values, saving CPU time. It is important to mention that only XFoil results are stored, while LEVEL0 results are always re-computed. Accordingly, follow-up errors produced by re-loading older results can be anticipated. The one-time computation of the required XFoil values to be utilised by LEVEL0 can require about thirty minutes, heavily depending on the defined boundaries, which is completely saved if all required values can be loaded from the data file in follow-up analyses. The alternative case of doing an "on the fly" analysis during the iterative mission analysis process, would require a multiple of the one-time calculation.

For the mission definition in LEVEL0, the possible aircraft velocity as well as the aircraft altitude is given in ranges. Therefore during the analysis process

of LEVEL0, different altitudes and velocities can be requested to analyse force equilibrium at current altitude and velocity. For example, a velocity of $5m/s \leq v \leq 50m/s$ and an altitude $15,000m \leq h \leq 20,000m$ can imply a great number of values to be computed. The algorithm requires a lift and drag coefficient at all altitudes and velocities in between boundaries to determine the best operating point. Computing all of these values using XFoil would require a high CPU time. Therefore, initial values, which have been computed for the velocity and altitude boundary values, a well as optional values in between, are used to interpolate the required values during the process of analysis. These values are further referred to as an aerodynamic performance map.
A sketched example for the value cluster with the minimum values required for later interpolation is shown in Figure 4.5.

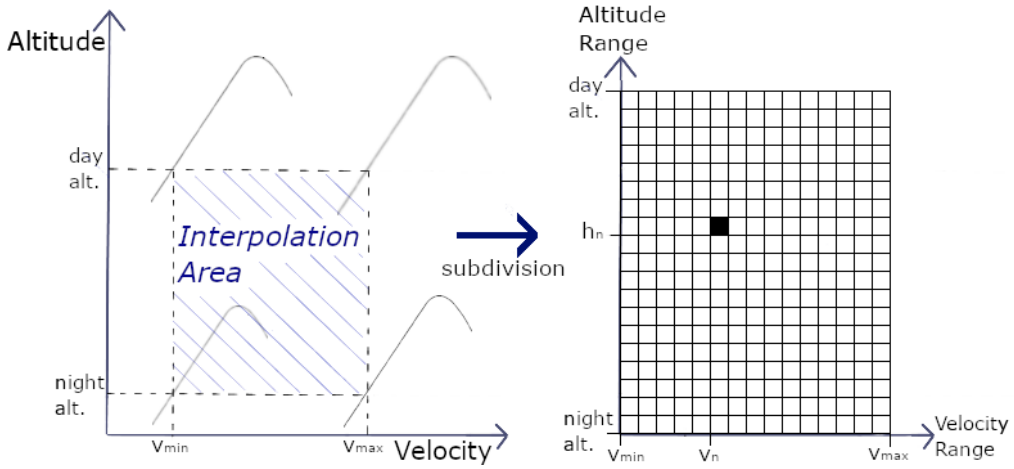

Figure 4.5: Simplified value cluster used for interpolation of 2D airfoil coefficients.

The marked area shows the simplest case for an area with the same minimum velocity for all altitudes to be computed. The boundaries of this area are influenced by the options for Reynolds number in the user input, as well as altitude and velocity range chosen in Table 4.1. While altitude and velocity directly influence the mission boundaries, the Reynolds number parameters primarily influence the accuracy of the analysis and secondarily influence the mission boundaries.
As graphically described in Figure 4.5, the initial boundaries with $v_{min} \leq v_{max}$, $h_{night} \leq h_{day}$, Re_{min} and Δ_{Re} are subdivided into smaller areas. This increases the accuracy of the interpolation process used by LEVEL0 and saves CPU time by reducing the XFoil values to be computed. Exemplary interpolation processes are used in verification examples in Section 5.1 and are further appended in Section B.1.

The XFoil analysis process can further deliver ranges of computed lift and drag versus angle of attack based on the boundary points required. They must not

coincide for different altitudes and velocities. Therefore, it is sometimes necessary to interpolate between curves with a different number of data points. Test cases in LEVEL0 have shown that normalisation prevents several errors and shows the best overall fit with directly computed 3D wing results. This normalisation has been included in the error analysis and verification process discussed in Section 5.1.

4.3.3 Mass Analysis

Generally, mass analysis is implemented in accordance with the theoretical description from 3.4. The mass analysis module is implemented as a stand-alone interface, used by the referring class for aerodynamic surfaces or the fuselage. It computes the initial mass on instantiation and re-evaluates all values every time a relevant parameter changes.

The interface used to compute component mass uses the workflow illustrated in Figure 4.6.

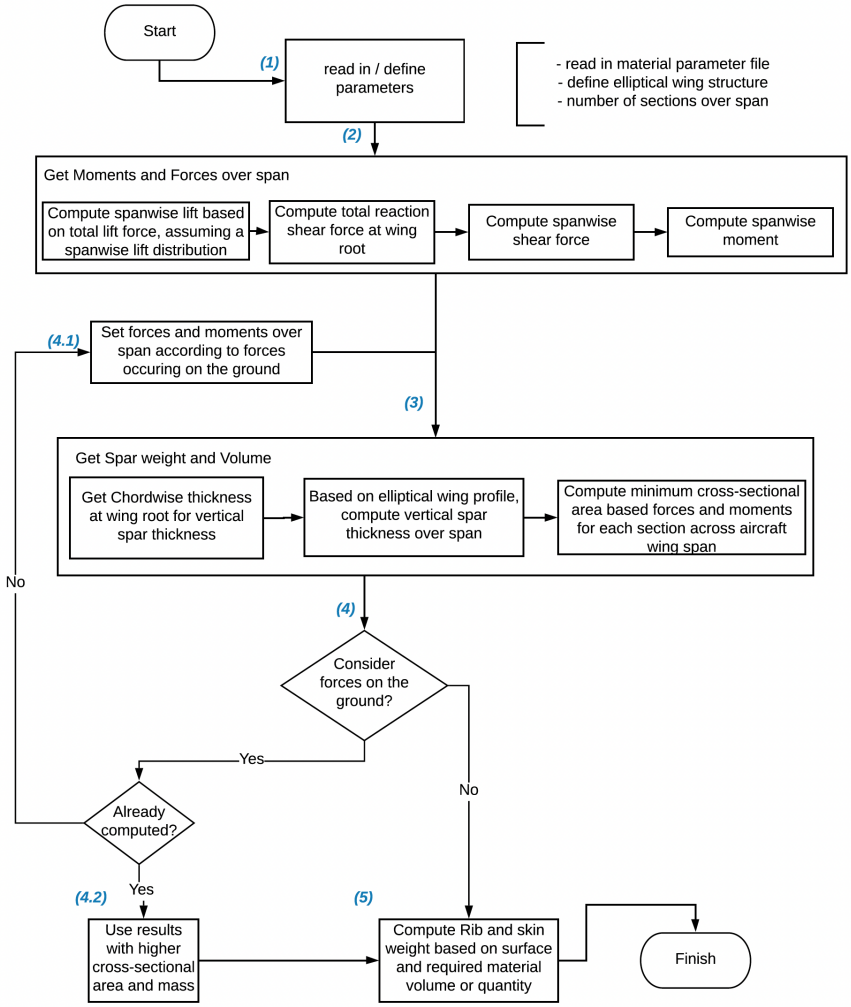

Figure 4.6: Flow chart of mass analysis within the interface, using the example of aerodynamic surfaces.

The analysis of mass for a given wing requires different input parameters. These parameters – wing geometry or exerted force – are required to describe the force on the wing and to size the wing internals to compute mass. The referred method within the interface is the only public method available and starts with the process described in Figure 4.6, utilising internal interface methods. To define a material thickness for the structure, the strength and the specific material mass is required. This data, introduced in **(1)**, is given as an input file using a comma-separated values (CSV) format and includes all values required for structural analysis and mass estimation, including

- Upper skin or laminate surface mass per square metre,
- Lower surface skin mass per square metre,
- Solar cell mass per square metre,

- Rib material mass per cubic metre,
- Spar material mass per cubic metre and
- Spar material strength modulus in x and y direction as well as maximum tensile stress.

Calculated forces can then be used to analyse the moments occurring over the wing span based on the given forces exerted on the aircraft. The following explanation is supported by LEVEL0's exemplary plotted analysis steps in Figure 4.7.

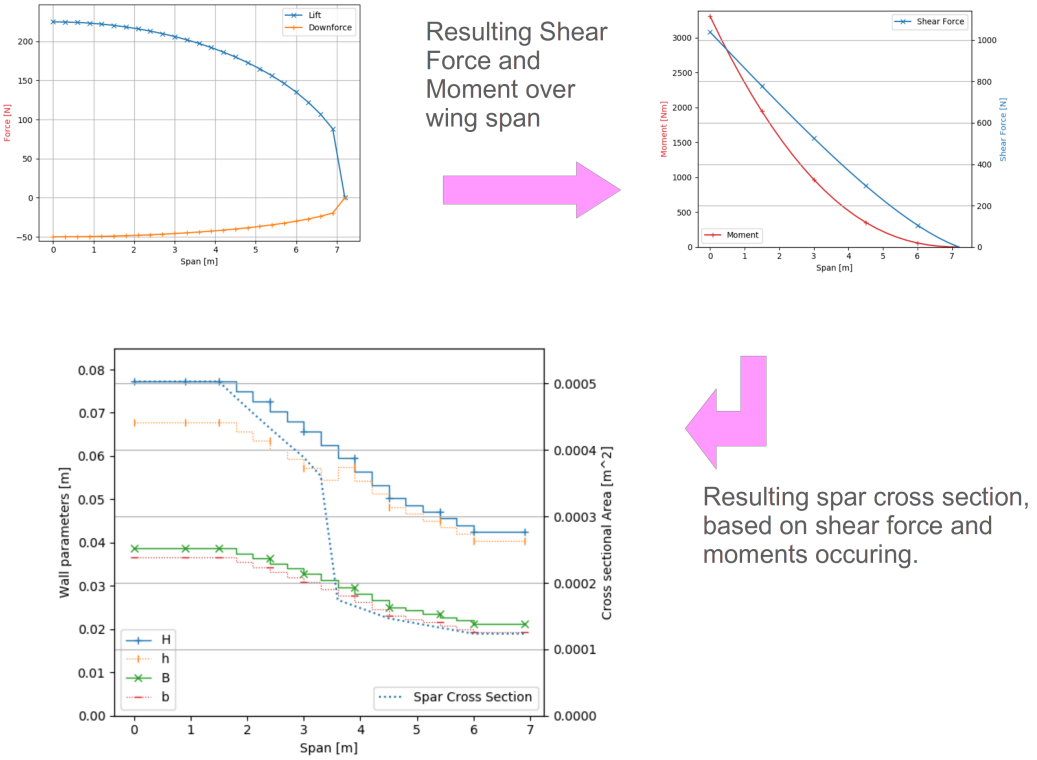

Figure 4.7: Spar cross-section over a wing based on lift and downforce over half wing span, as computed by the referring mass analysis module based on exemplary parameters with $b = 15m$, $AR = 25$, $L \approx 2650N$, downforce $W \approx 600N$, $v = 32.5\frac{m}{s}$, $\rho = 0.165\frac{kg}{m^3}$.

To compute the span-wise moment, a necessary step for sizing the aircraft spar, the shear force must first be computed, as shown in Figure 4.6 at **(2)**. This shear force, following Equation (3.25), is based on the forces working in the z direction on the wing, as displayed in Figure 4.7. The resulting shear force F_z, based on Equation (3.25), is thus computed using the integral of these occurring forces. LEVEL0 assumes that the downforce uses an elliptical distribution over the span. This elliptical assumption has been chosen to model the volume distribution inside the wing. It is assumed that the available storage volume

is distributed according to the wing's geometrical form. The required batteries and systems are asummed to be stored within this available volume, resulting in a quasi-elliptical mass distribution over span.

The shear force F_z occurring at the wing root represents the maximum shear force over the wing span. In the span-wise direction, this shear force is reduced by the distributed force. The resulting moment M_x at the wing root and the span-wise bending moment $M'_x(y)$ are exemplary plotted in Figure 4.7. Following the load distribution, the span-wise bending moment $M'_x(y)$ reduces towards the wing tip. Following the assumption of a super elliptical wing planform, the reduction of wing planform and the bending moment becomes handy due to the reduction of the required spar cross-sections.

Finally, the distributed moments and forces are used to obtain the required spar cross-section to support the given forces and moments. A rectangular spar is adapted to the internally available wing volume at the thickest chord-wise position. By maximising the thickness, the bending stiffness can be increased. Assuming that the spar is box shaped, the outer and inner dimensions are varied and analysed using Equation (3.26) to determine the minimum possible cross-sectional area. Resulting on the load distribution and the following bending moment, the resulting spar cross-section in Figure 4.7 shows the relation between spar volume and layer thickness over half wing span. The belonging spar dimensions have been introduced in Figure 3.4.

The resulting spar dimensions in Figure 4.7 illustrates various phenomena. First, the outer spar height is reduced towards the wing tip. With this reduction, other parameters, such as outer spar width B, are also reduced. The inner thickness in height is a little thicker and also reduces towards the wing tip. This is based on the increased moment at the wing root. The dimensions of the spar are chosen using the following short guidelines.

1. Working section-wise, while starting from root, going to wing tip.
2. A possible cross-section in every section is chosen under the following boundary conditions:
    - The maximum direct stress occurring in the spar is lower than the maximum allowed stress.
    - The spar cross-section in wing-tip direction is lower than in earlier sections.
3. Under the possible cross-sections, the algorithm chooses the lowest possible value based on the spar cross-section.

To reach this, for every section of the wing, the algorithm creates a list, section by section. LEVEL0 evaluates all possible values for the boundary conditions

and chooses the one with the lowest cross-section possible. It would also be possible to use a function and solve for the lowest possible values. However, because it uses Python methods, this requires more CPU time than a simple list evaluation. It would require less memory, but for modern workstations, this limit can be neglected.

The forces on the wing differ on the ground and in flight. Without lift force, the wing mass tends to bend the wing downwards, perhaps even with higher acceleration due to landing manoeuvres. Therefore at **(4)**, it is possible to include this case in the mass assumption by re-evaluating the cross-sectional analysis with the corresponding forces included.
Finally, using the input parameters, computed wing spar volume and the outer wing geometry, the final wing mass and available internal volume can be returned at **(5)**. Mass analysis of other aircraft components follows a similar approach and is therefore not further discussed.

4.4 Quality Criteria

Most HALE aircraft are on the cutting edge of what is technically possible. Consequently, most configurations will not converge. This, in combination with the chosen iterative approach, is a problem for a potential parameter optimisation, as finding a continuous function is difficult. A divergent analysis can be based on aerodynamic conditions, excessive mass or just the surrounding atmospheric conditions, mostly combinations of different effects. Effectively, the configuration is not sufficient to fulfil a mission at the given conditions. These non-converging aircraft configurations cannot be compared to each other, as the aircraft mass during the iterative approach increases until the defined boundaries have been exceeded. For a tool which is supposed to enable a comparison between different configurations, this is a central problem.

Different cases can occur, leading to either a convergent and feasible approach or a failed approach. Examples of a convergent approach (Table 4.2) and a non-convergent approach (Table 4.3) are given below.

	(1) Iterarion nr. [−]	(2) Bat. Mass out [kg]	(3) Aircraft Mass out [kg]	(4) Battery capacity required [Wh]	(5) Irradiation power capacity [Wh]	(6) Battery capacity out [Wh]	(7) Mass converged [−]	(8) Aircraft feasible [−]
(a)	0	19.36	68.63	4909.33	38236.38	4909.33	0	0
(b)	1	23.9	73.17	6059.71	38293.73	6059.71	0	0
(c)	2	27.17	76.43	6888.41	38321.48	6888.41	0	0
(d)	3	29.14	78.41	7389.16	38321.29	7389.16	0	0
(e)	4	30.5	79.77	7733.76	38322.14	7733.76	0	0
(f)	5	31.24	80.51	7922.11	38328.85	7922.11	0	0
(g)	6	32.05	81.32	8127.98	38358.78	8127.98	0	0
(h)	7	32.89	82.16	8340.1	38370.66	8340.1	0	0
(i)	8	33.82	83.09	8575.29	38377.24	8575.29	0	0
(j)	9	34.73	84.0	8806.58	38390.45	8806.58	0	0
(k)	10	34.7	83.97	8799.82	38389.98	8799.82	1	1

Table 4.2: Example of convergent aircraft convergence history.

	(1) Iterarion nr. [−]	(2) Bat. Mass out [kg]	(3) Aircraft Mass out [kg]	(4) Battery capacity required [Wh]	(5) Irradiation power capacity [Wh]	(6) Battery capacity out [Wh]	(7) Mass converged [−]	(8) Aircraft feasible [−]
(a)	0	21.44	70.71	4909.33	38236.38	4909.33	0	0
(b)	1	27.8	77.06	6365.26	38304.04	6365.26	0	0
(c)	2	33.03	82.3	7564.25	38322.31	7564.25	0	0
(d)	3	37.44	86.71	8574.3	38377.15	8574.3	0	0
(e)	4	40.89	90.16	9364.75	38404.19	9364.75	0	0
(f)	5	44.36	93.62	10157.74	38399.91	10157.74	0	0
(g)	6	47.77	97.04	10938.87	38429.45	10938.87	0	0
(h)	7	51.51	100.77	11794.84	38456.38	11794.84	0	0
(i)	8	54.4	103.67	12457.73	38455.76	12457.73	0	0
(j)	9	58.09	107.36	13303.4	38452.74	13303.4	0	0
(k)	10	62.32	111.59	14270.85	38512.23	14270.85	0	0
(l)	11	68.43	117.69	15669.5	38285.23	15669.5	0	0
(m)	12	75.67	124.94	17329.45	38311.04	17329.45	0	0
(n)	13	84.46	133.72	19340.71	38256.58	19340.71	0	0
(o)	14	96.23	145.5	22037.73	38243.36	22037.73	0	0
(p)	15	113.76	163.02	26050.14	38264.67	26050.14	0	0
(q)	16	144.66	193.93	33127.79	38281.58	33127.79	0	0
(r)	17	167.01	216.28	142057.83	38245.65	38245.65	0	0
(s)	18	166.76	216.03	184560.76	38187.83	38187.83	1	0

Table 4.3: Example of non-converged aircraft convergence history. Non-Convergence occurs due to available irradiation power.

The most convenient cases for a convergence or non-convergence are as follows.

- Table 4.2:

  Battery capacity required *(4)* and battery capacity available *(5)* do not diverge.

  → Mass converged *(7)* is true, as the aircraft mass does not change significantly during iterations. The available capacity coincides with the required

capacity and is lower than the total irradiation capacity in *(5)*. Additionally, the aircraft mass without battery does not diverge. Therefore, this analysis fulfils all boundary conditions for a feasible and convergent aircraft configuration.

- Table 4.3:

  Battery capacity required *(4)* and battery capacity available *(6)* diverge due to irradiation capacity available *(5)*. The battery capacity available *(6)* is limited by the irradiation capacity available *(5)*, which in this case, is not sufficient to power the aircraft at that mass throughout the day.

  → Mass converged *(7)* is true, as battery mass converges due to the given limit, leading to a converging aircraft mass. However, in this case, the available capacity is not sufficient to power the aircraft during the defined mission, which would lead to a failed or non-feasible but converged aircraft design, as displayed in *(8)*.

The main reason to recognise a suitable configuration is thus the battery capacity or the general power balance. The aircraft requires excessive energy and therefore increases in mass until one parameter, such as the irradiation capacity available, is no longer sufficient. Other reasons which can lead to a failed or non-feasible configuration are as follows and can be found within column *(8)*.

- The lift force available within boundaries is not sufficiently high to carry aircraft mass.
- The available storage volume is not sufficient in order to carry the battery capacity required.
- The possible spar size within the wing structure is not sufficient to support occurring forces.

As can be seen in Table 4.2, in a normal convergence, the aircraft battery capacity in *(6)* increases with every iteration to fit the required battery capacity in *(4)*, which is required to fulfil the defined mission with the aircraft mass in *(3)*. The battery capacity – and therefore the battery mass and capacity – increases with iterations and therefore the delta between the available irradiation power in *(5)* and the capacity to be stored reduces with every iteration. In this case, the aircraft increases in mass until the required battery capacity to fulfil the mission in *(4)* fits the available battery capacity in *(6)* but is also much lower than the available irradiation power in *(5)*, while the lift force of the aircraft is also sufficiently high to carry the aircraft's mass. These two conditions mean that the aircraft is "feasible", as in *(8)*.

As can be seen in Table 4.3, the aircraft's mass may well converge, but the aircraft may nevertheless be infeasible. In this case, the available irradiation

energy in *(5)* is not sufficient to power the aircraft for the defined mission. In this case, the aircraft mass still converges, as the battery capacity of the aircraft can never exceed the irradiation power available. Nevertheless, the aircraft may still be infeasible because the energy available would be insufficient. In such a case, the required battery capacity in *(4)* increases drastically, as the theoretical aircraft analysed in LEVEL0 is not able to maintain the required altitudes – mostly the higher day altitudes. This results in many climbing phases throughout the mission, drastically increasing the required energy.
As in Table 4.3, an infeasible aircraft is mostly the result of a divergent battery capacity and mass. The aircraft mass, in this exemplary case displayed in Table 4.2 and Table 4.3, differs by $> 50\%$ between the feasible and the infeasible approach for nearly the same aircraft configuration. The difference between these cases is just the assumed specific battery energy density $\Delta_\omega \approx 25 Wh/kg$.

Most documents about aircraft comparisons for HALE aircraft use total aircraft mass or relative battery mass, neither of which can be applied in this case. Thus, to compare infeasible and feasible aircraft with each other, an independent parameter must be defined for comparison. A parameter which shows a trend between different configurations, regardless of whether or not they would be feasible under normal conditions.
The specific battery energy density ω indicates the energy stored per unit mass. Thus, a higher value for ω implies that the same mass of batteries can store a higher amount of energy. Applying this to two different aircraft only differing by ω, the aircraft with the higher value for ω requires less mass for the same performance. Therefore, ω has been chosen as an overall aircraft quality parameter.

In earlier studies, there has been no possibility to directly assess and compare infeasible aircraft configurations and therefore no possibility to get a design direction. The use and manipulation of this parameter as quality criteria allows an assessment and comparison of different aircraft, even if the configurations are not feasible originally, which is an advantage of LEVEL0.
Further, using a weight function, it is also possible to display a compromise for two different quality parameters as aircraft mass and specific energy density. As earlier research used the aircraft mass as a quality parameter, a weighted function including the battery energy density and aircraft mass could deliver comparable results, while also including normally non-convergent parameter combinations. Such a weighted function can use parameters to prioritise one factor over the other. The prioritisation for a solar HALE aircraft can be based on battery cost per mass or other factors.

4.5 LEVEL0 Levels - Battery Evaluation Process

To identify the lowest possible value for ω, several values must be tested for convergence. The following example in Table 4.4 displays a simple example search interval for a converging specific energy density with $225 Wh/kg$.

	(1) 1st run	(2) 2nd run	(3) 3rd run	(4) 4th run
(a)	$100 Wh/kg$	$100 Wh/kg$		
(b)		$200 Wh/kg$	$200 Wh/kg$	$200 Wh/kg$
(c)				**225**Wh/kg
(d)			$250 Wh/kg$	$250 Wh/kg$
(e)	$300 Wh/kg$	$300 Wh/kg$	$300 Wh/kg$	
(f)	$500 Wh/kg$			

Table 4.4: Example specific energy density search interval using $25 Wh/kg$.

A search starts with two boundary points, in this case $100 Wh/kg \leq \omega \leq 500 Wh/kg$. Afterwards, the tested boundaries are reduced from *(1)* to *(2)* using a lower, non-converging value and a higher, converging value in Table 4.4. They are further reduced until the error between these two boundaries is reached, as with ongoing columns in Table 4.4. Values for ω which already have been computed are reused by loading the result files to save CPU time. For higher number of CPU cores available, the intervals are computed in parallel using as many boundaries as cores are available, if defined in the user input file.

The workflow for an ω-search is displayed in Figure 4.8.

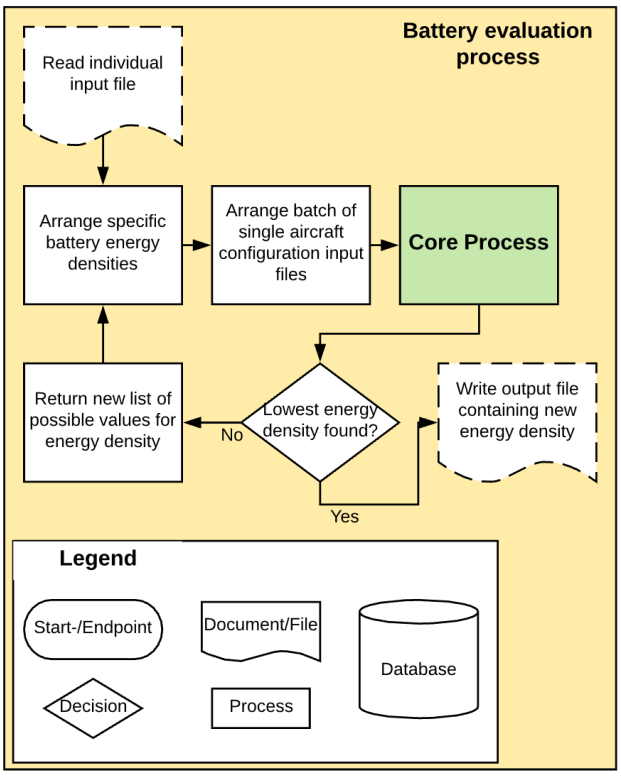

Figure 4.8: Workflow for the LEVEL0 battery evaluation process.

The individual input file includes a range for values of ω. Otherwise it is a single aircraft configuration definition, as mentioned in Section 4.1.1. The tool arranges a batch of input files with an individual value for ω and executes the core process from Section 4.3 for each of the created configuration files. Afterwards, these results are evaluated. If the lowest value for ω under consideration of a specific error has not found, the process restarts with changed boundaries and creates a new batch to analyse and evaluate. After finishing the search algorithm, the final result is returned as an output file containing the desired values for ω.

4.6 LEVEL0 Levels - Experiments

The requirements for LEVEL0 demand the possibility of comparing different aircraft and comparing for modularity. To compare different aircraft with each other, the outer level "Experiments" is wrapped around the battery evaluation and core process, as illustrated in Figure 4.1.

The lower levels described in Section 4.3 and Section 4.4 are based on performing an analysis on an aircraft with a defined configuration of parameters. Within these lower levels, it is possible to adapt aircraft battery capacity to find the correct mass and performance of a single configuration. If no converging result

can be achieved using the defined parameters, LEVEL0 uses ω, as described in Section 4.4 to obtain a convergent and comparable result.
The outer level “Experiments”, which is graphically described in Figure 4.9, is an example of a wrapper which utilises the lower analysis levels.

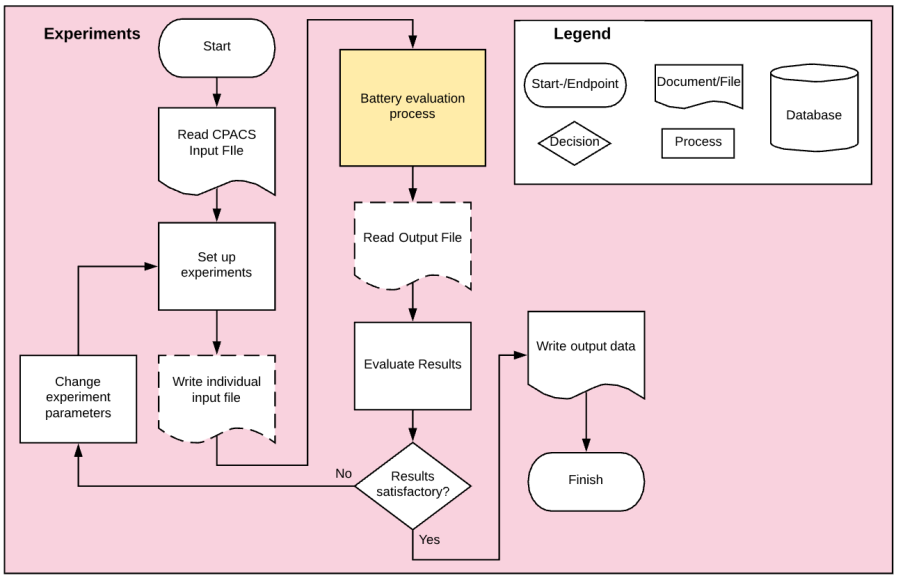

Figure 4.9: Workflow for the outer LEVEL0 ”Experiments” level.

Based on the given input data and the required comparison analysis, the tool defines a batch of individual input files with aircraft parameter configurations. These individual files are automatically distributed into a number of threads and computed using the lower levels, “Battery Evaluation Process” or “Core Process”, which were described earlier.
The individual results returned by the lower levels are gathered and processed by the “Experiments” level. Based on the analysis requested by the user, the results can be reused for new aircraft or mission configurations within an iterative approach, or directly passed further for results evaluation. In the scope of this thesis, some example experiments have been set up for aircraft comparison. Otherwise, this outer wrapper level is customisable and provides software interfaces for the further use of LEVEL0.

Chapter 5

Examples, Verification and Comparison

The differing modules implemented in LEVEL0 produce a variety of data, which is processed for delivering results and outputs for the user. To determine the reliability of these results, the underlying methods have to be verified. This can be done by comparing these methods using differing methods, tools or research. For the case of LEVEL0, some example outputs have been used in order to be compared with other results or research.
These results were produced using different analysis procedures for the aircraft components, in accordance with the theory in Chapters 3 and 4, and the respective methodology in . It is important to notice, that the results are not validated, but verified. A validation would require a real world example to compare, which is not available. Instead the verification process is based on other researcher's results, or well known tools.

5.1 Aerodynamics

To verify the aerodynamic analysis, a variety of situations and airfoils with different properties were chosen based on the following values.

- velocity: $5\frac{m}{s} \leq v \leq 50\frac{m}{s}$
- altitude: $16,000m \leq h \leq 20,000m$
- span: $25m$
- wing area: $20m$
- Re_{min}: 5,000
- $\Delta_{Re} = 10,000$

To cover different situations, the analysis procedure was verified using different airfoils. The verification using the PF25-airfoil is shown within this section, while other examples are appended in Section B.1. The aerodynamic 3D analysis is based on 2D results. These 2D results are computed using XFoil and interpolation, following Section 3.3.1 and Section 4.3.2. While the 3D analysis is determining for the final LEVEL0 results, and utilises the 2D results, the precision of the 2D results has a substantial influence on the 3D result. As explained in Section 4.3.2, the XFoil results form a mesh of aerodynamic values to be interpolated. The mesh density, based on Δ_{Re}, has thus substantial influence on the results and will be verified first, before verifying the belonging 3D results.

2D Analysis Verification

The lift and drag coefficient of a PF25 airfoil have been compared between XFoil and an interpolated LEVEL0 result in Figure 5.1.

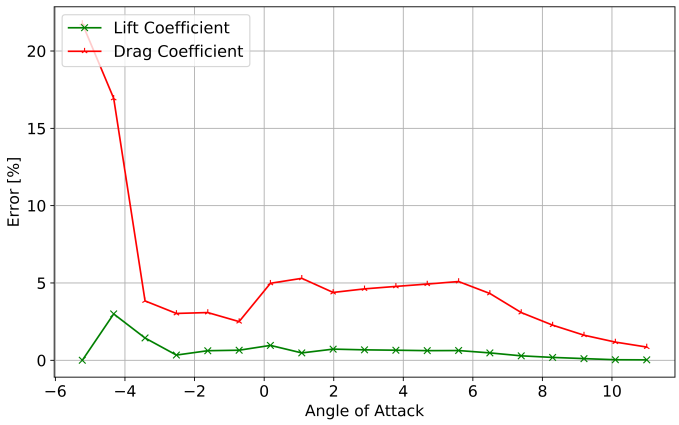

Figure 5.1: Relative error of interpolated lift and drag coefficient compared to computed XFoil results.

The error for the PF25 is relatively high at negative angles of attack. For the actual mission simulation, this range with $\alpha \leq 0$ normally is not required and is only plotted for better situation awareness. The required angles of attack normally fall between a range of $0° \leq \alpha \leq 10°$. For positive angles of attack, an error $\leq 5\%$ for lift and drag coefficient shows that the interpolation comes close to a direct analysis of the PF25 airfoil in that situation. In agreement with the project supervisor an error of under $+/-10\%$, which is acceptable in pre-design, is also an approximate value to be accepted for the used modules. Therefore these values may be accepted as verified.

3D Analysis Verification

The 3D wing analysis assumes a near optimal elliptical lift distribution, as mentioned earlier in Section 3.3.1. LEVEL0 is supposed to be able to compute an arbitrary wing, having access to a broad range of airfoils, to deliver a performance estimate to be used in the performance analysis. The desired aircraft specifications are based on glider aircraft, with specific differences.
A third-party analysis tool has been chosen, enabling the modelling of a 3D wing and therefore allowing the comparison of the chosen estimation method with a well-proven method. The tool of choice is XFLR5 [29]. In XFLR5, the results have been computed using LLT (Lift Line Theory) and VLM (Vortex Lattice Method), to evaluate the differences. It has been chosen to go with the LLT-method.

The lift coefficient for a 3D wing is derived from the 2D airfoil lift coefficient using Equation (3.9). The drag coefficient is based on Equation (3.11) and implies that the 3D wing drag coefficient is composed from $C_{D,0}$, based on the 2D airfoil drag coefficient and $C_{D,i}$, which is the component for induced drag in Equation (3.13), based on 3D wing lift C_L. The referring airfoils are used on an elliptical wing planform, this planform has been exported for use for a 3D wing geometry in XFLR5. The comparison of the assumed results, using interpolated XFoil values from LEVEL0 and the results from XFLR5, are used to verify some exemplary LEVEL0 results. For the lift as well as the drag coefficient, the error is computed only for values of α which have been computed by both, XFLR5 and LEVEL0.

For the PF25 airfoil verification, depicted in Figure 5.2, LEVEL0 returns a result which deviates very little from the XFLR5 reference values.

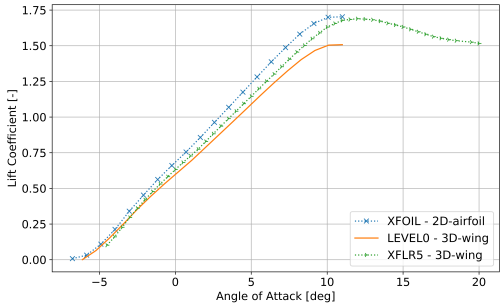

(a) Lift coefficient source and interpolated curve.

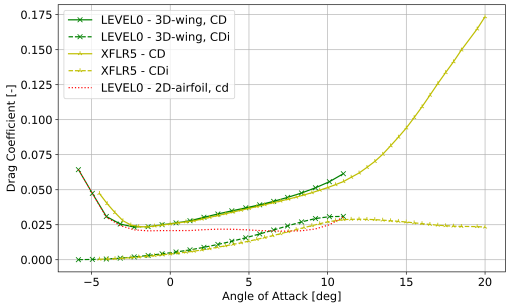

(b) Drag coefficient source and interpolated curve

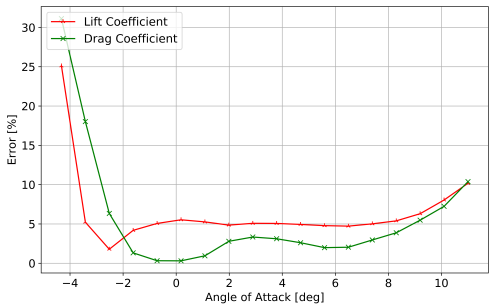

(c) Relative error of interpolated lift and drag coefficient compared to computed XFoil results.

Figure 5.2: Comparison between XFLR5 and LEVEL0 coefficient curves for an elliptical wing using a PF25 airfoil.

The PF25 does have an extremely low zero-lift angle of attack $\alpha_0 \approx -6°$, as depicted in the appended Figure 5.2a. Moreover, the XFoil analysis for the 2D airfoil approaches this value but never becomes $c_l = 0$ for the chosen range of α. For such cases, LEVEL0 extrapolates a value for α_0 and applies it to the given formulas in Section 3.3.1. This results in a high deviation between reference values in XFLR5 and values computed by LEVEL0 for negative angles of attack, close to α_0. This area is only essential to determining a starting point to compute the 3D wing curve for C_L and is not used by LEVEL0 for mission analysis, as the resulting lift forces are normally too low. Angles of attack $\alpha \geq -2°$ show much better behaviour with a mean error of $\approx 5\%$ and therefore return a usable estimate of the elliptical wing performance. The other airfoils used for verification, as are appended in Section B.1, show similar behaviour for the required angles of attack. The error for 2D interpolation is very low with a maximum of $\approx 5\%$. Additionally, while error increases in 3D wing analysis, the resulting error of $\approx 10\%$ for the required angles of attack is acceptable. Therefore, this approach can be used for mission analysis.

5.2 Mass Analysis

Mass analysis is based on earlier research discussed in [8, 13]. The glider-like structure allows the use of a simple approach which incorporates structural components of the wing and assumes main elements, such as the wing spar and ribs. The mass analysis approach has been verified for the complete aircraft, rather than single components. The different elements for mass analysis in LEVEL0, described earlier in Section 3.4 and Section 4.3.3, have been proven to be correct through a step-by-step examination, as appended in Section B.2. Nevertheless, that approach lacks a comparison with an already verified approach. Therefore, to verify the chosen approach, the results are compared to the mass relations based on earlier research by Noth [1].

Noth gathered several mass estimation models. The Brandt mass estimation model uses a very low specific mass per square metre wing projected area and therefore represents the lowest possible structure weight. The other models by Rizzo or Noth utilise a broad basis of aircraft data to represent a true-to-life aircraft weight. All models have been incorporated into a graphical comparison and compared with LEVEL0 results in Figure 5.3.

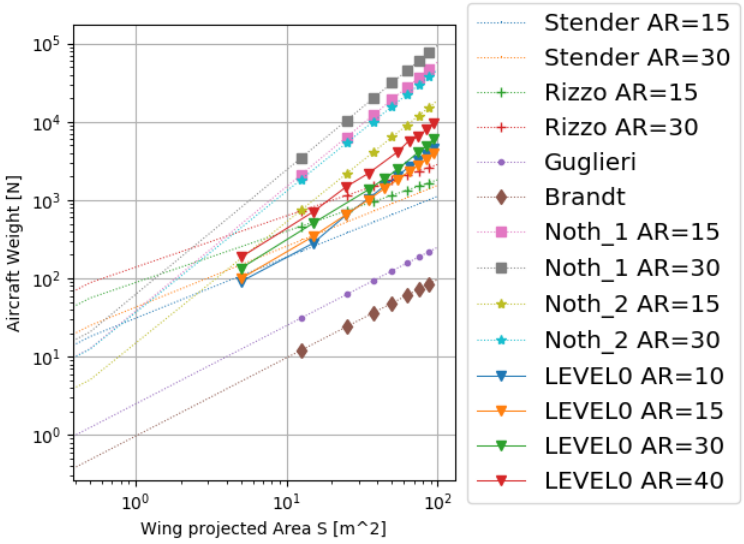

Figure 5.3: Total aircraft weight vs. wing projected area for AR configurations based on differing weight prediction models.

The models by Brandt and Noth mark the outer boundaries of the reference models available, returning a minimum and maximum possible aircraft weight, following the available aircraft weight model range. Figure 5.3 shows that the range of the LEVEL0 weight results fit within the main boundaries of these given models.

The progress of the weight plot for the LEVEL0 model is nearly the same as the Noth model and is closer in range to the upper aircraft weight boundaries. For an increasing AR, the aircraft weight plot shows that a higher AR leads to increased aircraft weight. This effect is based on the higher required cross-section of the wing spar due to moments occurring over span, while the area for the outer foils and the rib volume stays the same, in accordance with the assumptions mentioned in Section 3.4.
The minimum aircraft weight for an aircraft with an $AR = 10$ to $AR = 15$,span $b = 5m$ is tight across $10^2 N$. This result nearly corresponds with that of the Stender model for an $AR = 15$, which is a little lower, or the Noth_2 model for $AR = 15$, which is somewhat higher. Furthermore, the model of Rizzo is close to the result of LEVEL0. The trend continues for different aspect ratios AR as well as wing area S. The models which are closest to LEVEL0 predictions are based on high-altitude aircraft, NASA prototypes and glider aircraft. In general, the LEVEL0 model is within the range of other researcher's models, this result verifies the structural model utilised in LEVEL0.

5.3 Mission Analysis

The mission analysis procedure used in LEVEL0 is relatively unique. It makes use of simplifications on the one hand and includes constant evaluation of effects between irradiation, battery mass and altitude profile on the other hand. Nevertheless, it would be useful to have some comparisons with already known data from other authors. Therefore, an example mission is compared to a parameter study conducted by Schopferer in [8] Since this also includes a result calculation conducted by LEVEL0, this can also be seen as a first example.

It is important to note that the parameter study by Schopferer shows highly estimated values, following [8]. The study was meant to reflect the behaviour in different situations, rather than a reliable result. Nevertheless, the results can be compared to identify differences in results and behaviour. Especially because these platforms are still not fully researched, there is rarely any data available.

In the parameter study from [8], aircraft mass and geometry parameters are fixed, while the mission has been computed and optimised using a 3D trajectory analysis by Schopferer. The main difference is, as mentioned in Section 2.1, that LEVEL0 introduced an altitude and time-based analysis with a performance estimate, reducing CPU time required. In contrast to the parameter study conducted by Schopferer, LEVEL0 always tries to find the lowest possible aircraft mass. The specifications of the aircraft and mission to be analysed are appended in Table C.4. The aircraft is analysed for the following locations, taking place in June.

- Andoya, Norway (69° latitude)
- Brunswick, Germany (52° latitude)
- Dubai, United Arab Emirates (25° latitude)

The results in Table 5.1 put the different results into perspective.

Maximum Altitude [m]	Solar Cell Coverage [%]	Line Nr. [–]	Position [–]	Latitude [°]	Aircraft Mass LEVEL0 [kg]	Battery Mass LEVEL0 [kg]	Battery Mass Schopferer [kg]	Difference [%]	Battery mass LEVEL0 [%]	Battery Mass Schopferer [%]
20000	50	(1)	AN	69	54	7.61	7.32	8.81	13.8	9.15
		(2)	BS	52	76.63	21.93	18.64	15.0	28.2	23.3
		(3)	DU	25	94.97	29.99	27	9.97	31.2	33.75
	90	(4)	AN	69	50.93	4.28	1.24	71.13	8.3	1.55
		(5)	BS	52	71.89	18.45	11.6	37.13	25.3	14.5
		(6)	DU	25	81.01	24.53	23.52	4.12	29.9	29.4
17000	50	(7)	AN	69	55.09	8.03	7.32	8.84	14.3	9.15
		(8)	BS	52	78.67	23.12	18.64	19.38	29.0	23.3
		(9)	DU	25	-	-	27	-	-	33.75
	90	(10)	AN	69	51.09	4.81	1.24	74.22	9.2	1.55
		(11)	BS	52	74.78	19.88	11.6	41.65	25.2	14.5
		(12)	DU	25	-	-	23.52	-	-	29.4

Table 5.1: Aircraft parameter comparison with parameter study from [8]. Based on a mission in June for an aircraft mass of $80kg$, as appended in Table C.4.

There is a clear difference between the results, as far as the maximum altitude allowed. As can be seen in lines (7)-(12), the results only come close for a mission at a northern latitude and with fewer solar panels. The further south the mission is assumed to take place, the further the results deviate. Further south, the flight phases without irradiation become longer. Therefore, the battery required increases rapidly, influencing the aircraft's mass and feasibility. Even for a mission above Dubai, LEVEL0 fails to result in a feasible aircraft due to the excessive capacity required. Generally, this effect is the same in the results of Schopferer and LEVEL0; the solar cell coverage or flight altitude does not matter. A general difference is that LEVEL0 results in a higher relative battery mass.
After increasing the maximum flight altitude to $20,000m$ in lines (1)-(6), the results look different. As discussed in Section 3.2, LEVEL0 includes an extra margin of altitude to store some potential energy, potentially decreasing the required battery capacity. This effect is reflected in the generally lower aircraft mass results and the less battery mass required. Using this extra energy potential, the results of LEVEL0 and Schopferer approach each other. The resulting aircraft and battery mass of LEVEL0 show that at high northern latitudes, the battery capacity required is very low, also leading to a low aircraft mass. Going further south, the aircraft mass increases, as does the battery mass. However, aircraft and battery mass do not increase at the same rate, which is based on the increasing structural loads to be compensated with increasing battery mass. In general, the results for an altitude of $20,000m$ and a solar panel coverage of 50%, in lines (1)-(3) are very similar to the results of Schopferer, especially for southern latitudes. Another interesting result is the change in results for a solar

panel coverage of 90% in lines (4)-(6). The battery mass of Schopferer for a solar panel coverage of 90% is clearly lower than with a panel coverage of 50%, while LEVEL0 results show a smaller difference. This is an interesting result, as most research showed that the critical component is actually the battery capacity available. The batteries are required to fly through the night. As long as solar cells are sufficient to charge the batteries during the day, there should only be a minor difference in the final required capacity. The change in LEVEL0 may be based on the possibility of holding at high altitudes for longer; furthermore, the larger solar cells enable the aircraft to start climbing earlier the day. Therefore, there is a small difference in required capacity. The assumption is, that this is also the case for Schopferer.

In total, the results show a similar behaviour and are very close to each other, depending on the situation. In this list, another difference of LEVEL0, relative to other projects, comes to an eye. LEVEL0 makes a clear difference between feasible and not feasible configuration, as also the aircraft component strength is constantly evaluated in order to fit the required battery mass. This leads to a changing aircraft mass, while the payload and aircraft size stay the same. With a missing consideration of the required aircraft component strength and storage volume, the aircraft is mostly feasible and a lot of borderline cases will not be noticed. LEVEL0 includes these evaluations and therefore also provides an analysis of aircraft feasibility, which otherwise is restricted.

5.4 Single Aircraft Analysis Procedure

For further examples, the parameter study by Schopferer, shown in Section 5.3, is used for a single aircraft output results within this section. The result output in LEVEL0 utilises a HTML based report. This report includes the most important mission parameters, results and graphically worked out analysis steps, as mentioned Section 4.1.3.

In the beginning of every report, the basic aircraft input parameters are shown, as can be seen in Figure 5.4.

1. Wing Area: 16.67 [m^2]
2. Wing Span: 29.5 [m]
3. Altitude Range: [15000, 17000] [m]
4. Altitude Delta: 200 [m]
5. Velocity Range: [15, 50] [m/s]
6. Latitude: 52 [-]
7. Longitude: 11 [-]
8. Mission Time: ['2018-06-01T00:00:00.000Z', '2018-06-04T00:00:00.000Z'] [date]
9. Time Delta: 1800 [seconds]
10. Maximum G: 1 [-]
11. Propulsion Efficiency: 0.75 [-]
12. Panel Efficiency: 0.2 [-]
13. Panel coverage: 0.5 [-]
14. Energy Density Batteries: 240.0 [Wh/kg]
15. Payload: 1 [kg]
16. Maximum iterations: 50 [-]
17. Maximum error for convergence: 5.0 [%]

Compute aircraft ascend: True [-]
Compute aircraft descend: True [-]
Compute propelled descend: True [-]
Take battery volume into account: False [-]
Take ground loads into account: False [-]
Take maximum possible wing spar into account: False [-]

Figure 5.4: Basic aircraft input parameters.

This helps to identify obvious errors within the input, as well as it identifies the analysed configuration. As there are different cases in [8], the displayed case is based on the a scenario with medium wind speeds and is located in Brunswick, Germany. The results are discussed and compared afterwards, including a result display of the slightly changed scenarios.

A mass breakdown, as displayed in Figure 5.5, is one of the central properties of a solar HALE aircraft.

1. MTOW: 76.63 [kg]
2. Payload: 1.0 [kg]
3. Battery Mass: 21.93 [kg]
4. System Mass: 8.0 [kg]
5. Wing Mass: 32.97 [kg]
6. Fuselage + Tail Mass:13.73 [kg]
7. ---> Wing Loading: 4.6 [kg / m^2]

Mass penalty: 0 [kg]
Mass scaling factor: 0 [-]
Drag scaling factor: 0 [-]

(a) Table of resulting absolute component masses and option indicators for penalty or scaling factors.

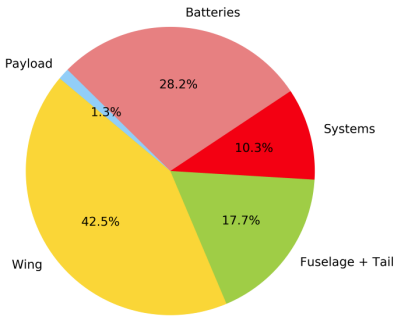

(b) Mass diagram showing the relative mass amounts of the main components.

Figure 5.5: Mass results based on single aircraft analysis.

The proportional battery mass is a particularly important factor in comparing two aircraft with each other. The first thing to notice is the large relative amount of battery mass. In accordance with different studies such as [8, 1], this large amount can be expected for an aircraft flying at $50° - 60°$ latitude. Battery mass is thus a main aircraft mass component in these latitudinal oper-

ation areas. As previously discussed in Section 5.3, this result is similar to the assumptions made in [8].

The aircraft geometry is based on the input parameters given to LEVEL0 – the aircraft wing span and wing area. Using these values, LEVEL0 estimates a total aircraft geometry based on discussed theory in Section 3. The input geometry and the geometry assumed by LEVEL0 are always shown to give a rough overview of the aircraft geometry result, such as in Figure 5.6.

1. Wing Area: 16.67 [m^2]
2. Span: 29.5 [m]
3. MAC: 0.57 [m]
4. Aspect Ratio: 52.2 [-]
5. Fuselange Length: 12.33 [m]
6. Profile: PF25
7. HTail Area 0.55 [m^2]
8. HTail Span 4.13 m
9. HTail MAC 0.13 [m]

(a) Table of geometric parameters for final LEVEL0 configuration.

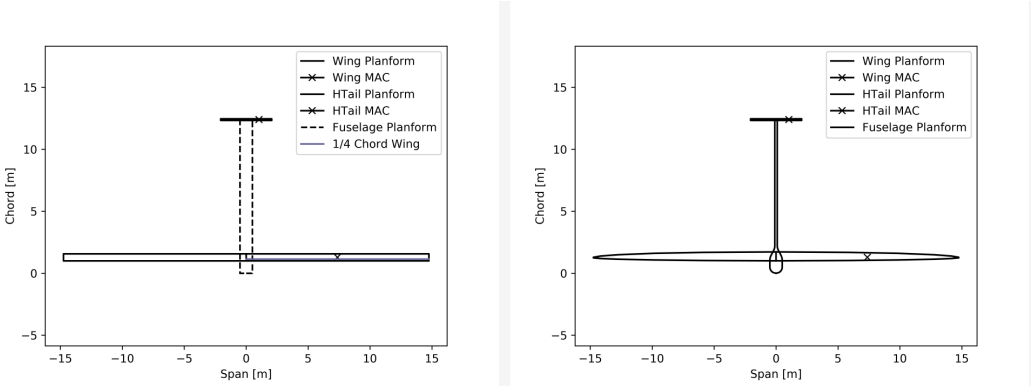

(b) Input geometry for LEVEL0 versus geometry assumed in LEVEL0.

Figure 5.6: Geometric data utilised in LEVEL0.

For this analysis, the following plots in Figure 5.7 may be the most interesting. They show the progress of aircraft altitude, power harvested, energy stored and the power deficit. These basic parameters represent central elements of aircraft performance defined over mission progress, as discussed in 3.2.

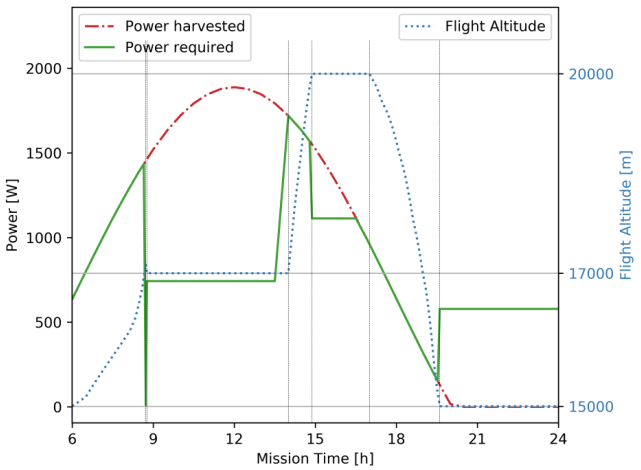

(a) Power required versus power harvested

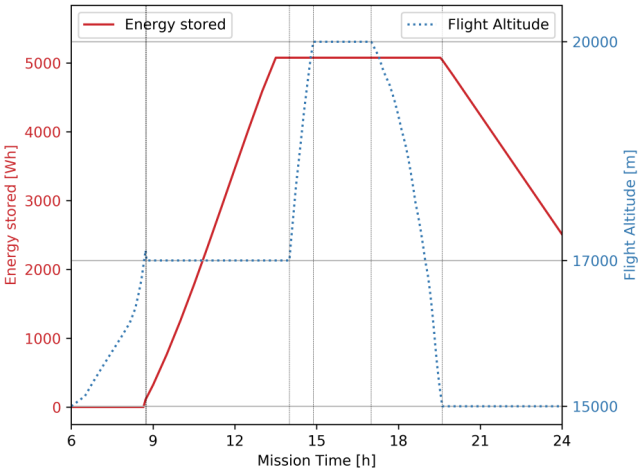

(b) Energy stored

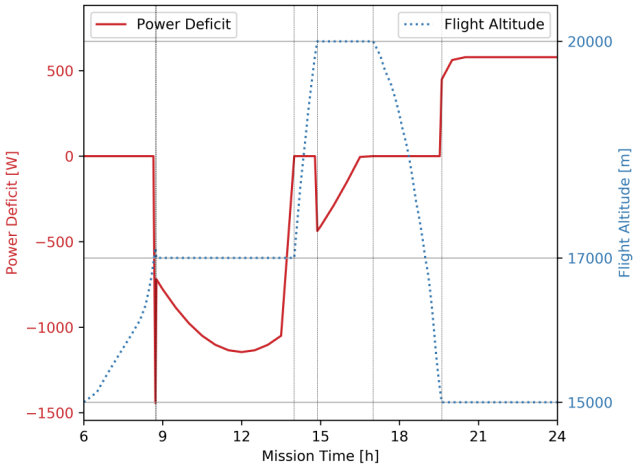

(c) Power deficit

Figure 5.7: Power balance during a day of flight, as analysed by LEVEL0.

These plots reveal the algorithm's behaviour computing the assumed descent

and ascent rates of the aircraft. A detail that may attract attention is that the aircraft altitude always somewhat lags behind the power required and power delivered. This is based on the analysis algorithm and follows a time-based analysis logic, thus having no negative influence on the results of the analysis.

The first plot in Figure 5.7a shows the power harvested, the flight altitude and the power required. The relation between the power delivered and power required is one of the main relations which contribute to mission success. The aircraft directly starts climbing as soon as the power required is higher than required for level flight. This is also the selected start point of the displayed plots. As the total harvested energy is used, $P_{def} = 0W$, and, thus, no energy is stored at this point. The aircraft climbs to the defined altitude of $h = 17000m$. Upon reaching the defined altitude, slight oscillation can occur around the target altitude, as is also visible in the plots. The aircraft then starts to hold its altitude. This results in a decreased P_{req} in Figure 5.7c, leading to $P_{def} \leq 0$ in Figure 5.7c, while P_{av} still increases. Therefore, there is overshoot power, which is used to load the batteries, as is shown in Figure 5.7b. Because of $P_{req} \leq P_{av}$ at full battery capacity, the algorithm choses to use overshoot power for further energy storage. The stored energy E_{bat} in Figure 5.7b does not change at this point. The aircraft climbs, such that $P_{req} \leq P_{av}$, and stays at the maximum allowed altitude until $P_{av} = P_{req}$. When $P_{req} = P_{av}$, the aircraft starts to decrease in altitude, such that $P_{req} = P_{av}$. This can happen in propelled descent or pure gliding flight, dependent on P_{av}. At the lowest allowed altitude, the aircraft starts with battery-based level flight. Therefore, $P_{def} \geq 0$ and E_{bat} decreases with time. This is an actual example based on a parameter study from literature, which showed progress close to the described theoretical optimum in Section 3.2. The figure describes the altitude progress and also graphically describes the difference in the parameter study between a maximum altitude of $17,000m$ and $20,000m$, as found in Table 5.1. The rate of climb can be limited using the user inputs, based on the maximum climb angle. Both values are therefore displayed in Figure 5.8. This way, the user can see an overview of the aircraft behaviour and if all boundaries are adhered too.

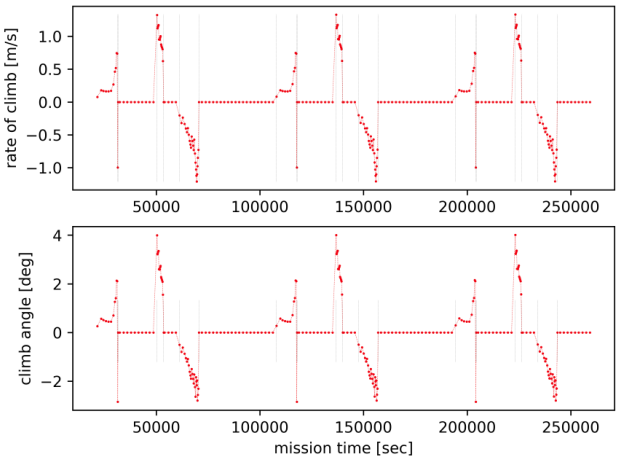

Figure 5.8: Rate of climb and rate of descent history during a three-day mission, as analysed by LEVEL0.

As previously mentioned, wind speed is an important variable for the mission success. The wind speed at the specific altitude is defined by the user. At high altitudes, wind speed normally increases and can therefore limit the aircraft speed minimum used for aerodynamic and structural analysis reasons. In Figure 5.9, the aircraft velocity is clearly higher than the wind speed. Therefore, wind speed is not a limiting factor, and even slightly higher wind speeds would not have any influence on the result.

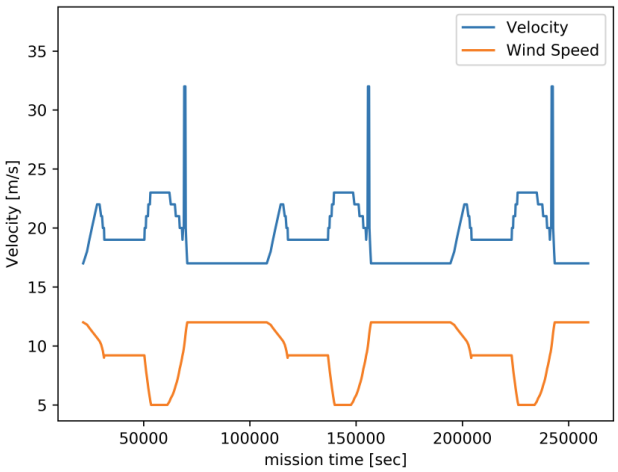

Figure 5.9: Wind speed versus aircraft speed over mission time as analysed by LEVEL0.

The final convergence history in Table 5.2 gives an overview of the mass history during iterative mission analysis. The first iteration is completely based on the assumed values for such an aircraft, the battery and the aircraft mass are adapted iteratively to the required battery capacity. Based on input parameters, these iterations are stopped if all conditions succeed and the aircraft mass

converges within the defined error. In this successful case, the aircraft can fulfil all boundaries and is thus a feasible aircraft. This means that the aircraft spar, which uses a defined volume within the wing, can carry wing loads. All other parameters are also suitable based on the conditions considered in Section 3 and Section 4.

Iteration nr. [−]	Total run time [s]	Aircraft mass wo bat. [kg]	Bat. mass out [kg]	Aircraft mass out [kg]	Battery capacity required [Wh]	Irradiation power capacity [Wh]	Battery capacity out [Wh]	Mass converged [−]	Aircraft feasible [−]
0	25.83	50.58	14.02	64.6	3364.86	18583.34	3364.86	0	0
1	29.61	52.53	17.72	70.26	4253.72	18632.18	4253.72	0	0
2	54.85	53.99	21.16	75.15	5078.02	18676.81	5078.02	0	0
3	86.33	54.7	21.93	76.63	5262.26	18690.92	5262.26	1	1

Table 5.2: Aircraft parameters for comparison with [8]

This report shows the result of the comparison analysis based on the example discussed earlier in Section 5.3. How the results of other methods compare to those of LEVEL0 have already been illustrated. The output files show what happened during the mission and if these results can make sense. It can also help to determine at which points during the mission the critical points appear.

As the CPU time required is an important argument for LEVEL0, this may not be neglected. For a single aircraft analysis like this, LEVEL0 takes about five minutes in an optimal case. This means, that all aerodynamic and irradiation values have been computed and stored before, such that they just have to be loaded and utilised. If this is not the case, LEVEL0 can require between thirty minutes and probably an hour for a complete analysis. However, this is still faster than a full three-dimensional trajectory analysis, requiring about 24h+ for a single analysis. These values are based on test on an Intel i7-6700HQ mobile processor using a single thread. For the analysis of multiple aircraft, LEVEL0 utilises multiple threads.

Another important result, which was already mentioned earlier, is that the aircraft's mass and battery are not limited by the energy which can be harvested. The limitation in this case is the number of batteries required to fly through the night. In Figure 5.7c, it can be seen that the maximum battery capacity was already reached mid-flight. Still, the battery is – per implemented definition – completely drained overnight. Therefore, in other cases, the battery could also be a limiting factor. This has also been shown in Table 5.1, where a reduction in solar cells did not change the aircraft's mass by much.

5.5 Multiple aircraft comparison procedure

The single aircraft analysis in Section 5.4 was computed following the configuration given in [8]. This configuration was set up based on a fixed aircraft mass and uses fixed components as an example for analysis. However, is it actually the optimal solution, or is there a better alternative for a flight above Brunswick, Germany? This question could also be asked for other example configurations, but the procedure is the same; therefore, this has been selected as an example.

Configuration Comparison - Aircraft Mass

The aircraft configured with a $MTOW = 80kg$ has been estimated using the values in Table C.4. These values fix the aircraft's geometry and thus the LEVEL0 result. Nevertheless, it is not clear whether these values are optimal or if there is a better alternative. Therefore, the following example shows an automatic comparison for a similar aircraft, based on Table C.4 for variable parameters in Table 5.3.

Name	Value	Unit
Aspect Ratio	20 to 52.5	-
Span	7.5 to 35	m
Airfoil Wing	PF25	-
Altitude Profile	15000, 1700, 20000	m
Time of the year	01.06.2016 - 03.06.2016	-
Maximum load factor	4.5	-
Specific battery energy density	240	Wh/kg
Solar panel efficiency	0.25	-
Solar panel coverage	0.9	-
Payload mass	10	kg

Table 5.3: Table of aircraft configuration parameters used for an aircraft comparison example, based on Table C.4.

The aircraft in Table 5.3 includes varying aspect ratios and a range of air craft wing spans. Therefore, the "Experiments"-level creates a batch of aircraft configurations, using different span and aspect ratio combinations, to identify the lowest mass possible with the given parameters. In reality, the solar cell efficiency can reach up to $\eta_{solar} \approx 25\%$, and the battery energy density of $\omega = 240Wh/kg$ has been reached in demonstrator aircraft. In contrast, a payload mass of $m_{pl} = 10kg$ could inherit a camera or communication module, while the assumed load factor has been chosen based on an educated guess. The deployment area and the time of flight have nonetheless been chosen to begin in June above Brunswick, Germany.

The results of this analysis are broken down to the basics and displayed in Figure 5.10. In this plot, the final aircraft mass after analysis is compared to those of all configurations from Table 5.3 related to aircraft span and AR. The combinations which led to an unfeasible approach were blanked out automatically, as the resultant aircraft mass would not have been comparable.

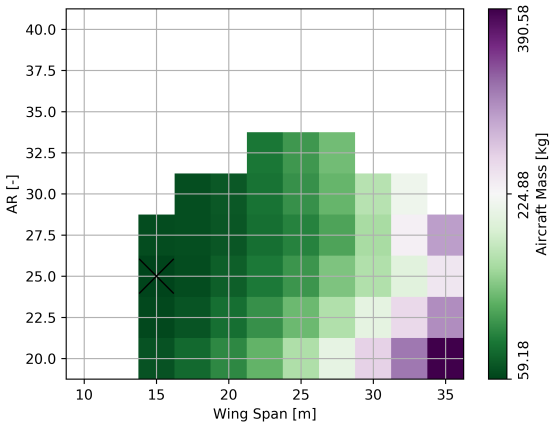

Figure 5.10: Mass of aircraft configurations based on the parameters of Table 5.3 including converged (coloured) and non-converged (blank) results.

Due to an increased maximum load and payload, the example configuration discussed in Section 5.4 is not feasible under the chosen conditions in Table 5.3. To obtain a more realistic aircraft, the results in Table 5.3 used realistic values for load factor and payload. Otherwise, all parameters were set in line with earlier research and can thus be achieved. For an increased maximum load and payload, the optimal solution was marked as $b = 15m$ and $AR = 25$ in Figure 5.10 with $\approx 60kg$.
The result seems rather lightweight for an aircraft of this size, but compared to other known estimation systems for high-flying autonomous aircraft in Figure 5.3, they are within range of estimations and the outer boundaries. The best possible aircraft configuration results according to Figure 5.10 mostly have a higher aspect ratio and smaller wing span.
An aircraft with a much higher AR would reduce wing volume, which reduces storage volume for batteries. A large aircraft span leads to forces far away from the aircraft fuselage substantially influencing the wing spar construction. Therefore, under the conditions given in Table 5.3, LEVEL0 results tend to reduce the wing span and AR in comparison to the example in Section 5.4.

Configuration Comparison - Weighted function

The earlier result showed, that it is possible to use a fixed specific battery energy density to compare different aircraft. However, as seen in Section 4.4, this is not always possible. In Figure 5.10, many configurations do not converge and therefore do not deliver a feasible and comparable result. Consequently, the example from Table 5.3 has been reused, and a variable value of $240Wh \leq \omega \leq 500Wh$ has been applied. As in this case ω is not constant, the aircraft mass is not the only quality parameter to be used. As already mentioned in Section 4.4, a weighted function is applied for aircraft assessment. The weight has been chosen in favour of ω with a value of 80% in Figure 5.11c. This choice is an example and is based on the thought, that a more efficient value for ω can only be reached with high expenses, and thus keeping this factor as low as possible is desirable. Exemplary results are shown below in Figure 5.11.

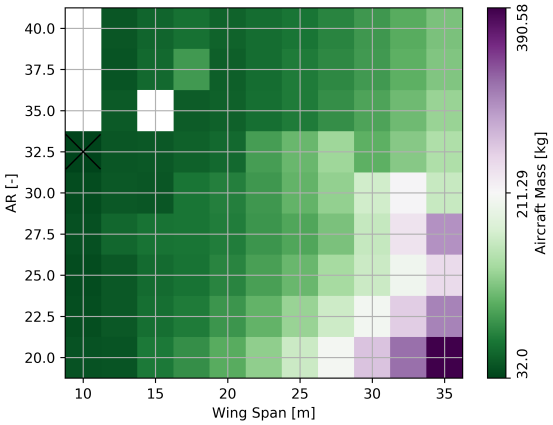

(a) Aircraft mass

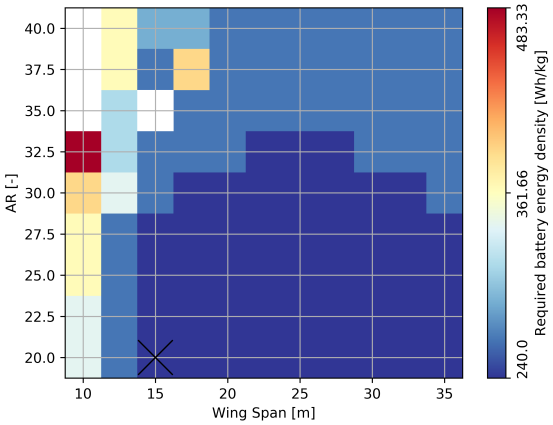

(b) Specific battery energy density

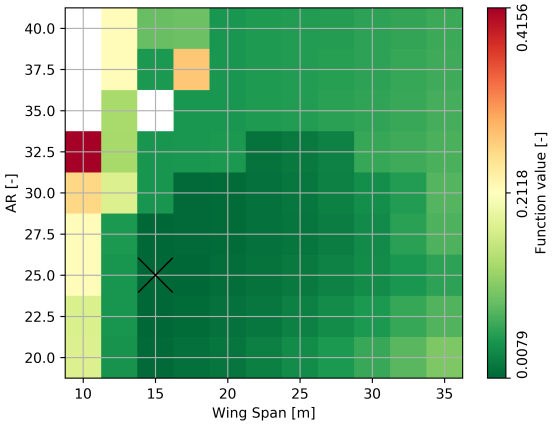

(c) Weighted function value of $f(x) = 0.8\frac{\omega-240}{\omega_{max}-\omega_{min}} + 0.2\frac{m-m_{min}}{m_{max}-m_{min}}$ based on aircraft mass in Figure 5.11a and aircraft specific battery energy density in Figure 5.11b.

Figure 5.11: Aircraft comparison based on variables of specific battery energy density ω based on Figure 5.10, with reduced range of AR and wing span.

As has been seen in Figure 5.10, for a fixed battery energy density, the aircraft mass increases with a larger wing span and a lower aspect ratio. This is based on the increased number of batteries required for lower aspect ratios and the related aerodynamic efficiency of the aircraft. A large wing span and a low aspect ratio increase the amount of material required and therefore the aircraft's structural mass.
In Figure 5.11a, the aircraft mass is related to aircraft wing span and AR. The results basically show the same trends as in Figure 5.10. The aircraft mass increases with a larger wing span and a lower aspect ratio. This time, the aircraft which were not included earlier have been included. With increasing wing span, the mass and moment exerted on the wing spar increase, thereby increasing the wing spar mass. A low aspect ratio also implies a high amount of material required as the wing surface increases. However, more importantly, a large wing span also leads to a less favourable lift-to-drag ratio and thus also increases the number of batteries required due to required energy, which again has a negative influence on the wing spar mass. As induced drag proportionally decreases with increasing AR, lower wing AR leads to a larger number of batteries required and is therefore less favourable. It is important to note that nearly all aircraft show a possible result. Thus, even the aircraft configurations which returned an "empty" result in Figure 5.10 contain a possible result. Thus, in this case, if only looking at the aircraft mass, a minimal wing span and a high AR would be the favourable result.

In Figure 5.11b, it is evident that the minimum required specific battery energy density is related to aircraft wing span and AR. As the lower boundary for ω is the same as what was already used in Figure 5.10, these results also show the same result for $\omega = 240Wh/kg$. The other configurations, or combinations of wing aspect ratio and span, are basically the results which were neglected in Figure 5.10. These aircraft configurations would require a higher battery energy density $\omega \geq 240Wh/kg$. As mentioned in Section 4.4, this implies a less favourable aircraft performance but makes these aircraft configurations also comparable.

Combining the results from Figure 5.11a and Figure 5.11b, Figure 5.11c displays the result of a weighted function. Such a function includes aircraft mass along with the battery energy density ω and results in a weighted compromise from the two chosen criteria. This can help with multi-objective optimisation of the given specifications to identify a better aircraft configuration which may include other quality criteria.

Geolocation Comparison

Another question would be at which other scenarios, locations or dates the chosen aircraft with a span of $b = 15m$ and an aspect ratio $AR = 25$ can be deployed. This can broaden the scope of the use of a single aircraft configuration, reducing costs through reuse over alternative scenarios around the globe. Consequently, a parameter configuration can be tested for alternative deployment possibilities. The incoming irradiation is the determining factor; thus, the result should coincide with the solar irradiation and the day-night rhythm at the particular location. An exemplary result, based on the given configuration, is displayed in Figure 5.12. It is important to note here that whether this test is conducted on an existing aircraft or for parameters in LEVEL0 makes a difference. An existing aircraft has a specified structural mass which is not changed for a new battery mass and is not built to carry extra mass. A parameter configuration in LEVEL0 has the optional possibility of switching off the re-evaluation of aircraft structure with changing battery mass, but normally, a change in battery mass introduces an adaptation of the required aircraft structure. Thus, the informative value is based on the chosen input in LEVEL0. In the following results, the aircraft structure is re-evaluated.

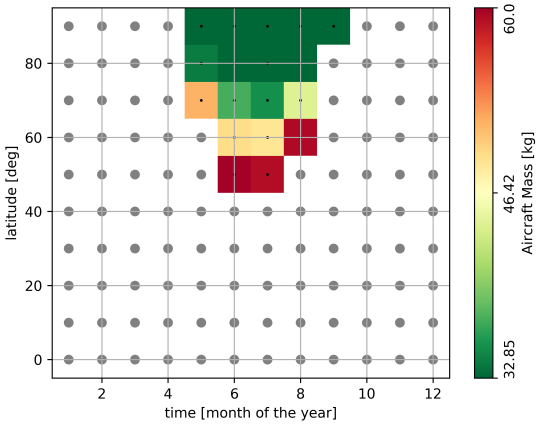

(a) Based on resulting aircraft mass.

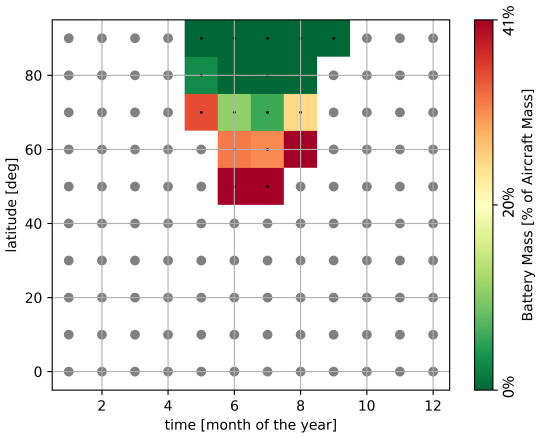

(b) Based on resulting partial battery mass.

Figure 5.12: Possible deployment area of a solar aircraft based on the found ideal configuration with $b = 15m$ and $AR = 25$, based on Table 5.3.

With an area of deployment for an aircraft based on the same wing planform from Table 5.3, Figure 5.12 shows that the same aircraft can only be used in areas with higher or more constant irradiation than the original deployment area. An influence on battery mass can simultaneously be observed.

The time of year on the x-axis is defined as the period between the first and third day of each month through the whole year, which also explains some asymmetry in the results, as the irradiation level is based on the Earth's position relative to the sun. Between May and September, it is summer in northern latitudes, which means a constant irradiation or extremely short nights. With these northern latitudes, the battery mass decreases to $m_{bat} = 32,85kg$ in Figure 5.12a. Theoretically, it is possible to reach a minimum battery mass closer to $0kg$ in absolutely perfect conditions at 90° northern latitude, as there is always

irradiation available.

The amount of energy which needs to be stored thus increases when going further south. The total aircraft mass in Figure 5.12a increases up to $m \approx 60kg$ at a latitude of 50°. This is close to the computed optimal aircraft mass of $\approx 60kg$, at a latitude of 52°, which was previously computed in Section 5.5. The large total aircraft mass is mainly based on the required battery mass. Therefore, the relative battery mass required increases in the south, as illustrated in Figure 5.12b. The required battery mass below 50° in southern latitudes is excessively high for convergence.

Chapter 6

Conclusion and Outlook

The analysis processes and the referring implementations discussed within this thesis, are part of the development of a design and assessment process for simple and fast solar HALE aircraft configuration evaluation.

Research Questions and Summary

The parameters and requirements for a solar HALE aircraft platform are based on a minimum weight aircraft with an optimised aerodynamic performance for low speeds, while all parameters are sized based on the battery required. The battery required must be sized according to the defined mission and individual irradiation profile over time, which results in a constantly evaluating aircraft sizing process. The required analysis methods, like aerodynamics, structural analysis, mission analysis and an irradiation module can be implemented into a tool for automated analysis and assessment of solar HALE aircraft. The software-based process must be able to analyse a broad range of aircraft parameter configurations and deliver comparable results in any case. Furthermore it must include mechanisms required to estimate aircraft and performance data not given by the user.

It is important to consider what is required in terms of input and estimated data to model a solar HALE aircraft. Such aircraft relies on solar energy, which requires it to be a low-speed, efficient and lightweight aircraft.
In this field, several authors have proposed the use of a glider-like aircraft. Therefore, the aircraft structure can be estimated to be similar to a glider aircraft, which allows a possible estimation of the aircraft structure. The aerodynamics must be close to an optimal aircraft, therefore an elliptical lift distribution can be assumed, with small efficiency factors. For the mission, the lateral motion has less impact on performance than the altitude profile. Therefore, the general altitude profile can be estimated based on the optimal energy preservation scheme possible. Furthermore, the altitude profile can be adapted to the available irradiation, based on location, altitude and time.

Consequently, only a few parameters are required for a minimum input. The required payload data and the general mission location, date and altitude boundaries. All other data can be estimated using handbook formulas for aerodynamic forces or structural analysis, while aircraft geometry is assumed using earlier research data.

With the above described data, it is possible to perform an estimation of missing parameters, used for an analysis process of a total aircraft. Earlier research either included a simple analytic approach or a CPU intensive 3D mission analysis approach, as mentioned in Section 3.2. The chosen process in Section 3.2 is optimised to save required calculations, by using an intermediate process based on a time-based altitude profiles, using aerodynamic and structural assumptions and performance estimates. The altitude profile reduces the required DOF and therefore the CPU-time, while keeping the correlations between the aircraft components. The aerodynamic theory is based on the assumption of an elliptical lift distribution, applied to an electric glider-like high-AR aircraft. Using this estimation the basic performance coefficients can be computed for a 2D-airfoil, and applied to a 3D-wing using handbook formulas as in Section 3.3.1. The required structural theory is based on the assumption of a glider-like aircraft. The relations between wing, fuselage and tail size can be evaluated using statistical data of other aircraft and handbook formulas, as mentioned in Section 3.1. By assuming a light-weight aircraft, several components can be chosen normally used for glider aircraft or even human powered aircraft. Further, the required structural component sizing, like the required wing spar dimensions, can be estimated using the exerted aerodynamic forces. The required mission analysis can now utilise these aircraft theory components, together with irradiation theory in accordance with [14]. The mission profile of a solar HALE aircraft is based on maximum energy preservation using altitude boundaries from [8], based on wind speeds and optimum irradiation income. The theoretical aircraft analysis can run through an optimised altitude profile, based on the irradiation available over time. The aircraft parameters during this analysis can be used within an iterative sizing approach, sizing the aircraft structural components and battery required until convergence occurs. The results can be used for further evaluation and display the required aircraft parameters and estimated performance during mission.

The final analysis process for solar HALE aircraft, is the implementation of the abovementioned process into a software-based tool. This tool is based on a three-level-structure using an object oriented approach. This approach has been chosen for modularity as well as fast and structured data access.
On the lowest level, the corresponding theory of aerodynamics, structural analysis and irradiation analysis, is implemented into independent modules. These modules are used by an aggregation ("Aircraft Assembly") in order to fulfil the mission analysis for a single aircraft. This is the "Core"-level, described in Section 4.3. Apart from the mission analysis process, the aerodynamic analysis is

strongly optimised for a fast and robust analysis process. XFoil is used as a basis for the 2D airfoil analysis, as it is a verified and robust tool, which is also able to compute small Reynolds number $Re \leq 50,000$. The required CPU time of an XFoil- analysis can not be reduced, but LEVEL0 decreases the required calculations by using interpolation techniques, aerodynamic performance maps and performance databases, as described in Section 4.3.2. Another module optimised for a low CPU-time is the irradiation analysis, based on [14], as it has been equipped with a database and an interpolation algorithm in order to deliver results instantly instead of requiring CPU time during a LEVEL0 analysis.
The upper levels "Battery Evaluation" (Section 4.5) and "Experiments" (Section 4.6) include all required tool functionalities to set up experiments and comparisons, while it uses the "Core"-level for all mission and aircraft analysis functionalities.

The verification of all included processes and modules returned single digit errors for the single theoretical modules in Sections 5.1 to 5.2. Comparing the final tool results with parametric studies from [8] in Section 5.3, showed similarities as also differences. The systemic trends are comparable, while the results deviate strongly for more challenging mission definitions, as above northern latitudes. Possible causes for this are the constant evaluation of the batterie mass required and the referring structural aircraft components to carry the battery mass for the defined mission. Further result evaluation included a detailed single aircraft analysis and comparison between different solar panel mounting approaches. LEVEL0 was able to find the boundaries of technical feasibility and show differences between the different approaches, while finding the same correlations between parameters as expected from [2, 8]. Therefore, this thesis's approach is able to add value to the known tools and methods, while questioning other results.

Findings

The correlations between the mission altitude profile, irradiation and aircraft parameters had a more significant influence on the final results than expected from earlier research. The difference between the results in this study and the results from the literature was significant in some areas, as mentioned in Chapter 5. The technical feasibility for a solar HALE aircraft have boundaries based on today's battery technology. LEVEL0 clearly draws a line for multiple scenarios and shows the differences between different solar panel mounting technologies, as well as limits of older research. While on the other hand, the adaptability of parameters enables to find the best configuration possible for each scenario, independent on today's technology. This means that the overall theoretical approach of LEVEL0 returns valuable results. This approach approximates a

full 3D analysis, requiring much less CPU time (based on Section 5.4 about a minimum factor of twenty-four) and still delivering a clear estimation of aircraft performance. However, it was not expected that all connections of the various parameters could cause so many exceptions and cases to be considered for a flight. This has been compensated in LEVEL0 by spending a lot of attention to exception handling and data consistency, keeping the tool's approach robust and reliable.

Impact

The results of this thesis include several ideas and approaches which can help in future solar HALE projects. Most projects today are based on first prototypes and ideas, as mentioned in Chapter 1. But as the battery management and and flight path management are interdependent and unknown in advance, the potential performance of these platforms is unknown. The chosen approach can help to further assess the potential for different parameter combinations, missions and use cases, as shown in the example in Section 5.5. If the solar HALE aircraft is unknown until that point, this study's approach can help to conduct a rapid aircraft sizing and battery capacity estimation for the desired mission. However, the analysis process from this study can also be adopted for and incorporated into a new assessment or optimisation tool. The altitude-profile based approach, in particular, showed that it is capable to be used for aircraft performance estimation, while using less performance than known 3D approaches like Schopferer. Additionally the iterative approach, in combination with the chosen quality paramters (Section 4.4) also evaluates boundaries for parameter configurations and trends for all aircraft sizes, which also adds value to this process and for future HALE aircraft designers.

Further, based on the results for solar HALE aircraft examples in Chapter 5, different recommendations can be made to solar HALE aircraft designers. In general, the technological bottleneck for these aircraft is the battery capacity available in relation to battery mass. The solar cells required do not have a significant influence, as this study revealed in Section 5.5. Under the assumed conditions, modern solar cells are in general efficient enough to power aircraft. An important factor related to the solar cells is their integration into the aircraft's structure to keep their structural performance.

Limitations and Outlook

Despite all advantages, the process and the resulting tool presented within this thesis have several limitations.

Even though Section 5.2 showed agreement with other weight estimation modules, there is a big necessity for validation and calibration data for a more detailed method. Due to the high dependence on the weight estimation model, small changes in aircraft weight already have a high influence on result feasibility. The chosen approach is based on many assumptions and estimations from earlier research. A more sophisticated weight estimation model would have a huge influence on result precision and usability for future projects. Further, there is a need for validation and calibration data for the total aircraft. Most research for solar HALE aircraft is based on either small demonstrators showing concepts, as in [2], but never working at high altitudes, or theory-based approaches, as in [8, 13], with a lot of estimations or assumptions used. Also as there are big uncertainties, leading to wide-spread results, this further shows the necessity for further research in this sector.

The software-tool is based on an idea to model and assess a wide range of aircraft sizes, missions and also aircraft configurations. The ability to model a wide range of aircraft sizes and missions already substantially complicates the required analysis methods. LEVEL0 enables the user to model every size desired, also enabling for some changes of the configuration, while delivering a comparable result for all given inputs. To increase the use cases of LEVEL0, additional versatility in the implemented modules would be valuable.

The chosen mission analysis approach involves a constant evaluation of all aircraft components. Additionally, the mission analysis can return a divergent or infeasible aircraft approach, while still being able to compare those infeasible parameter configurations by using ω for compensation. The chosen aircraft performance estimation approach is also faster than a full-scale analysis of a single aircraft. With this in mind, against the background of the parameter studies shown in Section 5, LEVEL0 can potentially be used for an automated optimisation approach of aircraft parameters. Despite this potential, several attempts with optimisation algorithms showed that, due to non-convergent parameters combinations, big parameter ranges and the required CPU time, LEVEL0 in its current state is not yet ready for a fully automated optimisation. The potential for optimisation could be further improved in future research work. A first step would be to increase the performance by implementing the process into a compiled language, or simply using a high-speed computation platform in order to find and eliminate optimisation referred problems within the given software tool.

Concluding all results, the tool shows added value compared to research and for potential use in future aircraft and mission design projects. The given process is able to define feasibility and asses and design all given solar HALE aircraft parameter configurations. This is based on the implemented mission analysis process and versatility and robustness of the software tool, enabling LEVEL0 to deliver fast and reliable results. Additionally, due to the given flexibility of the designed tool structure, there is potential for future improvements. Therefore,

this thesis and the resulting software tool deliver a valuable contribution to solar HALE aircraft research.

Appendix A

Theory - Addendum

A.1 Mission Trajectory - Altitude-Profile Assumption

In line with [30], the turn radius of an aircraft flying at $25\frac{m}{s}$ at a bank angle of about $5[°]$ is $R = 730[m]$. As this radius is relatively small compared to the aircraft flight altitude, a bank angle of $\Phi <= 5[°]$ may be assumed for a stationary mission using a circular pattern. Solar irradiation harvest for a simple solar panel can be computed for different mission scenarios using the Brizon's tool, as mentioned earlier. The scenarios are distributed between a latitude of $0[°]$ to $90[°]$, as well as between the different seasons during the year occurring in January, March and June.
This simplified analysis based on the values in Table A.1 shows, that the difference in harvested irradiation is negligible with a difference of maximum $<= 4\%$. Still, the influence is measurable and can thus have an impact on a mission analysis. The power harvested for a simulated circular pattern trajectory (3) over a duration of 24 hours can be compared to the total power harvested in straight flight in (4), resulting in a difference in harvested power between (5) and (6).

However, a constant trajectory flight also influences the power required by the aircraft. The required force has been estimated by evaluating the change in force equilibrium. Depending on aircraft settings, trajectory flight negatively influences the flight performance, resulting in a difference in P_{req} of $g\sqrt{g}$ for the load factor. For the assumed bank angle $\Phi = 5\,[°]$, this results in difference for P_{req} of 0.57%. For other flight modes the difference is negligible due to low bank angle $\Phi <= 15\,[°]$, in line with [31].

(1) Latitude [°]	(2) Month	(3) Total power harvested including trajectory $\left[\frac{W}{m^2}\right]$	(4) Total power harvested in straight flight $\left[\frac{W}{m^2}\right]$	(5) Absolute difference $\left[\frac{W}{m^2}\right]$	(6) Relative difference [−]
0	January	4655.29	4588.44	66.85	0.01
0	March	4909.41	4873.69	35.72	0.01
0	June	4242.07	4343.45	-101.38	-0.02
30	January	2688.34	2612.35	75.99	0.03
30	March	3775.12	3726.15	48.97	0.01
30	June	5244.27	5372.84	-128.56	-0.02
60	January	294.18	282.17	12.01	0.04
60	March	1631.94	1576.13	55.81	0.03
60	June	5190.24	5142.6	47.64	0.01
90	January	0.0	0.0	0.0	0.0
90	March	0.0	0.0	0.0	0.0
90	June	5979.96	5922.87	57.09	0.01

Table A.1: Difference of a mission simulation using a simple trajectory versus a straight flight, measured in total power available during flight.

A.2 Trajectories

Following [8], there are four possible trajectories which have been incorporated into a tool by Simon Schopferer. Based on the operation site, time of day (day or night), altitude and mission duration, wind conditions and determined boundary conditions, the tool tries to identify an optimised trajectory. The trajectories to be examined are shown in Figure A.1 and are described below, as given in [8].

a Simple pattern: Starting with a heading matching the wind direction, a 360° turn is indicated. The driftage is compensated for the following straight leg. This pattern is close to a circular when comparing the solar irradiance incidence angle during flight.

b 8-shaped pattern: At the starting point the wind-relative course over ground is $0° < x_{rel.W} \leq 90°$. A turn is indicated until the negative wind-relative course is reached; this course crosses the start course at about 90°. The driftage is compensated for the straight legs to remain at the same stationary point.

c Meandering pattern: This is a flight with alternating left and right turns against the wind direction. The wind-relative course over the ground is between $90° < |x_{rel.W}| < 180°$. Between the turns, there is a straight leg, which is not used to compensate for the driftage. As the turns are always against the wind, they are used to compensate for driftage. Relative to the surrounding air, the aircraft's trajectory can be described as a meandering flight path.

d Meandering pattern: This pattern is the same as c, just with steeper turns and shorter straight legs.

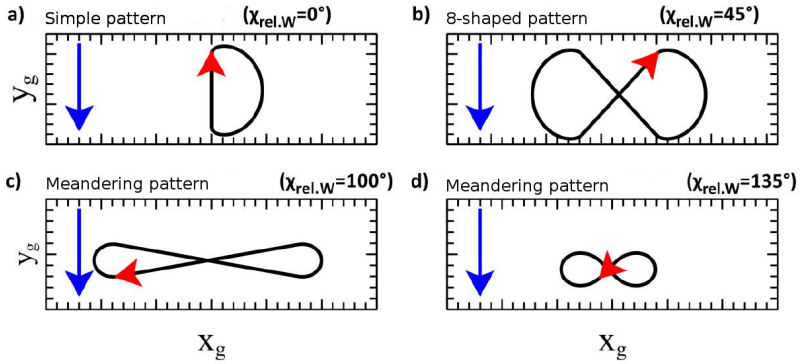

Figure A.1: Flight path trajectories following the concept of Simon Schopferer in [8]

Appendix B

Examples and Verification - Addendum

B.1 Aerodynamics - Interpolation and Verification

For every value requested, LEVEL0 first checks internally stored variables. If results are not available in storage, they are computed using XFoil. However, not all values are computed using XFoil. LEVEL0 evaluates the boundaries and divides them into smaller blocks based on the Reynolds number, using Δ_{Re}, as schematically shown in Figure 4.5. All values requested later which are not included in this aerodynamic performance map are interpolated. The user can influence the interpolation process used in the LEVEL0 aerodynamics module by changing parameters for the interpolation area, displayed in Figure 4.5, or by adjusting the interpolation precision and CPU time. The interpolation can be influenced through adjusting the following parameters.

- Altitude range:
  Minimum and maximum altitude from mission boundaries.
- Velocity range:
  Fixed initial boundaries to be considered, including a minimum and maximum velocity to be taken into account by LEVEL0.
- Minimum Reynolds number to be considered:
  As Reynolds number can become $Re \leq 50,000$, such low Reynolds numbers can cause problems for XFoil. It is therefore possible to choose a minimum Reynolds number, which can increase the minimum velocity computed at low altitudes and therefore reduce the range of possible velocities for the aircraft to be considered and analysed.
- Density of Reynolds number to be computed by XFoil:
  This number is given by a maximum Δ_{Re}. Therefore, between the initial

boundaries of altitude and velocity, the algorithm evaluates the Reynolds numbers to maximise Δ_{Re} between the Reynolds numbers computed by XFoil. Therefore, a lower Δ_{Re} does not change the initial boundaries but increases and condenses the coefficients computed and used for interpolation in between the original boundary values.

The final precision of the interpolation process is mostly influenced by the number of source values viable, based on Δ_{Re}. An example is displayed below Figure B.1.

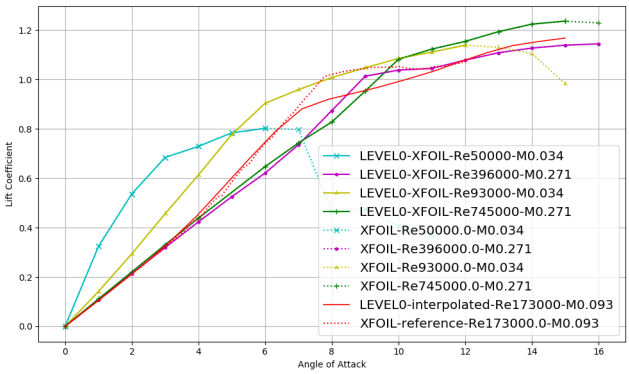

(a) Low $\Delta_{Re} = 10,000$, boundaries set by user.

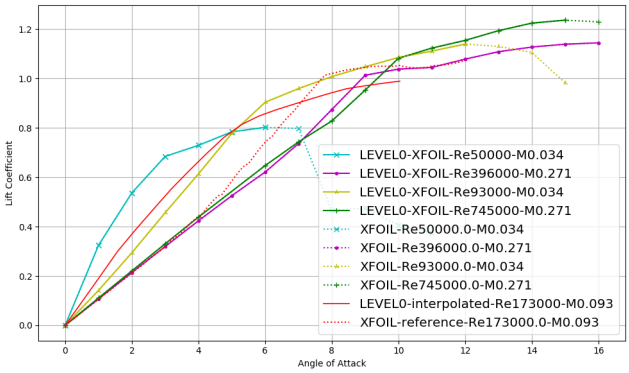

(b) High $\Delta_{Re} = \infty$, boundaries set by source values based on altitude and velocity range.

Figure B.1: Lift coefficient of a NACA0020 airfoil comparison between XFoil and LEVEL0 for source curves and interpolated curve.

An aircraft with a velocity range of $5\frac{m}{s} \leq v \leq 50\frac{m}{s}$ and an altitude range of $15,000m \leq h \leq 20,000m$ has been computed in an exemplary manner in different versions using a NACA 0020 airfoil with an estimated span of $25m$ and a projected wing area of $20m$. The minimum Reynolds number defined is $Re_{min} = 50,000$ for better exemplary results.

The non-interpolated curves from LEVEL0 and from XFoil overlap, which means that the implementation of XFoil delivers correct results. As stated before,

LEVEL0 computes all values between α_0 and $c_{l,max}$ and stops at these points to reduce CPU time. Accordingly, the plotted results reflect this behaviour as all LEVEL0 plots stop at an earlier position.
The interpolated curve for $Re = 173,000$ and $M = 0.093$ have been computed based on different boundary conditions in Figure B.1b and Figure B.1a. In Figure B.1b, the only curves computed by XFoil are the four boundary value-based curves shown within the plot. In Figure B.1a, a value for Δ_{Re} revealed that LEVEL0 does compute coefficients for all Reynolds numbers with a maximum difference of $\Delta_{Re} = 10,000$ between the minimum and maximum Reynolds numbers given. Therefore, this version inherits many more source coefficients to use for interpolation, resulting in higher accuracy in the interpolation. Analysing the interpolated results in Figure B.1b, the result for the interpolates curve shows a low cl_{max}, compared to the XFoil result computed. Moreover, the range for angle of attack α is lower than for the results computed by XFoil. Increasing the density of Reynolds numbers for which the results have been computed in Figure B.1a, this changes. The maximum lift coefficient cl_{max} and the number of angles of attack computed increased as well. The results of the interpolation in Figure B.1a, are much closer to the results directly computed by XFoil. Conducting the same analysis for a range of Δ_{Re} and airfoils revealed an error of $\approx 5\%$ (mostly lower) for $\Delta_{Re} \leq 50,000$ This error is caused by interpolation only and can theoretically be reduced by decreasing Δ_{Re} or disabling interpolation.

This interpolation and aerodynamic calculation process used in this thesis has been further analysed, focusing on complete aerodynamics analysis, rather than on Δ_{Re} and 2D interpolation alone. Using the mission example in Table B.1, some airfoils have been used for verification of the aerodynamic 3D wing analysis process.

Property	Description	value	Unit
velocityrange	Velocity Range	[5,80]	$\frac{m}{s}$
altituderange	Altitude Range	[16000,17000]	m
maxaltitude	Maxium altitude to gather potential energy	20000	m
span	Total wing span	25	m
area	Projected wing area	20	m
ReBoundary	Maximum Δ_{Re} for XFoil source values	10000	–
ReMin	Mimimum Reynolds number to consider for XFoil	50000	–

Table B.1: Essential wing properties used for verification purposes.

The 3D analysis assumes a near optimal elliptical lift distribution. LEVEL0 is meant to be able to compute an arbitrary wing with a broad range of airfoils to deliver a performance estimate to be used in the performance analysis. The desired aircraft specifications are based on glider aircraft, with specific differences. A third-party analysis tool has been chosen, enabling the modelling of a 3D wing and therefore the comparison of the chosen estimation method with a well-proven method. An available and well-proven open-source tool for this use case is XFLR5. XFLR5 is a tool based on XFoil, including different theories,

such as lifting line theory or the vortex lattice method, as stated by [29]. It is safe to assume that the results compared can be regarded as an estimation, which is what is required for LEVEL0. To analyse a 3D wing, XFLR5 delivers different capabilities for this case. A lifting line theory-based approach has been chosen, as it is considered the standard approach with the smallest number of limitations.

The comparison between the elliptical wing assumption in LEVEL0 and the XFLR5 analysis has been made using the same airfoils and parameters as already used for the verification of the 2D airfoil results. The referring airfoils are used on an elliptical wing planform and are exported to be used for 3D wing geometry in XFLR5. The comparison of the assumed results, using interpolated XFoil values from LEVEL0, and the results from XFLR5 are used to verify some exemplary LEVEL0 results.

All airfoil comparisons from Figure B.2 to Figure 5.2 are following the same system.
The lift coefficient for a 3D-wing is derived from the 2D-airfoil lift coefficient using Equation (3.9). This implies that the 3D-wing lift coefficient has a smaller slope than the 2D-airfoil coefficient curve.
For the lift as well as the drag coefficient, the error is computed only for values of α which have been computed by XFOIL as well as by LEVEL0.

The NACA0020 airfoil compared in Figure B.2 has a mean error $\leq 10\%$ and a maximum error of $\approx 17.5\%$, as shown in Figure B.2c.

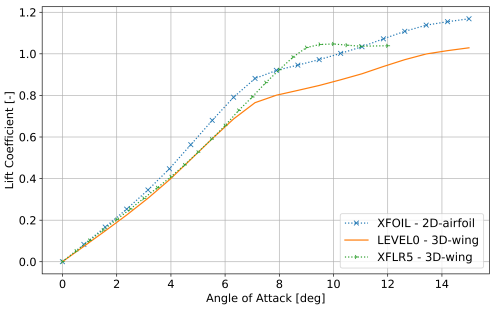

(a) Lift coefficient source and interpolated curve.

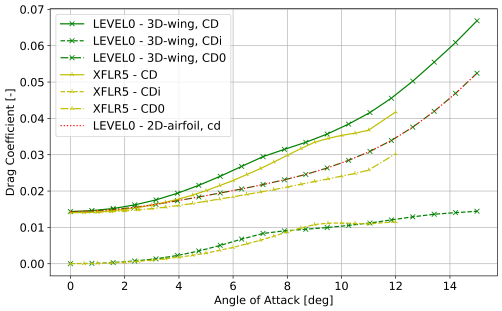

(b) Drag coefficient source and interpolated curve

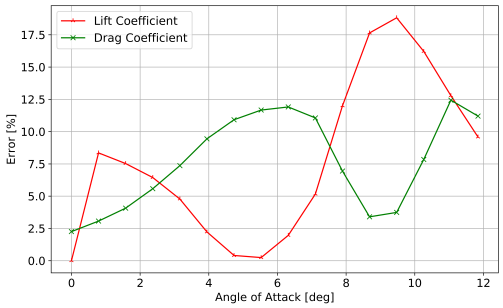

(c) Relative error of interpolated lift and drag coefficient compared to computed XFoil results. (Only results with available α were compared.

Figure B.2: Comparison between XFLR5 and LEVEL0 coefficient curves compared for an elliptical wing using a NACA0020 airfoil.

The high maximum error for the lift coefficient is based on the differing lift slope computed by XFLR5, which shows a lower $C_{L,max} \approx 1.05$ at $\alpha = 9.5°$, while the interpolated 2D coefficients computed by LEVEL0 show a higher maximum lift coefficient of $C_{L,max} \approx 1.03$ at $\alpha = 14.5°$. This is a worst-case scenario for the chosen interpolation method. The source curves show a strong difference in behaviour at higher ranges of α. This means that the final result could use an angle of attack which may be above the α_{stall} computed by XFLR5. This error could be reduced by using a smaller Δ_{Re}, but even in this range, most of the resulting range for angle of attack α can be used to estimate the chosen wing performance. The error in lift coefficient in Figure B.2c increases drastically for an angle of attack $\alpha \geq 8°$. According to most of the analysis results in this thesis, a normal angle of attack for climbing flight should not exceed $\alpha = 5°$. Which then again reduces the used range of angle of attack, and thus makes this still valid for later use. Nevertheless, this clearly shows the

downsides of interpolations for 2D analysis and later estimation of an elliptical wing planform, even if this is an extreme example. In accordance with the supervisor, these results have been claimed as satisfactory.

The verification for a wing using the FXS 02-196 airfoil is shown in Figure B.3.

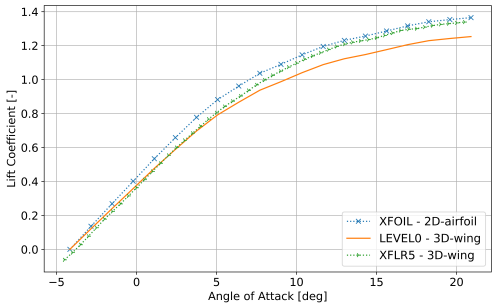

(a) Lift coefficient source and interpolated curve.

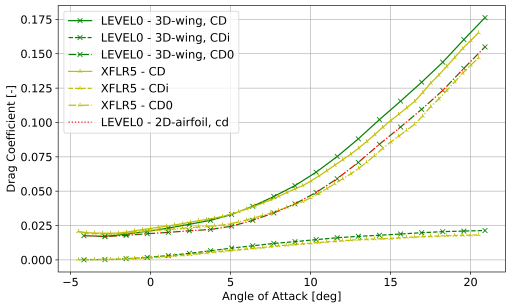

(b) Drag coefficient source and interpolated curve

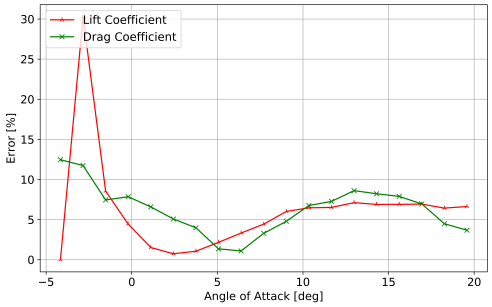

(c) Relative error of interpolated lift and drag coefficient compared to computed XFoil results.

Figure B.3: Comparison between XFLR5 and LEVEL0 coefficient curves compared for an elliptical wing using a FXS 02-169 airfoil.

Figure B.3a shows that the results of the interpolated curve and the reference curve from XFLR5 are closer to each other. Compared to Figure B.2 in this case, the range of angles of attack α is the same. Based on the formulas used, the lift coefficient assumed by LEVEL0 is lower than for a 2D airfoil, which is the intended effect. XFLR5, in contrast, is very similar to the 2D interpolated value of LEVEL0. The drag coefficient shows a low deviation between XFLR5 reference and the results computed by LEVEL0 in Figure B.3b. For both coefficient curves, the error at low angles of attack is extremely high, caused by the small absolute values, resulting in high relative errors. Normally, such low angles of attack should not be required during analysis, as the angle of attack normally is $\alpha \geq 0°$. Thus, these results also can be regarded as valid and usable results.

For the Wortmann FX 60-126 airfoil in Figure B.4, the situation can be described the same way as the previous airfoil assumption in Figure B.3.

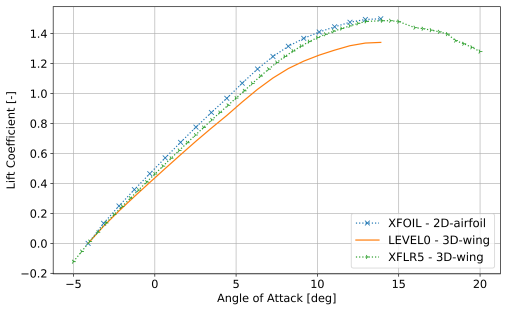

(a) Lift coefficient source and interpolated curve.

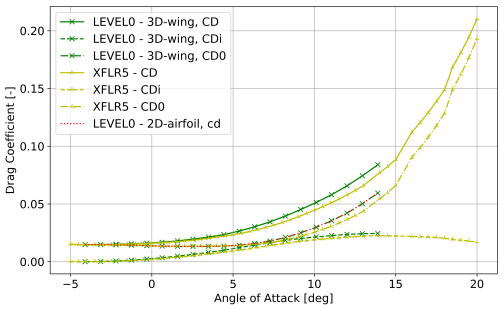

(b) Drag coefficient source and interpolated curve

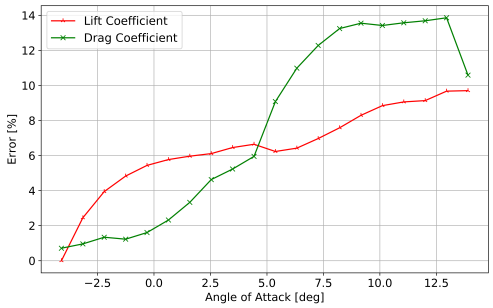

(c) Relative error of interpolated lift and drag coefficient compared to computed XFoil results.

Figure B.4: Comparison between XFLR5 and LEVEL0 coefficient curves compared for an elliptical wing using a Wortmann FX 60-126 airfoil.

The assumed elliptical values by LEVEL0 show a lift curve in Figure B.4a, with lower values for the lift coefficient C_L, and a drag curve, with a slightly higher drag than XFLR5 in Figure B.4b. The only difference in this case is that the error in Figure B.4c shows a much smaller deviation for low angles of attack α, while the error increases for angles of attack $\alpha \geq 5°$. This is based on the deviation in lift or drag slope and in resulting coefficient values close to α_{stall}.

B.2 Mass Analysis

To compare the LEVEL0 mass analysis approach, different aircraft configurations have been tested based on mission specifications from Noth [1]. These specifications do not define specific boundaries. The aircraft is supposed to fulfil a mission profile in the summer at a central German location for a duration

of longer than a day. The specifications for solar cells, propulsion and other parameters have been estimated based on earlier experiments by Noth, the DLR in Brunswick and earlier work regarding HALE aircraft. A mission takes place at about 51° latitude during June. An altitude of between $16,000m$ and $20,000m$ has been chosen, following the general theoretical considerations in 3.2. The aerofoil used for the exemplary aircraft is the "PF25".

The exemplary aircraft configuration is initiated using a mass model based on aircraft wing surface area and aspect ratio. The specified exemplary mission is analysed, and the resulting parameters are evaluated for the partial masses of the aircraft components.
To compare different configurations, even if they do not ultimately converge in LEVEL0, the results have been gathered in Table B.2 to obtain some assumptions for such non-convergent results and create a surrogate model for the chosen example.

	(1) Span $[m]$	(2) Area $[m^2]$	(3) Aspect Ratio $[-]$	(4) Aircraft mass $[kg]$	(5) Battery mass [%]	(6) Fuselage + Tail mass [%]	(7) Wing mass [%]	(8) Payload mass [%]	(9) System mass [%]
(a)	29	42	20,0	279,83	48,73	6,01	38,26	0,36	7,00
(b)	29	33,64	25,0	185,91	37,50	8,18	45,70	0,54	8,62
(c)	29	29	29,0	185,71	39,59	7,85	44,21	0,54	8,35
(d)	29	21	40,0	192,74	42,80	7,19	42,09	0,52	7,91
(e)	29	17	49,5	233,86	46,32	5,84	40,47	0,43	7,38
(f)	20	20	20,0	112,89	49,51	9,43	33,71	0,89	7,35
(g)	20	13,3	30,1	124,92	63,77	7,74	23,06	0,80	5,42
(h)	20	10	40,0	118,74	63,37	7,92	23,19	0,84	5,51
(i)	-	-	-	-	48,95	7,52	36,34	0,61	7,19

Table B.2: Exemplary mass breakdown for several configurations, with minimum assumed payload mass, based on the example for mass verification resulting from LEVEL0 analysis.

For both exemplary aircraft in Table B.2, the total mass *(4)* is reduced while increasing the aircraft AR up to a specific point for *(a)* to *(c)* and for *(f* to *(g)*. The reason for this is the consistent aircraft span *(1)* with a reducing projected wing area *(2)*. This reduces the available wing surface and thus also the wing chord and the required material. In the cases of *(d)* and *(e)*, the aircraft span *(1)* is the same, the AR *(3)* still increases with a decreasing wing projected area *(2)*. For these aircraft configurations, the total aircraft mass increasing is related to a higher AR. This is caused by the wing mass required impacting the aerodynamic requirements of the aircraft. As the span is the same, the higher AR requires LEVEL0 to increase the spar cross-section and the ribs required, which again increases the wing mass. An increased wing mass also leads to the an increased required lift and therefore increased drag. This increases the energy required to fulfil the mission, influencing the required battery mass and the specific battery energy density.

The results from the exemplary mission analyses are used to estimate the required mean battery mass. Following the results in Table B.2, the mean battery mass for such a mission is at $\approx 50\%$ in line *(5i)*. This result can be used for battery mass estimation for different aircraft configurations for the same mission.

The results displayed in Table B.2 in line *(i)* also show the mass distribution, which is typical for solar aircraft. In accordance with Ross [32] and Jürgenhake [13], the typical component mass distribution for an all-electric aircraft is displayed in Table B.3.

	(1) Battery mass	(2) Airframe	(3) Payload mass	(4) Systems mass
Ross	52%	36%	7%	5%
Jürgenhake	30%	35%	5%	30%

Table B.3: Component mass distribution according to Ross [32] and Jürgenhake [13].

Comparing the aircraft component weight from Table B.2 and Table B.3, the battery mass and airframe mass from Ross and LEVEL0 are fairly similar for the chosen examples. The battery mass from Jürgenhake as well as the mass of the aircraft systems have higher discrepancies. This is based on the total weight of the required systems assumed, including propulsive and electronic systems by Jürgenhake which were based on different solar and battery mass assumptions and systems assignments. In general, LEVEL0's chosen computed exemplary distribution can be assumed to fall in an acceptable range for total aircraft component mass.

Wing spar dimensions

Following Table B.2, wing mass is one of the main components of an aircraft's mass. Thus, an inaccurate result for wing mass would have a significant impact on the result.

The wing spar analysis is based on aerodynamic forces and on aircraft mass. As previously explained, this results in forces in positive and negative z directions – namely, lift and downforce. The data used to generate these plots is based on an exemplary study from [8] for an aircraft with a wing area $S = 9m^2$, a wing $AR = 25$ and a total aircraft mass of $m \approx 60kg$ at $n = 4.5$. Additionally, a PF25 aerofoil has been used. The aerodynamic forces are based on the mentioned elliptical lift distribution computed at an altitude of $h = 17500m$ and a velocity of $v = 20m/s$. These values have been chosen due to the altitude range for solar HALE aircraft and the possible wind speeds at this altitude. The lift and the downforce, as well as the resulting moment over span, are displayed in Figure B.5.

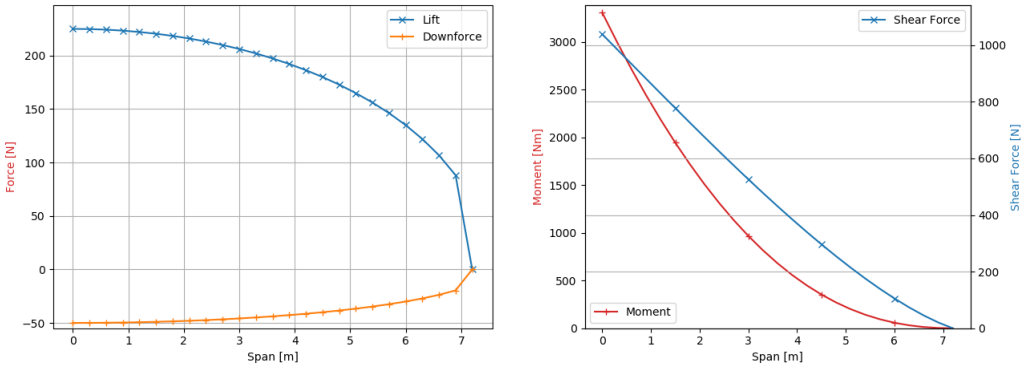

(a) Spanwise forces working on aircraft wing.

(b) Shear Force and moment exerted on wing spar.

Figure B.5: Forces and moments used to compute wing spar dimensions.

The lift and downforce are both dependent on the aircraft mass and the defined maximum load factor. The curves are elliptical, and an integration should return the total lift force required $F_z = 60kg \times 9.81\frac{m}{s^2} \times 4.5 = 2648.7N$. The integration of Figure B.5a return a force in z direction of $F_z = 2708.22N$ for a span-wise sectioning into 25 sections. This means that the sectioning, in this case, causes an error of 2.2%, which can be deemed acceptable. These forces in the z direction summed up and integrated over the span result in the shear force over span seen in Figure B.5b. The reaction force in the z direction at the wing root can be computed by integrating lift and downforce from Figure B.5b, obtaining a reaction force at the root of $\approx 1053.199N$. This also marks the shear force at the wing root, decreasing towards the wing tip. Integration of this shear force again yields the reaction moment M at the wing root, illustrating the maximum reaction moment in Figure B.5b. Integrating the shear force towards the wing tip, the resulting moment over span is used to determine the direct forces in the wing spar.
The direct forces within the wing spar are dependent on the cross-section and the material properties given. Therefore, the resulting wing spar is displayed in Figure B.6.

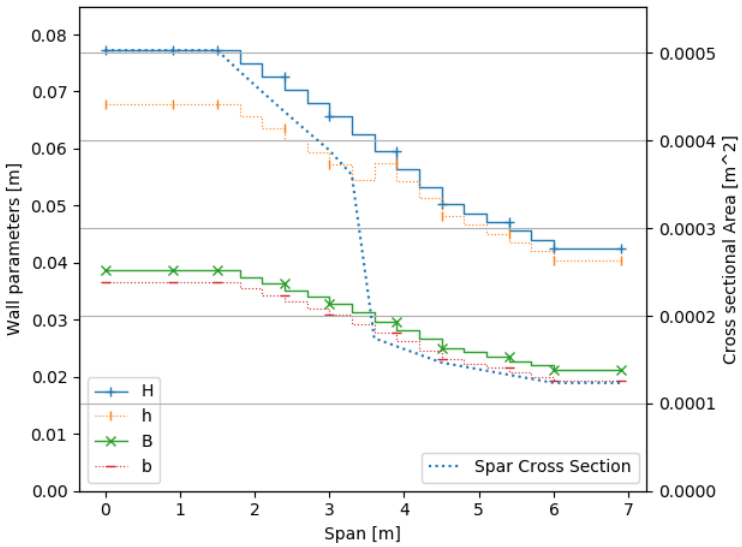

Figure B.6: Spar dimensions resulting from forces and moments working on the wing.

As explained in 4.3.3, the wall thickness of the spar is based on a minimisation process under several boundary conditions. The main parameters are the outer height of the spar H and the outer width B, followed by the inner values for height h and width b, as defined in Figure 3.4. The outer height H is always maximised based on the wing's elliptical outer shape. The outer width is assumed to be within $\frac{1}{2}H \leq B \leq H$. Based on this assumption, the outer width is maximally close to the wing root as the moment working on the spar is maximised at span $b = 0$. Because of the high moment leading to high stresses within the spar material, the spar cross-section is increased at this point. The most efficient way to strengthen the spar is to strengthen the upper and lower walls to withstand the forces in the z direction. The wall thickness is slowly lowered towards a higher span, as the moment also reduces with span. The estimation at this point tries to not drastically reduce wall thickness values but to achieve a gentle transition between wall thickness values. A drastic change in wall thickness at a specific point would lead to peak pressure occurring and would therefore be a predestined spot for material failure. With increasing span, the cross-section at the wing tip reduces towards the minimum value. This behaviour can be tracked through an examination of Figure B.7.

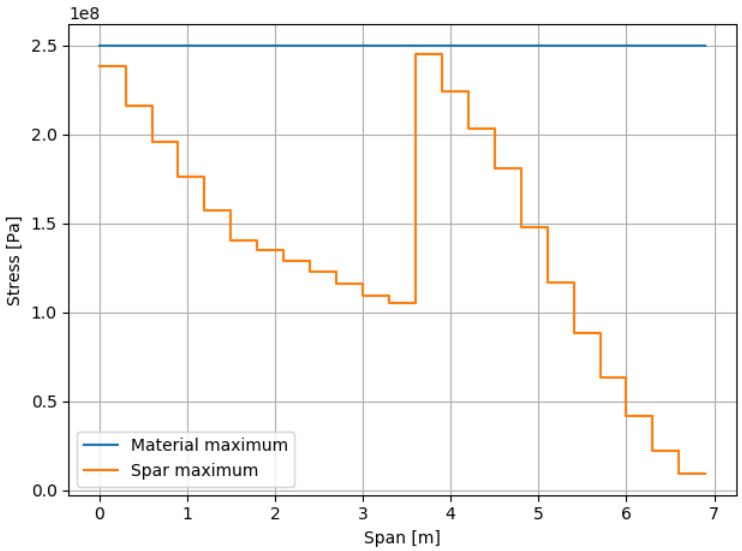

Figure B.7: Stresses working on the wing spar, resulting from span-wise moments, in relation to the maximum stress allowed.

The ”material maximum” is the maximum value which may occur and yet not cause the material to fail. The high stress, close to the allowed maximum and occurring close to the wing root, therefore shows that the spar width adjustment was necessary. Another effect can be observed when the spar cross-section drastically reduces at $b \geq 3m$. The stress occurring within the spar rises with the substantially decreasing cross-sectional area. In reality, it would also be important to avoid stress peaks within the spar, but for a mass assumption, this has been neglected. It is very important that the maximum occurring stress never exceeds the maximum allowable material parameters, and a real wing spar should thus come close to the estimated cross-sectional values.
If this cannot be reached during analysis, this can also be set as a boundary condition for a successful aircraft design.

B.3 Comparison with Keidel configuration

As already mentioned in Chapter 1, different possibilities for configuring aircraft have been developed. It is possible to either use wing-mounted solar panels with a body frame fixed alignment or use the solar panel configuration by Keidel in Figure 1.1b with a larger fuselage and adjustable mounted solar panels automatically oriented towards incoming irradiation. The experiments are the same as in Section 5.5, assuming a different solar panel configuration and an assumed 10% increase in aircraft mass and drag compared to the fixed solar cell configurations.

For the study about aircraft mass based on aircraft size in 5.5, the aircraft with adjustable solar panels shows a much larger potential in Figure B.8 than that with a fixed solar cell.

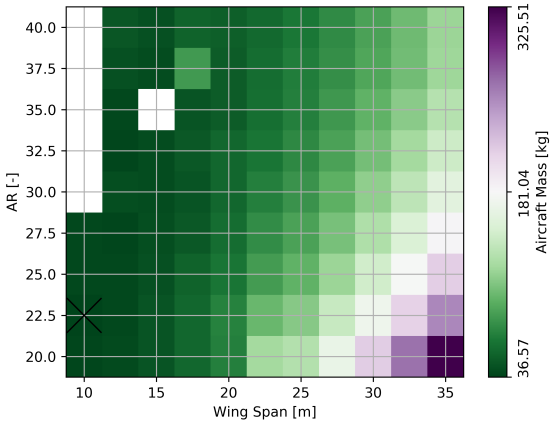

Figure B.8: Mass of aircraft configurations based on Figure 5.12 using Keidel's ideal solar panel configuration.

The range of possible aircraft configurations increases towards lower spans and higher aspect ratios. This implies that adjustable solar cells deliver more energy during flight, enables aircraft propulsion to be sustained for longer periods of time at beginning of the day and at the end of the day. This is reached due to an adjustment of the panels towards the sun, which increases the amount of harvested power. This again reduces the flight time which requires battery power and thus enables less efficient aircraft to also fulfil the mission scenario. The optimal aircraft in this case has a span of $b = 10m$ and an aspect ratio $AR = 22.5$, which is out of the possible scope for the fixed solar cell aircraft version shown in Figure 5.10.

For the study about the deployment area in Section 5.5, the aircraft with adjustable solar panels in Figure B.9 offers much more potential than the aircraft with a fixed solar cell.

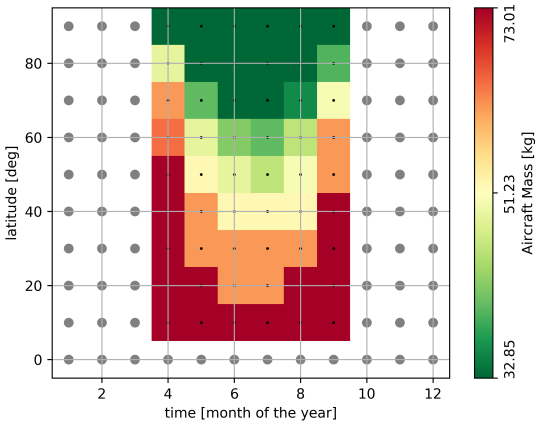

Figure B.9: Possible deployment area of a solar aircraft based on Figure 5.12, using Keidel's solar panel configuration.

Generally, in this case, the chosen base configuration in Section 5.12 already shows that it only can be deployed in northern latitudes during the summer. Every location or time with less usable irradiation distributed over a day is less favourable. A way to broaden the possible area and time of deployment of an aircraft of this size can thus be a configuration similar to that developed by Keidel [2]. The aircraft configurations possible are marked with colours which are scaled based on the required aircraft mass.
For the results which already showed a low mass, the added adjustable solar panels do not show any effect. This is the case for all settings which are close to the middle of the year and for far northern latitudes. As already shown in Figure 5.12 and now in Figure B.9, these settings need only a small number of batteries. This implies that the complete energy during flight is already based on incoming irradiation; thus, the fixed solar panels have already distributed a sufficient amount of energy, and the adjustable solar panels do not have any positive effect in these settings. The settings close to the boundaries in Figure 5.12 are still possible but with a reduced mass, while the results which already worked with a low mass show almost no added value.
However, in Figure 5.12, it can be seen that there are settings now feasible which were not feasible in the past. This is based on the adjustable solar panels harvesting more irradiation over the day. This does not increase the storage capacity of the batteries, but it enables the harvesting of irradiation for a low irradiation incidence angle in the morning and evening, shortening the battery flight time required. This this design has an increased area of possible use than a conventional approach with fixed solar panels mounted.

Appendix C

Tables

	Phase A-B	Phase B-C	Phase C-D	Phase D-E	Phase E-F	Phase F-G	Phase G-A
Indicator	$P_{req,asc} \leq P_{av}$ $RC \geq 0$			$P_{req} <= P_{av}$ $P_{req} <= P_{av}$ $P_{req} <= P_{av}$	$P_{req} = P_{av}$ $P_{req} = P_{av}$ $P_{req} = P_{av}$	$P_{req} \leq P_{av}$ $P_{req} \geq P_{av}$ $P_{req} <= P_{av}$	$P_{req} > P_{av}$ $P_{req} > P_{av}$ $P_{req} > P_{av}$
Power balance	$P_{req} <= P_{av}$ $P_{req} = P_{av}$ $P_{req} < P_{av}$	$P_{req} < P_{av}$	$P_{req} < P_{av}$	$P_{req} <= P_{av}$ $P_{req} <= P_{av}$ $P_{req} <= P_{av}$	$P_{req} = P_{av}$ $P_{req} = P_{av}$ $P_{req} = P_{av}$	$P_{req} <= P_{av}$ $P_{req} <= P_{av}$ $P_{req} <= P_{av}$	$P_{req} > P_{av}$ $P_{req} > P_{av}$ $P_{req} > P_{av}$
Power required	$P_{req,asc} + P_{pl}$	$P_{req,lvl} + P_{pl}$	$P_{req,asc} + P_{pl}$	$P_{req,lvl} + P_{pl}$	$P_{req,dsc} + P_{pl}$	$P_{req,dsc} + P_{pl}$	$P_{req,lvl} + P_{pl}$
Bat. loading	$P_{load} = 0$	$P_{load} >= 0$	$P_{load} > 0$	$P_{load} = 0$	$P_{load} >= 0$	$P_{load} = 0$	
Bat. status	$P_{load} = 0$	$P_{load} >= 0$	$P_{load} > 0$	$P_{load} = 0$	$P_{load} >= 0$	$P_{load} = 0$	

Table C.1: Change in power ratio over a 24-hour optimal mission scenario dividing changes within different phases.

Name	Type of Result	Explanation
Aircraft geometry	float values	To control the outcome, the geometric values are returned as a result. The values are used, stored and altered during analysis. Therefore this can be used to control the correct operation of the tool.
Mass breakdown	float values	The mass changes during iterations and is returned as a result.
Performance overview	list of values	Altitude, power consumption, power overshoot over time, and solar power delivered, velocity, rate of climb and altitude during mission are returned.
Conversion history	lists of floats	As the tool iterates, the differing values of every run are stored and returned within results.

Table C.2: Outputs for single LEVEL0 design.

	(1) Parameter Name	(2) Unit	(3) Description
(a)	maxiter	–	Maximum iterations for iterative mass analysis
(b)	maxclimbangle	–	Maximum aircraft climb angle
(c)	parallelComputation	–	Number of cores to be used in parallel
(d)	MinimumReynolds	–	Minimum Reynolds number to be assumed for XFoil
(e)	ReynoldsDelta	–	Difference between Reynolds numbers for interpolation
(f)	ncrit	–	NCrit for XFoil
(g)	maxiter	–	Maximum iterations for XFoil
(h)	save	–	Save 2d airfoil results
(i)	load	–	Load saved XFoilresults
(j)	solution	–	Safe minimum solution
(k)	solution2	–	Safe extended solution containing all internal computed values
(l)	ascend	–	Include ascent flight in analysis
(m)	descend	–	Include descent flight in analysis
(n)	prop	–	Include propelled descend in analysis
(o)	input	–	Save input with output again
(p)	batteryvolume	m^3	Include battery volume check in analysis
(q)	groundloads	–	Include load analysis without lift effect included
(r)	sparminimum	m	Include minimum spar cross-section as Boolean result
(s)	massscaling	–	Scale total aircraft mass
(t)	dragscaling	–	Scale total aircraft drag
(u)	masspenalty	kg	Include absolute mass penalty in analysis
(v)	solarincidence	–	Incidence angle for solar irradiation on the panels (”std”, ”ideal”)

Table C.3: Extended input parameters LEVEL0.

Name	Value	Unit
Aircraft mass	80	kg
Aspect ratio	52.36	-
Span	29.54	m
Maximum lift coefficient	1.6	-
Mean chord length	0.56	m
Projected wing area	16,67	m^2
Wing loading	4.79	km/m^2
Maximum spar thickness	67.01	mm
Solar panel efficiency	0.2	-
Specific battery energy density	240	Wh/kg
Payload mass	1	kg
Maximum load factor	1	-
Date of flight	30th of June 2016	-

Table C.4: Aircraft parameters for parameter study comparison with [8]

Appendix D

Figures

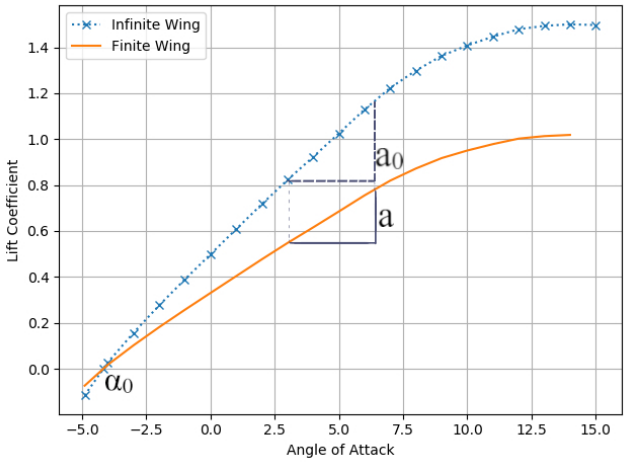

Figure D.1: Exemplary lift curves for an infinite wing versus a finite wing planform.

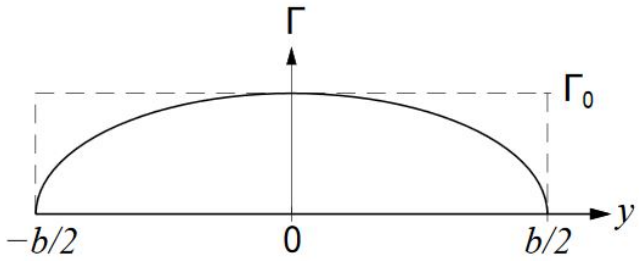

Figure D.2: Schematic description of elliptic circulation distribution.

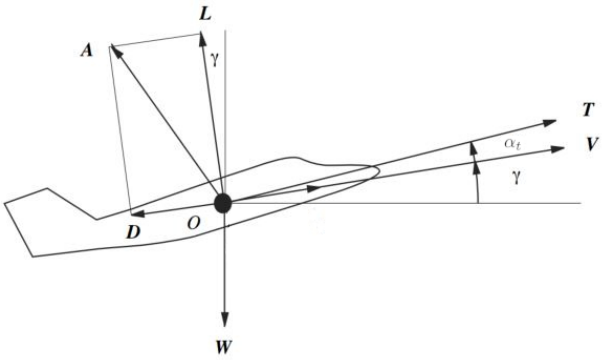

Figure D.3: Forces exerted on aircraft based on [33].

Bibliography

[1] Andre Noth, (2008), "Design of Solar Powered Airplanes for Continuous Flight", (Doctoral dissertation), *ETH Zuerich*

[2] Bernhard Keidel, (2000), "Auslegung und Simulation von hochfliegenden, dauerhaft stationierbaren Solardrohnen", (Doctoral dissertation), *Institute of Flight System Dynamics, Technical University Munich*

[3] M. Hepperle, A.Ruiz-Leon, W.Rack, H.Runge, (2007), "A solar powered HALE for arctic research", (Conference paper), presented on 1st CEAS European Air and Space Conference, Sept. 2007, Berlin, *German Aerospace Center, University of Canterbury*

[4] unknown, (2018), "Zephyr - Pioneering the Stratosphere", (Website), retrieved from *https://www.airbus.com/defence/uav/zephyr.html* on 21.11.2019

[5] unknown, (21.08.2010), "Zephyr HALE UAV endurance record", (Website), retrieved from *http://aviationdefence.blogspot.com/2010/08/zephyr-hale-uav-endurance-record.html* on 21.11.2019

[6] Arnaud Jordan, (2007), "Feasibility Study of Fixed-Wing Configurations for HALE UAV Platforms", (Technical Report), *Institute of Flight Systems, Technical University Brunswick*

[7] Craig Nickol, Mark Guynn, Lisa Kohout, Thomas Ozoroski, (2007), "High Altitude Long Endurance Air Vehicle Analysis of Alternatives and Technology Requirements Development", (Technical Report), *American Institute of Aeronautics and Astronautics*

[8] Sunpeth Cumnuantip, Sarah Froese, Michael Hanke, Thomas Immisch, Carsten Liersch, Simon Schopferer, Andre Suchaneck, (2016), "Entwurf und Auslegung Hochfliegender Plattformen", (Technical report), *German Aerospace Center*

[9] Benedict Bartels, (2017), "Literature Study - HALE", (report), *Technische Universiteit Delft*

[10] G. Girishkumar, B. McCloskey, A. C. Luntz, S. Swanson, W. Wilcke , (2010), "Lithium - Air Battery: Promise and Challenges", (Article), presented

in The Journal of physical Chemistry Letters, July 2010, *American Chemical Society*

[11] Takeo Oku, (2016) "Solar Cells and Energy Materials", (Book), *De Gruyter*

[12] Daniel P. Raymer, (1998) "Aircraft Design: A conceptual approach", (2nd ed.), (Book), *American Institute of Aeronautics and Astronautics, Inc*

[13] C. Jürgenhake, (2008),"Konstruktion und Bau eines Flügelabschnittsdemonstrators für eine hochfliegende, dauerhaft stationierbare Solardrohne", (Technical report), *German Aerospace Center*

[14] Mathilde Brizon, (2015), "Solar Energy Generation Model for High Altitude Long Endurance Platforms", (Master thesis), *KTH - Royal Institute of Technology, Stockholm, Sweden*

[15] B.W. McCormick, (1979), "Aerodynamics, Aeronautics and Flight Mechanics", (Book) *John Wiley & Sons*

[16] Fred Thomas, (1979), "Grundlagen für den Entwurf von Segelflugzeugen", (Book), *Motorbuch Verlag*

[17] John D. Anderson, (2011), "Fundamentals of Aerodynamics", (5th ed.), (Book), *McGraw-Hill Series in Aeronautical and Aerospace Engineering*

[18] John J. Bertin, Russel M. Cummings, (2014), "Aerodynamics for Engineers", (6th ed.), (Book), *Pearson*

[19] Johannes Drexler, Hans Galleithner, (1994), "Untersuchung der technischen Machbarkeit hochfliegender, dauerhaft stationierbarer Drohnen", (Technical report), *German Aerospace Center*

[20] unknown, (23.10.2013), "XFOIL - Subsonic Airfoil Development System", (Website), retrieved from *https://web.mit.edu/drela/Public/web/xfoil/* on 23.10.2017

[21] H.Glauert, (1983), "The Elements of Aerofoil and Airscrew Theory", (Book), *Cambridge University Press*

[22] Sighard F. Hoerner, (1965), "Fluid Dynamic Drag", (Book), *Hoerner Fluid Dynamics*

[23] Egbert Torenbeek, (2013), "Advanced Aircraft Design: Conceptual Design, Analysis and Optimization of Subsonic Civil Airplanes", (Book), *Wiley*

[24] W.Stender, (1969), "Sailplane weight estimation", (Book), *OSTIV*

[25] E. Rizzo, A. Frediani, (2004), "A Model for Solar Powered Aircraft Preliminary Design", (Article), *International Conference of Computational and Experimental Engineering and Sciences 04*, Vol. 1

[26] Russel C. Hibbeler, (2008), “Sterkteleer”, (2nd ed.), (Book), *Pearson*

[27] “CPACS - A Common Language for Aircraft Design; Simulation and Modeling”, (10.02.2016), retrieved from *https://software.dlr.de/p/cpacs/home/* on 05.11.2017 (Website)

[28] Unknown, ICAO, (1993), “Manual of the ICAO standard atmosphere - extended to 80km (262 500 feet)”, (Technical Report), *International Civil Aviation Organization*

[29] unknown, (07.2019), “XFLR5”, (Website), retrieved from *http://www.xflr5.tech/xflr5.htm* on 23.10.2017

[30] (2016) “Pilot’s Handbook of Aeronautical Knowledge”, (Book), *Federal Aviation Administration*

[31] Ger Ruijgrok, (2009), “Elements of airplane perfomance”, (Book), *VSSD*

[32] Hannes Ross, Solar Impulse, (2007), “Solarangetriebene Flugzeuge - Eine Übersicht = The True All Electric Aircraft”, (Article), *Deutscher Luft- und Raumfahrtkongress 2007*

[33] David G. Hull, (2007), “Fundamentals of Airplane Flight Mechanics”, (Book), *Springer*